# Development of Carrier-Flotation Technique for Finely Ground Copper Sulfides

A dissertation submitted in partial fulfillment of the requirements for the degree of Doctorate in Engineering

by

**MUHAMMAD BILAL**


Laboratory of Mineral Processing and Resources Recycling,
Division of Sustainable Resources Engineering,
Graduate School of Engineering,
Hokkaido University, Japan

September 2022

# Development of Carrier-Flotation Technique for Finely Ground Copper Sulfides

A dissertation submitted in partial fulfillment of the requirements for the degree of Doctorate in Engineering

by

**MUHAMMAD BILAL**

Supervisor and Chairperson of Examination Committee M. Ito
(Prof. Mayumi ITO)

Examination Committee Member
(Prof. Naoki HIROYOSHI)

Examination Committee Member
(Prof. Tsutomu SATO)

Examination Committee Member
(Assoc. Prof. Yasumasa TOJO)

Laboratory of Mineral Processing and Resources Recycling,
Division of Sustainable Resources Engineering,
Graduate School of Engineering,
Hokkaido University, Japan

September 2022

## Declaration

I, **Muhammad Bilal**, hereby declare that, except where a specific reference is made in the text, this dissertation is my own research work, and it has never—entirely or in parts—been submitted to any university for academic qualification.

**Signature:** M. Bilal
19/08/2022

**Acknowledgments**

First and foremost, I am thankful to Almighty ALLAH, by His grace and bounty, I am able to complete my Ph.D. thesis. I ask for sincerity in all my actions from ALLAH, and I quote the verse from the Holy Quran “Say, Indeed, my prayer, my rites of sacrifice, my living and my dying are for ALLAH, Lord of the worlds” (Al-’An‘am, verse 162).

I would like to express my sincere gratitude to my Ph.D. thesis advisor Prof. Mayumi Ito for the continuous support of my Ph.D. study and research, for her patience, motivation, enthusiasm, and immense knowledge. Her guidance helped me in all the time of research and writing of this thesis. I could not have imagined having a better advisor and mentor for my Ph.D. study.

To my co-supervisor, Prof. Naoki HIROYOSHI, who made complex phenomena seem easy. The saying by Albert Einstein “If you can't explain it simply, you don't understand it well enough” was realized after working under his supervision. You used to bring so many ideas during those long discussions, and I am forever grateful.

I wish to extend my sincere appreciation to Asst. Prof. Ilhwan Park, who generously helped me throughout my Ph.D. journey. In particular, I thank Ph.D. co-examiner Assoc. Prof. Yasuma Tojo and Prof. Tsutomu Sato for their valuable comments and advice that helped me improve the quality of my dissertation.

I would like to thank all the members of the Laboratory of Mineral Processing and Resources Recycling for their assistance and support.

I would like to thank my colleague Fawad Ul Hassan for his unconditional support during my research work.

Last but not least I thank my parents, my wife, my kids, and my sisters, for their patience, guidance, and support during my Ph.D. research.

**Abstract**

Copper (Cu) is one of the most important metals required to meet the world's growing energy production, storage, and transportation needs. Porphyry copper deposits (PCDs) make up a large portion of the world's economic copper resources. Porphyry copper deposits contain hundreds of millions of tons of ore averaging only a fraction of 0.44% copper. Although PCDs are low-grade, they are important because they can be mined at a low cost on a large scale.

Flotation is a common mineral processing method used to produce copper concentrates from copper sulfide ores. In this method, copper sulfide minerals are concentrated in the froth while associated gangue minerals are separated as tailings. However, some amount of copper is lost to tailings during the processing; therefore, tailings can be considered secondary resources or future deposits of copper.

The particle sizes of copper sulfide minerals present in tailings are typically very fine because of the adoption of the regrinding process before cleaner flotation for improving the degree of liberation. Ultrafine particles are least likely to collide with air bubbles in the flotation cell, resulting in the lowering of their recovery by conventional flotation techniques. Therefore, the development of flotation methods able to recover fine particles effectively is necessary for processing tailings. In this regard, this study investigated an innovative method called carrier flotation using coarse chalcopyrite and pyrite as carriers for improving the recovery of finely ground chalcopyrite particles.

Chapter 1 describes the statement of the problem and the objectives of this study.

Chapter 2 reviews the comparison of different techniques to recover copper sulfides from flotation tailings, including column flotation, microbubble flotation, nanobubble flotation, polymer flocculation, shear flocculation, oil agglomeration, and carrier flotation.

In Chapter 3, the effects of coarse chalcopyrite particles as a carrier on flotation behavior of fine chalcopyrite were investigated by the flotation experiments using fine chalcopyrite (particle size $D_{50}$ = 2.3 μm) with a varied amount of carrier particles of different sizes (–75 + 38 μm and –106 + 75 μm) using an agitated flotation cell. The addition of carrier particles improved the recovery of ultrafine particles into the froth from around 25% (without carrier) to around 80% (with 20 g of carrier, –75+38 μm size). Recovery of fine particles was higher with smaller carrier size (–75+38 μm) compared with larger carrier size (–106+75 μm), though the difference was not significant.

In Chapter 4, the effects of pyrite as a carrier for recovering finely ground chalcopyrite particles were investigated. Flotation experiments for finely ground chalcopyrite ($D_{50}$ = 3 μm) were conducted with and without coarse pyrite (–125+106 μm) using potassium amyl xanthate as a collector. The results showed that untreated pyrite did not act as an effective carrier and that the amount of fine chalcopyrite attached to pyrite was not significant; furthermore, Cu recovery into froth was around 65% both with and without pyrite. When pyrite was pre-treated with a $CuSO_4$ solution, its carrier ability improved owing to a significant amount of fine chalcopyrite becoming attached to the $Cu^{2+}$-activated pyrite particles and being recovered with pyrite into the froth (Cu recovery, >90 %).

In Chapter 5, a method to separate finely ground chalcopyrite particles from coarse pyrite particles was investigated. Results showed that at pH ~2, the collector adsorbed onto chalcopyrite/pyrite surfaces could be dissolved, and thus around 90% of fine chalcopyrite was detached from coarse pyrite particles.

In Chapter 6, a summary of this dissertation's findings and implications were provided.

## Table of contents

## List of Figures

## List of Tables

# CHAPTER 1: General Introduction

## 1.1 Background

Copper is commonly present in the earth's crust as copper–iron–sulfide, and copper sulfide minerals, such as chalcopyrite ($CuFeS_2$) and chalcocite ($Cu_2S$). The concentration of these minerals in an ore body is low. Typical copper ores contain from 0.5% Cu (open pit mines) to 1 or 2% Cu (underground mines). Pure copper metal is mostly produced from these ores by concentration, smelting, and refining. The copper concentrates from sulfide ores are usually produced by flotation and then processed by pyrometallurgical or hydrometallurgical methods to extract the copper as illustrated in Fig. 1-1 (de Lima et al., 2011, Tabelin et al., 2021, Park et al., 2020). Copper also occurs to a lesser extent in oxidized minerals (carbonates, oxides, hydroxy–silicates, sulfates). Copper metal is usually produced from these minerals by leaching, solvent extraction, and electrowinning (Schlesinger et al., 2011).

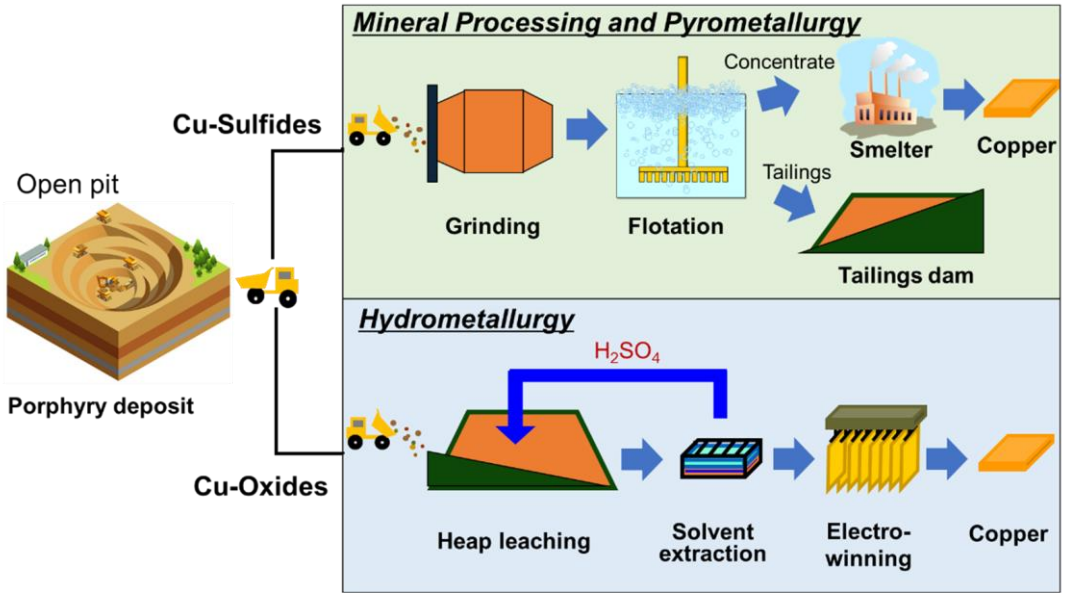


Fig. 1-1. Main processes for extracting copper from sulfide and oxide ores.

## 1.2 Problem Statement

Flotation is a common method used for the separation of sulfide minerals. Copper sulfides are the main source of copper and flotation is often used to concentrate it from its ores and remove most of the associated gangue minerals before extraction processes (e.g., smelting). Before flotation, the ore is ground to liberate minerals from gangue, which often results in excessive grinding thus producing fine particles. An increase in the percentage of fine particles (<10um) gives poor recovery in flotation (Leistner et al., 2017, De F. Gontijo et al., 2007). During the flotation process, a significant amount of fine chalcopyrite particles is lost in tailings. A major reason for the low recovery in flotation is

the low probability of collision between the bubble and fine particles. In mechanical flotation cells, the collision between fine particles and the rising bubbles becomes poor because of the small mass and low momentum of fine particles (Trahar, 1981). According to reports, copper mines lose about 10%–20% of copper in tailings (Chen et al., 2014). These tailings may be regarded as secondary deposits of copper, subjected to the development of an effective flotation method for recovering fine copper sulfide particles.

Many flotation methods have been developed to enhance particle–bubble collision efficiency and improve fine particle recovery either by increasing particle size or decreasing bubble size (Leistner et al., 2017, Tabosa and Rubio, 2010). The particle size of the targeted mineral is increased using shear flocculation, oil agglomeration, or carrier flotation technique (Leistner et al., 2016).

The Carrier flotation technique has been used to recover fine coal particles, however, in the case of copper sulfides, no study reports the use of carrier flotation and mechanism to recover fine copper sulfides.

### 1.3 Thesis objectives

The objective of this study is to develop a carrier flotation method to improve fine copper sulfides recovery, which can be used to recover fine copper sulfides efficiently from flotation tailings in the future.

### 1.4 Thesis outline

There are six chapters in this dissertation. The contents of each chapter are outlined below.

Chapter 1 gives a general background of copper processing methods, the problem statement, and the objective of this study.

Chapter 2 gives a detailed review of the tailing loss mechanism, the challenges, and the prospects of different flotation methods to recover copper sulfides from tailings.

Chapter 3 investigates the effects of coarse chalcopyrite particles as a carrier for improving the flotation recovery of finely ground chalcopyrite particles.

Chapter 4 investigates the use of pyrite as a carrier for recovering finely ground chalcopyrite particles.

Chapter 5 investigates the detachment of coarse $Cu^{2+}$–activated pyrite and finely ground chalcopyrite particles after flotation.

In chapter 6, the dissertation is summarized, and a general conclusion is presented along with proposals for future research.

## References


CHEN, D., YU, Y., LIU, L. M. & HAN, Z. B. 2014. Study on Flotation Technique to Recycle Copper from Tailings. *Advanced Materials Research,* 878**,** 322-329 DOI: https://doi.org/10.4028/www.scientific.net/AMR.878.322.

DE F. GONTIJO, C., FORNASIERO, D. & RALSTON, J. 2007. The limits of fine and coarse particle flotation. *The Canadian Journal of Chemical Engineering,* 85**,** 739-747 DOI: https://doi.org/10.1002/cjce.5450850519.

DE LIMA, G. F., DE OLIVEIRA, C., DE ABREU, H. A. & DUARTE, H. A. 2011. Water Adsorption on the Reconstructed (001) Chalcopyrite Surfaces. *The Journal of Physical Chemistry C,* 115**,** 10709-10717 DOI: https://doi.org/10.1021/jp201106e.

LEISTNER, T., EMBRECHTS, M., LEIßNER, T., CHEHREH CHELGANI, S., OSBAHR, I., MÖCKEL, R., PEUKER, U. A. & RUDOLPH, M. 2016. A study of the reprocessing of fine and ultrafine cassiterite from gravity tailing residues by using various flotation techniques. *Minerals Engineering,* 96-97**,** 94-98 DOI: https://doi.org/10.1016/j.mineng.2016.06.020.

LEISTNER, T., PEUKER, U. A. & RUDOLPH, M. 2017. How gangue particle size can affect the recovery of ultrafine and fine particles during froth flotation. *Minerals Engineering,* 109**,** 1-9 DOI: https://doi.org/10.1016/j.mineng.2017.02.005.

PARK, I., HONG, S., JEON, S., ITO, M. & HIROYOSHI, N. 2020. A Review of Recent Advances in Depression Techniques for Flotation Separation of Cu–Mo Sulfides in Porphyry Copper Deposits. *Metals,* 10 DOI: https://doi.org/10.3390/met10091269.

SCHLESINGER, M. E., KING, M. J., SOLE, K. C. & DAVENPORT, W. G. 2011. Chapter 1 - Overview. *In:* SCHLESINGER, M. E., KING, M. J., SOLE, K. C. & DAVENPORT, W. G. (eds.) *Extractive Metallurgy of Copper (Fifth Edition).* Oxford: Elsevier DOI: https://doi.org/10.1016/B978-0-08-096789-9.10001-0.

TABELIN, C. B., PARK, I., PHENGSAART, T., JEON, S., VILLACORTE-TABELIN, M., ALONZO, D., YOO, K., ITO, M. & HIROYOSHI, N. 2021. Copper and critical metals production from porphyry ores and E-wastes: A review of resource availability, processing/recycling challenges, socio-environmental aspects, and sustainability issues. *Resources, Conservation and Recycling,* 170**,** 105610 DOI: https://doi.org/10.1016/j.resconrec.2021.105610.

TABOSA, E. & RUBIO, J. 2010. Flotation of copper sulphides assisted by high intensity conditioning (HIC) and concentrate recirculation. *Minerals Engineering,* 23**,** 1198-1206 DOI: https://doi.org/10.1016/j.mineng.2010.08.004.

TRAHAR, W. J. 1981. A rational interpretation of the role of particle size in flotation. *International Journal of Mineral Processing,* 8**,** 289-327 DOI: https://doi.org/10.1016/0301-7516(81)90019-3.

# CHAPTER 2: Literature Review

## 2.1 Introduction

Copper (Cu), the second most-produced non-ferrous metal after aluminum, has been widely used for various applications due to its unique properties such as excellent electrical/thermal conductivities, high corrosion resistance, and outstanding malleability/ductility (Schlesinger et al., 2011b, Tran et al., 2019), and the demand for Cu is projected to be continuously increased because it is considered one of 17 materials/metals identified as critical materials/metals for realizing a low-carbon future (Tabelin et al., 2021, Kirsten Hund, 2020). Low-carbon technologies require more Cu than conventional fossil-fuel-based technologies; for example, a typical 3 MW wind turbine requires 4.7 t of Cu, photovoltaic (PV) cells need ~1% Cu, and electric vehicles (EVs) use 1.7–11 times more Cu than conventional cars (Tabelin et al., 2021, Park, 2022, Park et al., 2021b, Kirsten Hund, 2020, 2017). Thus, the establishment of a robust and sustainable supply chain of Cu is an important issue for humanity.

Copper sulfides are the primary source of metallic copper, which makes up 80% of copper resources (Schlesinger et al., 2011a). The major copper sulfide ores include chalcopyrite ($CuFeS_2$), bornite ($Cu_5FeS_4$), covellite (CuS), and chalcocite ($Cu_2S$). The copper concentrates from sulfide ores are usually produced by flotation and then processed by pyrometallurgical or hydrometallurgical methods to extract the copper (de Lima et al., 2011, Tabelin et al., 2021, Park et al., 2020b).

Froth flotation is widely used to separate sulfide minerals from gangue minerals such as quartz ($SiO_2$), based on the surface properties of minerals. The principle of the flotation process is illustrated in Fig. 2-1. In flotation, ground ore particles are suspended in water in the flotation cell and conditioned with various reagents (e.g., collector, frother, activator, depressant, and pH adjustor) to control the hydrophobicities of target and gangue minerals (Park et al., 2020a, Park et al., 2021a, Aikawa et al., 2021, Bulatovic, 2007). Afterward, air bubbles are induced into the pulp (mineral/water suspension), and hydrophobic copper mineral particles are attached to the bubble surface and recovered into the froth layer as a copper concentrate (Yuan et al., 1996, Sripriya et al., 2003). Hydrophilic gangue minerals such as quartz are not attached to air bubbles and remain in the pulp as a by-product called tailings.

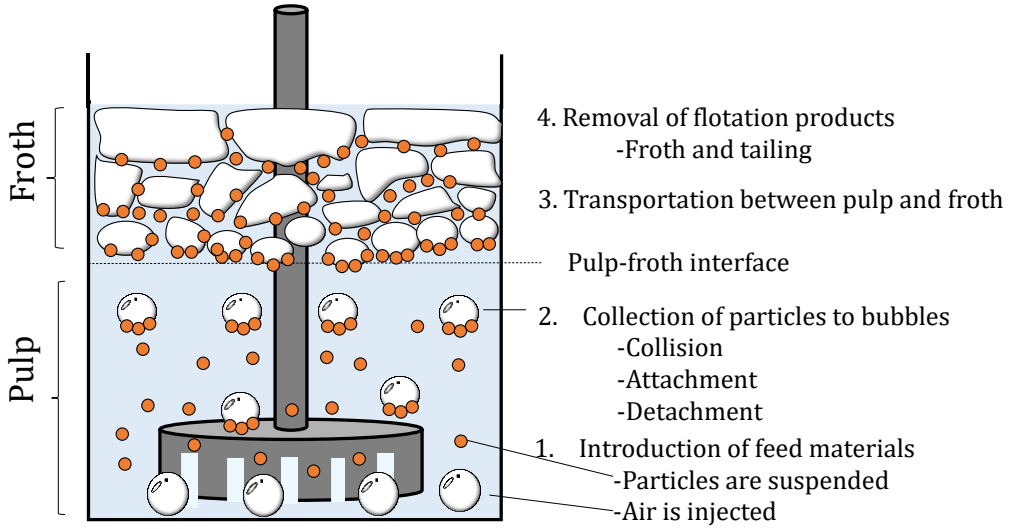


Fig. 2-1. Flotation mechanism.

In the actual flotation process, however, a significant quantity of copper sulfide particles is lost in tailings, which are disposed of in the tailings storage facilities (TSFs). Since the conventional copper ores have been getting depleted, copper tailings are gaining increasing attention as potential resources. For example, the amount of copper in TSFs is estimated to be the magnitude of 0.13 Gt, equivalent to ~15% of the current geogenic Cu reserves (Suppes and Heuss-Aßbichler, 2021, Kapur and Graedel, 2006, Ober, 2018). The recovery of copper sulfides from TSFs will not only add economic value but also protect the environment because the oxidation of copper sulfides causes the formation of acid mine drainage (AMD) that contaminates surrounding ecosystems (Park et al., 2019). In this chapter, the mechanism of the tailing loss during the flotation process is discussed and developed methods to recover copper from tailings are reviewed.

## 2.2 Tailing loss

### *2.2.1 Tailing amount*

Tailings from the flotation process account for ~98% of total ore fed to the concentrator and are usually stored in large tailings dams near the mine (Schlesinger et al., 2011c). Flotation tailings are termed the rejected product of the flotation process, and according to the reported literature data, 90–95% of plant tailings are produced from the flotation process (Han et al., 2018, Antonijević et al., 2008, Hansen et al., 2005). Flotation tailings mainly contain gangue minerals, while a significant amount of valuable copper sulfide particles is also contained. As shown in Table 2-1, it has been reported that around 10–20% of copper in the ore is lost in the tailings. The copper grade in the tailings is 0.04–0.2%, and this is very low in comparison with standard copper ores containing over 0.5% of copper. Because of this, low-grade tailings are not considered an economically

valuable copper source at present, however, when copper demand increases and methods to recover copper from tailings are developed, tailings can be considered as a secondary deposit or future resource of copper.

Table 2-1. Industrial flotation data from copper concentrators, 2010 (Schlesinger et al., 2011c).

| Concentrator | Ore treated, tonnes/ year | Concentrate, tonnes/ year | Cu recovery to concentrate, % | Cu loss to tailings, % | Tailings grade, %Cu |
|---|---|---|---|---|---|
| **El Soldado, Chile** | 7,700,000 (2010) | 67,000 | - | - | 0.18 |
| **Los Bronces, Chile** | 20,500,000 (2010) | 676,000 | - | - | 0.133 |
| **Africa (open Pit)** | 4,000,000 | 35,000 | 80 | 20 | 0.018 |
| **Africa (under Ground)** | 900,000 | 21,000 | 85 | 15 | 0.04 |
| **Mantos Blancos Chile (open pit)** | 4,500,000 | 125,000 | 89 | 11 | 0.12 |
| **Cerro Verde, Peru** | 39,000,000 | 750,000 | 88 | 12 | 0.075 |
| **Sierrita, U.S.A.** | 37,000,000 | 325,000 | 84.3 | 15.7 | 0.041 |
| **Ray, U.S.A.** | 10,000,000 | 150,000 | 90 | 10 | 0.035 |

*2.2.2 Mechanism*

The main part of copper mineral processing is generally composed of two steps: (i) comminution to liberate valuable copper minerals from non-valuable gangue minerals, and (ii) flotation to separate copper minerals from gangue minerals. After flotation, copper concentrates are sent to the smelter for the production of highly purified copper cathodes (>99.99% Cu), while tailings are disposed of in tailing dams near mine sites.

In an ideal mineral processing of copper ores, all copper mineral grains must be liberated from gangue minerals before separation in the comminution step (crushing and grinding). In an actual comminution step, perfect liberation is difficult, because the step consumes a lot of energy and generates excessively fine particles, which cannot be recovered in the separation step (Bagster and McIlvenny, 1985). Because of these reasons, as shown in Fig.

2-2, actual ground ores are a mixture of liberated (fine) copper minerals and gangue grains, and unliberated (coarse) copper minerals locked with gangue minerals.

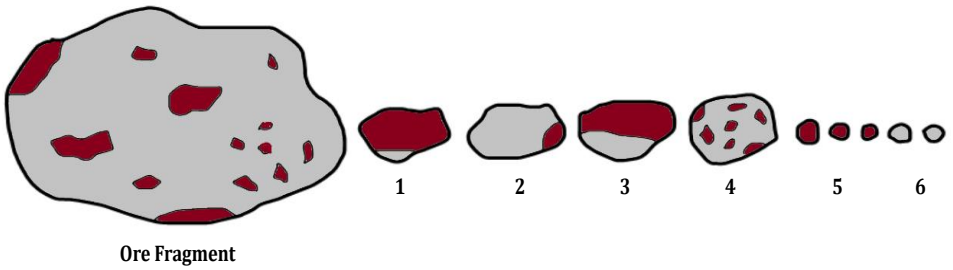


Fig. 2-2. Illustration of an ore fragment (mineralization in dark red) and the products of comminution: (1) highly liberated particle, (2) poor liberation or gangue-rich particle, (3) and (4) moderately liberated particles (middlings), (5) liberated fine mineral.

In the separation process, the behavior of unliberated grains depends on the copper mineral portion in the grain; that is, when the copper portion is large, an unliberated particle may act as a (liberated) copper mineral, while when the copper portion is small, it may behave as gangue mineral. Because of this, a part of copper minerals in unliberated grains is lost into tailings together with gangue minerals. This is one of the reasons (mechanisms) for copper loss in the tailings.

Another case of copper loss occurs even for fine liberated particles during separation using flotation. In flotation, mineral particles suspended in water collide and attach to air bubbles induced into the flotation cell, then they are floated to the surface of the water as a froth product. The flotation efficiency of mineral particles depends on particle size. Research on the relationship between particle size and floatability began in the early 1930s in work presented by Gaudin et al. (1931) (Mankosa et al., 2016), which showed that coarse and fine particles are more difficult to recover than intermediate size particles. In the case of chalcopyrite flotation, it has been reported that copper recovery to the froth was around 95% at particle size between 10–150 μm, while the recoveries were decreased to 50% when particle size decreased from 20 μm to 3 μm (Shergold, 1984, De F. Gontijo et al., 2007). The flotation process is more efficient in the particle size range of approximately 10–100 μm (Trahar, 1981, Jameson, 2012, Schubert, 2008), and it is usually poor with an increased percentage of ultrafine particles (−10 μm) in the system (Trahar and Warren, 1976, Sivamohan, 1990, Leistner et al., 2016). The majority of copper lost into flotation tailings at operating concentration plants occur in particle sizes smaller than 20 μm and larger than 105 μm. In general, liberating particles or increasing mineral surface area, can be increased by decreasing particle size (Asghari et al., 2019). In flotation, a particle's lower size limit varies for different minerals (Trahar and Warren,

1976), besides, some studies reported good recovery of ultrafine particles (Trahar, 1981, Leistner et al., 2017). Michael et al. (Mankosa et al., 2016) reported the effects of particle size on the distribution of copper to froth and tailings during conventional flotation. Recoveries of copper to froth were maximum at particle size between 30 and 150 μm, and there is a distinct drop in the recovery outside of this range, resulting in a loss of ultrafine and coarse particles into tailings (Fig. 2-3). It is evident from Fig. 2-3 that a substantial amount of valuable minerals is contained in the tailings in both the finest and coarsest fractions. The reason for the dependence of flotation efficiency on particle size can be described as below.

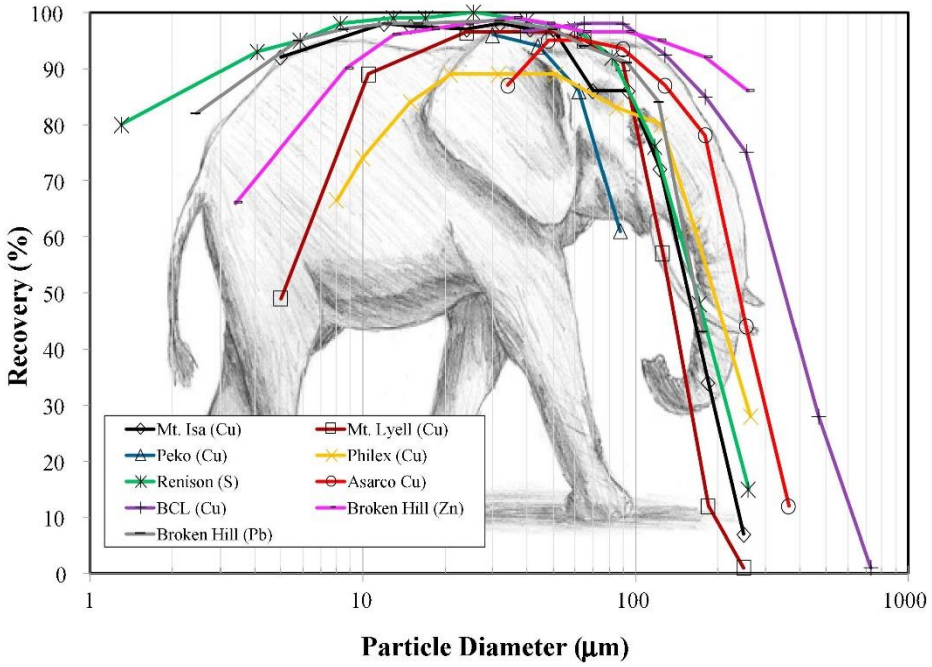

Fig. 2-3. Conventional flotation data for industrial sulfide flotation circuits (Mankosa et al., 2018).

In flotation, air bubbles are injected into mineral particle/water suspension, which rises by buoyancy and collides with suspended mineral particles. If the particle is hydrophobic, it is stably attached to the air bubble and is not detached from the bubble. This captured particle is then floated with air bubbles and recovered as a froth product.

Fig. 2-4 illustrates the process of particles captured with a rising air bubble. The probability of particles ($P$) captured by bubbles during the flotation process in the cell can be expressed as follows (Sivamohan, 1990, Yoon, 2000):

$$P = P_c \times P_a \times (1 - P_d), \qquad 2.1$$

where $P_c$ , $P_a$, and $P_d$ represent the probabilities of collision, attachment, and detachment, respectively. The collision between fine particles and the rising bubbles, in mechanical flotation cells, becomes poor because of the smaller mass and low momentum of fine particles (Trahar, 1981, Hornn et al., 2020b, Hornn et al., 2020c, Hornn et al., 2020d); fine particles follow fluid streamlines around the bubble.

Collision efficiency is linked with the size ratio of the mineral particle and air bubble Eq. (2.2).

$$P_c = A\left(\frac{D_p}{D_b}\right)^n, \qquad 2.2$$

where, $D_p$ and $D_b$ represent the diameters of particle and bubble, respectively; and $A$ and $n$ are empirical flow regime constants.

Attachment probability ($P_a$) and detachment probability ($P_d$) are mainly a function of the particle surface properties. For hydrophobic minerals like chalcopyrite, the values of $P_a$ and $P_d$ could be assumed as 1 and 0, respectively. In this case, $P$ is mainly dependent on $P_c$. Based on Eq. (2.2), the collision probability ($P_c$) is directly proportional to the particle to bubble diameters ratio. With a significant decrease in the diameter of particles ($D_p << D_b$) the collision probability is substantially decreased, which explains the very low recovery rates of fine particles. For excessively coarse particles, collision probability ($P_c$) is high; however, attached particles are easily detached from the air bubble by turbulent flow, i.e., $P_d$ is high (Nguyen-Van, 1994, Tortorelli et al., 1997, Nguyen and Schulze, 2003). This is because of the relatively small specific surface area of coarse particles, which reduces particle-bubble attachment strength. This is one of the reasons for the low flotation recovery of coarse particles into the froth.

As discussed above, there are two major reasons for tailing loss of copper in the flotation process: (i) tailing loss of ultrafine particles due to the excessively low collision efficiency between particle and air bubble in flotation cells, and (ii) coarse unliberated copper minerals associated with gangue minerals, which are easily detached from an air bubble in flotation.

For recovering copper from tailings, regrinding is needed to liberate copper minerals from locked grains. As a result, liberated but fine copper mineral particles are formed. This necessitates the development of flotation techniques to recover fine copper mineral particles from tailings. Numerous flotation methods have been developed to enhance

particle-bubble collision efficiency and improve fine particles recovery either by increasing the particle size or decreasing the bubble size (Leistner et al., 2017, Tabosa and Rubio, 2010). In this review paper, these techniques are reviewed concerning their applications on tailings, which contain mostly fine mineral particles.

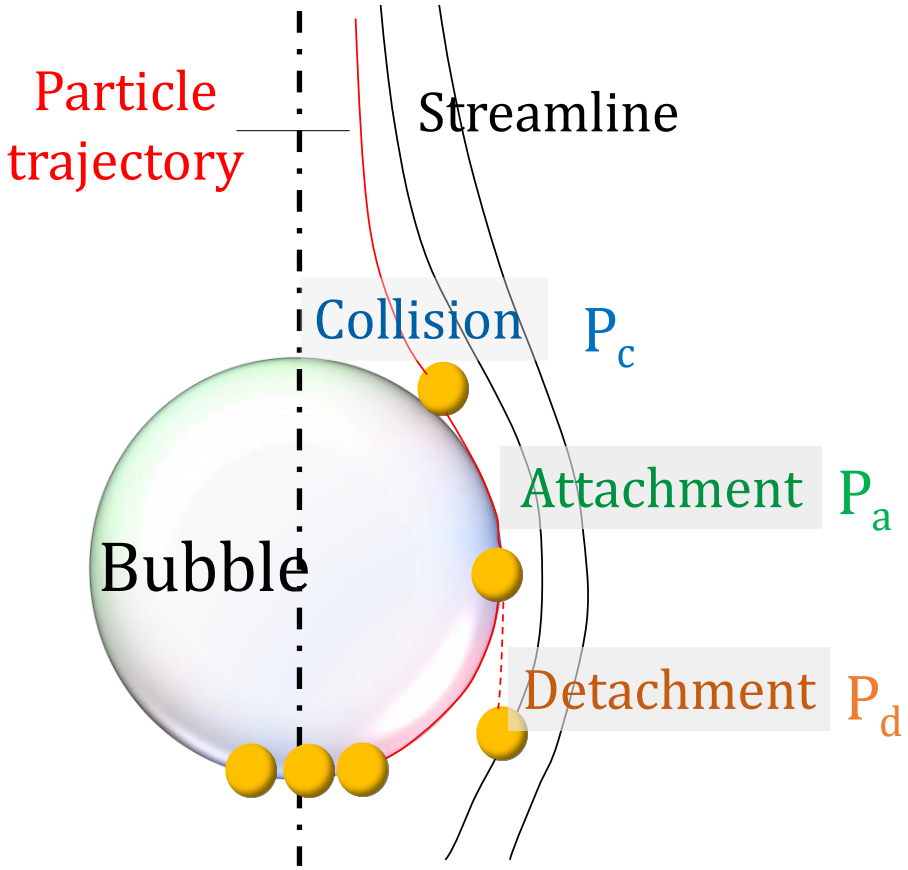


Fig. 2-4. Schematic representation of particle-bubble collision, attachment, and detachment. The thick lines represent particle trajectories whilst the thin lines represent the fluid streamlines (reprinted with permission from (Miettinen et al., 2010), copyright (2022) Elsevier).

## 2.3 Methods for copper recovery from tailings

### *2.3.1 Decreasing bubble size approach*

#### 2.3.1.1 Column flotation

Flotation circuits use multiple flotation cells in series to recover the maximum amount of desired minerals. Circuits consist of a set of cells called rougher, cleaner, and scavenger as illustrated in Fig. 2-5. Rougher flotation cells are usually mechanical-type and appear first in the circuit, to increase the recovery of the valuable minerals. To minimize valuable minerals loss from final tailings, tailings from rougher cells are fed to scavenger cells, and the froth from the rougher cells is reground to liberate the middlings. This product is then fed to the cleaner cells. For cleaner flotation, column-type flotation cells are frequently used that produce smaller bubbles than mechanical flotation units (Finch, 1995,

Rodrigues and Rubio, 2007). By using smaller bubbles, the collision efficiency of particles and bubbles increases, causing a higher copper recovery for fines in column flotation.

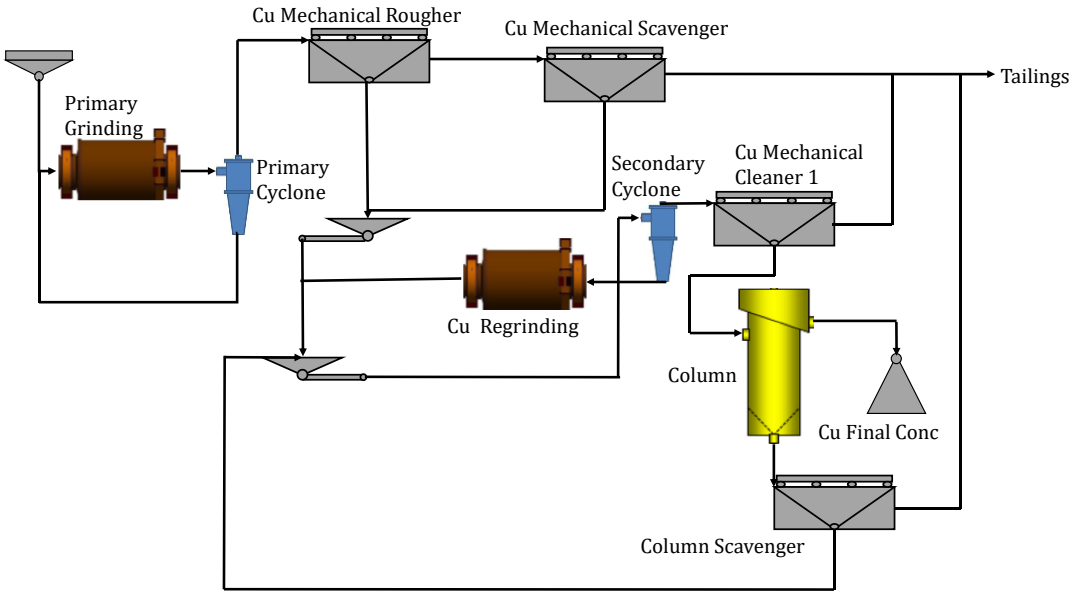


Fig. 2-5. A simplified flotation circuit.

The size of the air bubble in the column flotation cell depends strongly on the bubble generator/sparger. Different types of bubble generators/spargers are used in column flotation. Depending on the technique used to create the bubbles, there are three types of spargers. In one type, the air is pumped into a porous material, such as rubber or cloth, to produce bubbles. However, such spargers have durability issues (wear and tear), pore blockage by particles, and difficulties in consistently maintaining optimal bubble size. In the jetting type, air and water are forced through a small circular opening at high pressure (Finch, 1995, Fuerstenau et al., 2007). Lastly, the sparger type utilizes the shearing motion of a slurry-air mixture to generate fine bubbles after passing through a specially designed tube (Fuerstenau et al., 2007).

An in-line mixer bubble generator produced relatively large bubbles up to a diameter of 0.35 mm, according to laboratory studies (Patil et al., 2001). In a comparison of Microcel™ and jet-type spargers, it was found that the former produced smaller bubbles, thereby increasing the recovery (Pyecha et al., 2006). However, the mean diameter of bubbles produced by these two types of spargers (1–3 mm) is still relatively large. Considering this, according to Eq. (2.2), for particles having a size <10 μm, the ideal bubble size is <150 μm.

#### 2.3.1.2 Microbubble flotation

As already discussed in the above section, one of the possible ways to overcome the difficulties associated with fine-particle flotation is to reduce bubble size to a few micrometers. Microbubbles are defined as air bubbles with a diameter range of 1−100 μm (Vothy, 2020, Terasaka, 2014). To generate microbubbles several techniques are used, and these techniques are listed in Table 2-2. Due to microbubble stability problems in agitated flotation cells, microbubble flotation is primarily carried out in column-type flotation cells (Yoon, 1993). Laboratory experiments were performed using this technique to recover copper, zinc, and lead from a complex sulfide ore of <5 μm size (Vothy, 2020, Kusaka, 2014).

Even though microbubble flotation is promising, it has several drawbacks (Miettinen et al., 2010). When the bubbles are too small (<200 μm), their collision efficiency with fine particles is high, however, they will float too slowly due to their low buoyancy. On the other hand, if bubbles are large (>500 μm), they will float fast, however, they have low collision efficiency with fine particles (Farrokhpay et al., 2020). Due to the slow speed of the microbubbles rising with attached mineral particles, longer residence times are required in the flotation circuit. Furthermore, the microbubbles cause a higher water recovery, thereby increasing gangue mineral entrainment, which reduces the selectivity (Trahar and Warren, 1976, Liu and Wannas, 2004).

Table 2-2. Studies on the use of microbubbles in flotation.

| Name | Minerals studied | Process/effects | References |
|---|---|---|---|
| **Electro-flotation** | Chalcopyrite (<20 μm) | Bubble generation by electrolysis.<br>Improved recovery by electrolytic oxygen. | (Bhaskar Raju and Khangaonkar, 1982) |
| **Charged microbubble/ colloid gas aphrons (CGAs) microbubble** | CuO and $SiO_2$ (<10 μm) | The grade of CuO improved from 59 % to 82%.<br>Recovery of CuO improved from 58% to 77%. | (Waters et al., 2008) |
| **Microbubble flotation** | Pyrite ($FeS_2$), chalcopyrite ($CuFeS_2$), galena (PbS), and sphalerite (ZnS) | Microbubble flotation of ultrafine sulfide minerals. | (Kusaka, 2014) |
| **Microbubble flotation** | Galena (PbS) and sphalerite (ZnS) | Collector-less microbubble flotation using sodium hydrosulfide. | (Murao, 2014) |

| | | | |
|---|---|---|---|
| **Nano-microbubble** | Chalcopyrite fines (14–38 µm)<br>Ultrafine particles (5–14 µm) | Bubble size ($D_{90}$ = 100 µm) generated by hydrodynamic cavitation | (Ahmadi et al., 2014) |
| | | Improved recovery of fine and ultrafine particles (16–21%) | |

#### 2.3.1.3 Nanobubbles flotation

Flotation of fine particles can be enhanced by nanobubbles. Parker et al. were the first to propose nanobubbles to improve the flotation of fines (Parker et al., 1994). Nanobubbles (NBs), also called ultrafine bubbles, are gas cavities having a diameter of <1 µm (Uchida et al., 2011, Zimmerman et al., 2011, Wang et al., 2019). As shown in Fig. 2-6, Nanobubbles are adsorbed on fine mineral particles when they are pre-treated with them, they form nanobubble–particle aggregates; thus, increasing the apparent particle size and improving collision efficiency (Calgaroto et al., 2015, Azevedo et al., 2016, Zhou et al., 2020). In addition to enhancing the fine particle hydrophobicity and forming aggregates, NBs also act as secondary collectors (Fan et al., 2010a, Han et al., 2020, Atluri et al., 2019).

NBs are produced by different methods such as cavitation, gas oversaturation, and membrane module (Li and Zhang, 2022). Studies have shown that nanobubbles can significantly boost process efficiency by enhancing coarse bubble attachment onto adhered NBs and by aggregating the problematic fine particles (Sobhy and Tao, 2013, Calgaroto et al., 2015, Fan et al., 2010a, Fan et al., 2010b, Ahmadi et al., 2014). The NBs are considered to have significant potential in mineral processing due to the better recovery of ultrafine particles (Azevedo et al., 2019).

Flotation kinetics and recovery are reportedly higher for a fine fraction (−38 µm), while the grade and selectivity index tend to be higher for coarse size fraction (−150 µm) (Chipakwe et al., 2021b). With surfactants (collector and frother), nanobubbles may cause a decrease in grade, primarily due to increased entrainment (Chipakwe et al., 2021a, Chipakwe et al., 2021b). Nanobubbles should be used in the flotation stages (i.e., rougher, or cleaner) where recovery is of primary importance than the grade control. Optimizing the hydrodynamic conditions and surfactant types is required to reduce the amount of water recovery associated with NBs, which will reduce the entrainment rate (Chipakwe et al., 2021a).

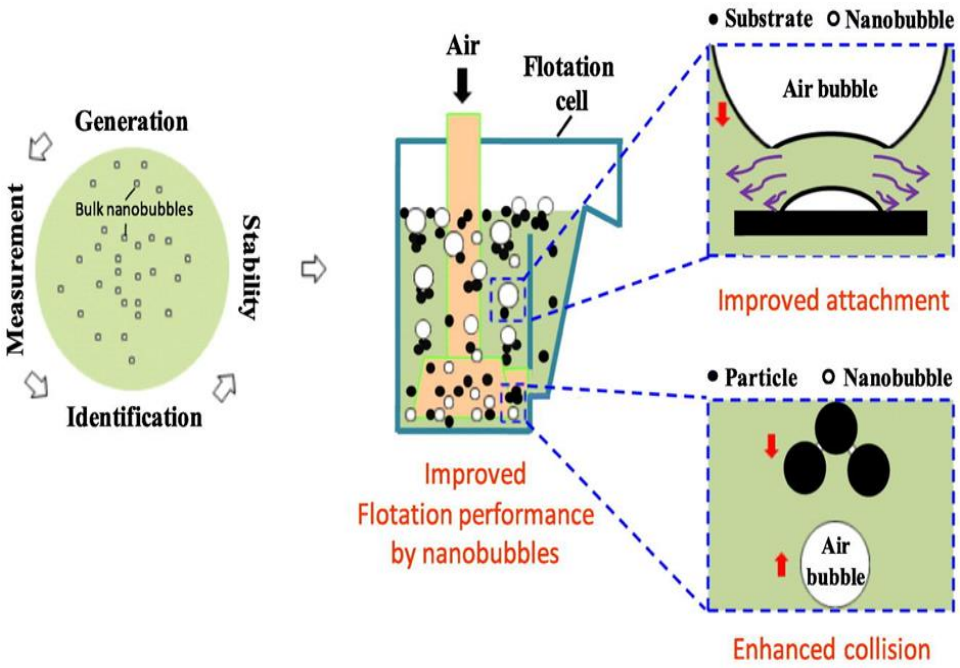


Fig. 2-6. Schematic mechanism of nanobubble flotation (reprinted with permission from Li et al. (Li and Zhang, 2022), copyright (2022) Elsevier).

*2.3.2 Increasing particle size approaches*

Theoretically and experimentally, it has been observed that the flotation rate elevates when the particle size is large (Sutherland, 1948, Trahar and Warren, 1976, Crawford and Ralston, 1988, Ralston and Dukhin, 1999, Duan et al., 2003, Pyke et al., 2003). As mentioned above, the agglomeration of fine mineral particles can be an effective method for improving collision efficiency between mineral particles and air bubbles during flotation. The recovery of fines by using this approach has been studied extensively, and several techniques have been developed. These techniques mainly include polymer flocculation, shear flocculation, oil agglomeration, and carrier flotation. Table 2-3 provides a brief overview of these techniques, and Fig. 2-7 presents a schematic diagram of the governing mechanisms.

Table 2-3. A brief description of different agglomeration techniques.

| Method | Reagents and Material | Types of Interaction |
|---|---|---|
| **Polymer flocculation** | Polymer, surfactant | Hydrophobic, chemical, hydroxyl functional group, electrostatic |
| **Shear flocculation** | Surfactant | Hydrophobic interaction |

| | | |
|---|---|---|
| **Oil agglomeration** | Oil, surfactant | Capillary forces |
| **Carrier flocculation** | Surfactant, Carrier material | Hetero coagulation, Hydrophobic interaction |

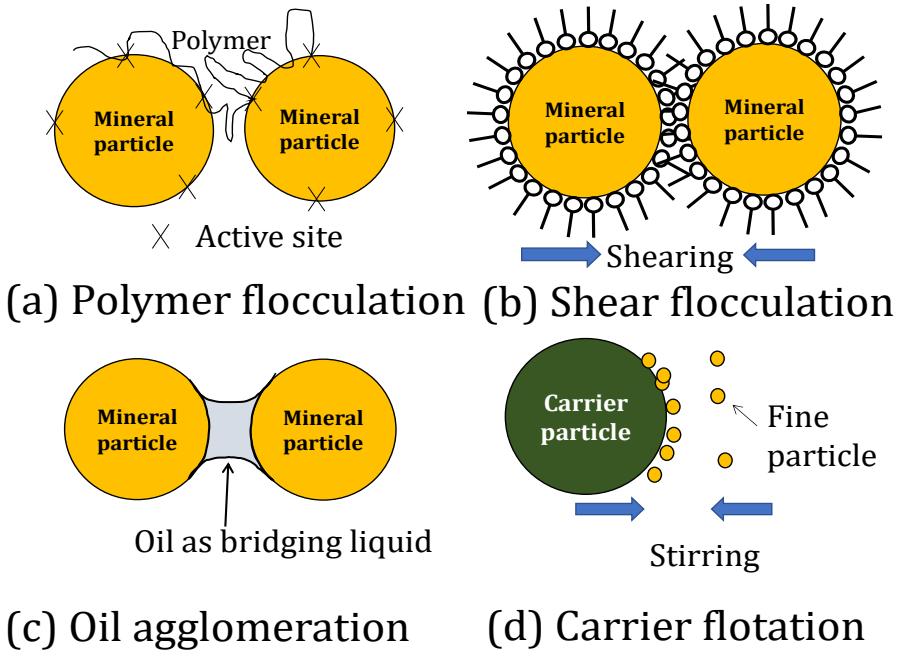


Fig. 2-7. Schematic representation of polymer flocculation, shear flocculation, oil agglomeration, and carrier flotation.

#### 2.3.2.1 Polymer Flocculation

In flocculation, organic polymers having a high molecular weight (>1 million) are used to form a molecular bridge between particles (Hogg, 2000, Pearse, 2003, Usher et al., 2009). A polymer induces flocculation of mineral particles by attaching itself to two or more particles consequently bridging the particles. If polymers are adsorbed on a specific mineral surface, selective flocculation occurs (Phiri et al., 2019, Wills and Finch, 2016). Selective flocculation is usually divided into feed preparation; selective adsorption of flocculant (polymers) on specific minerals; floc formation and conditioning. For separating flocs from dispersed particles, flotation or sedimentation can be used (Wills and Finch, 2016).

Usually, flocculation is possible with a small amount of flocculant. This is an advantage of the flocculation technique, in comparison with other techniques discussed below. Selective flocculation is, however, proven a challenging technique (Wills and Finch, 2016).

Cellulose-type compounds are typical flocculants and their effects on the flocculation of ground chalcopyrite, pyrite, and quartz were investigated using silylated cellulose nanofibers (SiCNF) (Zhou et al., 2021). The results showed that all minerals are flocculated in the presence of SiCNF, suggesting that cellulose-type compounds cannot be used for the selective flocculation of typical copper ores containing chalcopyrite, pyrite, and quartz. In another study (Mandre and Panigrahi, 1997), synthesized polymer xanthate was used as flocculant before flotation of complex sulfide ores, demonstrating a good recovery. However, the grade of the concentrate was very low, indicating that the flocculant was non-selective.

#### 2.3.2.2 Shear Flocculation

Shear flocculation is a technique to improve flotation kinetics. Mineral particles suspended in water have an electrical surface charge, and this causes a repulsive energy barrier between the homogeneously charged particles, suppressing their flocculation. In shear flocculation, kinetic energy is mechanically imparted to hydrophobic particles to make them collide together, in a mechanical mixing tank. High-intensity stirring of hydrophobic mineral particles overcomes the energy barrier causing repulsion due to homogeneously charged particles (Subrahmanyam and Forssberg, 1990, Bilgen and Wills, 1991, Patil et al., 2001). Warren initially proposed this technique (Bilgen and Wills, 1991), concluding that, subject to provision of sufficient kinetic energy to the system using agitation overcomes the energy barrier, forming flocs/aggregates of hydrophobic particles. Warren proposed that shear flocculation occurs in three steps: in the turbulent movement, the average collision energy is much higher than thermal energy that allows colloidal particles to approach each other; the formation of flocs/aggregates is preferred with the energy of "hydrophobic bond" in the event of a collision in direct contact between hydrophobic particles; likely, the resistance to the thinning and removal of the water layers separating the approaching particles is less in the case of hydrophobic particles than with colliding hydrophilic particles (Warren, 1975a).

The flotation of galena or sphalerite having a particle size less than 20 μm after shear flocculation has been reported (Song et al., 2001). Over 80% recovery was obtained for both galena and sphalerite when shear flocculation was applied. Due to selectivity issues and high energy demands, shear flocculation has not been frequently used despite its potential.

#### 2.3.2.3 Oil agglomeration

The oil agglomeration technique was developed in the early '20s for coal cleaning, modified, and improved many times since then (Mehrotra et al., 1983). This technique uses oil as a bridging liquid to aggregate minerals (Bensley et al., 1977, Wu et al., 2005, Hornn et al., 2020b, Hornn et al., 2020c, Hornn et al., 2020d). Kerosene, vegetable oil, and diesel oil are used as bridging liquids for agglomeration to increase apparent particle size leading to improved flotation of ultrafine particles (Jiangang et al., 2012). The capillary force of the bridging liquid between particles causes an attraction force between particles (Mehrotra et al., 1983). The application of this technique has been researched for the purification of coal (Mehrotra et al., 1983, Laskowski and Yu, 2000, Gray et al., 2001, Aktaş, 2002, Alonso et al., 2002, Cebeci and Sönmez, 2002, Cebeci and Sönmez, 2006, Sahinoglu and Uslu, 2008), recovery of gold (Moses and Petersen, 2000, Sen et al., 2005), molybdenite (Jiangang et al., 2012), and chalcopyrite (Hornn et al., 2020b, Hornn et al., 2020c, Hornn et al., 2020d).

Dosage and type of oil, hydrophobicity of minerals, and agitation strength are the key parameters for oil agglomeration (Aktaş, 2002, Alonso et al., 1999, Bos and Quast, 2000, Slaghuis and Ferreira, 1987, Wheelock et al., 1994). Oil is expensive and required in large amounts which need to be reduced to improve economic viability. This is a major disadvantage associated with oil agglomeration for industrial-scale operations (Bensley et al., 1977).

To reduce the amount of oil used in the agglomeration, the use of oil-water emulsions has been proposed (Bensley et al., 1977). Using emulsifiers decreases oil droplet size and increases the surface area (Sahinoglu and Uslu, 2013, van Netten et al., 2014, Zhang et al., 2021). In a recent study (Hornn et al., 2020a), emulsified oil agglomeration flotation was conducted on fine chalcopyrite/quartz mixture by varying different parameters, i.e., agitation strength, collector dosage, and amount of oil. Emulsified oil agglomeration flotation significantly improved copper (Cu) recovery from around 45% without agglomeration to over 80% with agglomeration as well as separation efficiency from around 30% without agglomeration to 70% with agglomeration.

It was observed that strong agitation strength is required to produce a large number of oil droplets, which is important to produce a larger agglomerate of mineral particles. However, this process consumes a lot of energy, making it expensive, and difficult to incorporate into flotation circuits. Later a new method was developed to overcome this problem by using emulsified oil stabilized by a surfactant to produce a stable oil-water

emulsion that does not require strong agitation strength (Hornn et al., 2020c) and this method can be easily integrated into the existing flotation circuits.

A major problem of oil agglomeration is the amount of oil and high agitation speed. This problem can be overcome when emulsified oil is used: small oil droplet becomes stable (Gao et al., 2022), and strong agitation is not needed. However, when the number of copper minerals becomes smaller, agglomerate size becomes small and the flotation rate is low. Therefore, it is difficult to use oil agglomeration for Cu recovery from tailings having a very minute amount of copper mineral particles.

#### 2.3.2.4 Carrier Flotation

Carrier flotation is a method to improve fine particle recovery in flotation. In this method, coarse carrier particles are added to the flotation cell and agitated together with fine mineral particles. The fine particles are then attached to the surface of coarse carrier particles and floated together.

The carrier flotation technique was initially developed to remove impurities from kaolin clay using coarse limestone as a seed or carrier (Ateşok et al., 2001). Normally, coarse particles are present in the ore, so adding extra coarse particles is not desirable in that case. If coarse particles are already present, they may act as a seed, introducing extra carrier particles may not work then (Ateşok et al., 2001, Warren, 1975b). When fine particles are attached to coarse particles (carrier or seed) of the same mineral, the process is termed autogenous carrier flotation (Valderrama and Rubio, 1998). Heterogenous carrier flotation uses coarse carrier particles different from target fine minerals. Autogenous carrier flotation was first carried out on wolframite (Hu et al., 1982) and later used for coal (Hu et al., 1988). With heterogeneous carrier flotation, numerous research works have been reported. Jorge Rubio and Heinz used polypropylene treated with oleic acid as a carrier for different minerals (Rubio and Hoberg, 1993).

Requirements for carrier flotation are the presence of coarse particles (carrier or seed); and hydrophobic coarse and fine particles (Subrahmanyam and Forssberg, 1990). The collision rate between fine and coarse particles is comparatively greater than fine and fine particles, also, fine particles attach well to the surface of coarse particles (Valderrama and Rubio, 1998, Dianzuo et al., 1988, Lange et al., 1997, Hu et al., 2003). The schematic mechanism of carrier flotation is presented in Fig. 2-8. It can be seen that when coarse carrier particles are agitated together with fine mineral particles, the fine particles are selectively attached to the surface of carrier particles.

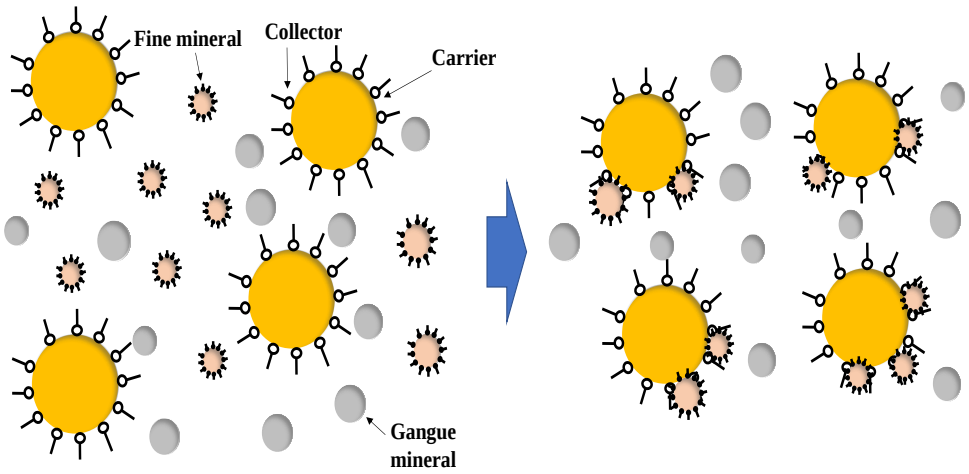

Fig. 2-8. Schematic mechanism of carrier flotation.

In carrier flotation, agitation time and intensity, pulp density, carrier particle size, coarse-fine particles ratio, and chemical factors such as pH, collector dosage, the extent of hydrophobicity, the surface charge of the particle, and geometry of the cell, are important variables, affecting the recovery of fines. Among these variables, the coarse-fine ratio may be the most important variable.

When the carrier (coarse particle) amount is increased, fine particle recovery is also increased (Lange et al., 1997). However, too large amounts of coarse particles are harmful. If the amount of coarse particles is too large, collision rates between coarse particles become high, which may cause detachment of already adhered fine particles (Subrahmanyam and Forssberg, 1990).

In a study by Li et al. (Li et al., 2017), interactions between coarse and fine hematite particles were studied. When the amount of coarse and fine hematite particles was equal, attachment of fines to coarse carrier particles was maximum, causing maximum flotation recovery of fines. However, In the case of copper sulfides, there is no literature available using the carrier flotation technique to recover fine copper sulfides.

As already discussed, considering tailings as future deposits, polymer flocculation, oil agglomeration, and shear flocculation are difficult to apply for copper recovery from tailings. This is mainly because of the low copper grade in tailings: floc/aggregate size depends on the number of copper minerals, and the size is limited when the amount of copper mineral is small.

Tailings consist primarily of gangue minerals with a minute amount of valuable/target minerals, so the above-mentioned methods are unlikely to efficiently recover fine minerals from tailings. On the other hand, in carrier flotation, aggregate size is mainly

dependent on the carrier size. This gives carrier flotation an advantage over other mentioned techniques (polymer flocculation, shear flocculation, and oil agglomeration) for recovering fine particles from tailings. However, the autogenous carrier flotation technique using coarse chalcopyrite as a carrier and heterogenous carrier flotation using a different carrier for fine chalcopyrite particles is not investigated.

This chapter was modified from **Bilal, M.;** Ito, M. ; Hornn, V. ; Hassan, F.U. ; Jeon, S. ; Park, I; Hiroyoshi, N. The Challenges and Prospects of Recovering Fine Copper Sulfides from Tailings Using Different Flotation Techniques: A Review. *Minerals* **2022**, *12*, 586.

**References**


2017. *Copper Drives Electric Vehicles* [Online]. CDA (Copper Development Association Inc.). Available: https://www.copper.org/publications/pub_list/pdf/A6191-ElectricVehicles-Factsheet.pdf [Accessed March 15, 2022 2022].

AHMADI, R., KHODADADI, D. A., ABDOLLAHY, M. & FAN, M. 2014. Nano-microbubble flotation of fine and ultrafine chalcopyrite particles. *International Journal of Mining Science and Technology,* 24**,** 559-566 DOI: https://doi.org/10.1016/j.ijmst.2014.05.021.

AIKAWA, K., ITO, M., KUSANO, A., PARK, I., OKI, T., TAKAHASHI, T., FURUYA, H. & HIROYOSHI, N. 2021. Flotation of Seafloor Massive Sulfide Ores: Combination of Surface Cleaning and Deactivation of Lead-Activated Sphalerite to Improve the Separation Efficiency of Chalcopyrite and Sphalerite. *Metals,* 11 DOI: https://doi.org/10.3390/met11020253.

AKTAŞ, Z. 2002. Some factors affecting spherical oil agglomeration performance of coal fines. *International Journal of Mineral Processing,* 65**,** 177-190 DOI: https://doi.org/10.1016/S0301-7516(01)00074-6.

ALONSO, M. I., VALDÉS, A. F., MARTíNEZ-TARAZONA, R. M. & GARCIA, A. B. 1999. Coal recovery from coal fines cleaning wastes by agglomeration with vegetable oils: effects of oil type and concentration. *Fuel,* 78**,** 753-759 DOI: https://doi.org/10.1016/S0016-2361(98)00218-X.

ALONSO, M. I., VALDÉS, A. F., MARTíNEZ-TARAZONA, R. M. & GARCIA, A. B. 2002. Coal recovery from fines cleaning wastes by agglomeration with colza oil: a contribution to the environment and energy preservation. *Fuel Processing Technology,* 75**,** 85-95 DOI: https://doi.org/10.1016/S0378-3820(01)00233-8.

ANTONIJEVIĆ, M. M., DIMITRIJEVIĆ, M. D., STEVANOVIĆ, Z. O., SERBULA, S. M. & BOGDANOVIC, G. D. 2008. Investigation of the possibility of copper recovery from the flotation tailings by acid leaching. *Journal of Hazardous Materials,* 158**,** 23-34 DOI: https://doi.org/10.1016/j.jhazmat.2008.01.063.

ASGHARI, M., NAKHAEI, F. & VANDGHORBANY, O. 2019. Copper recovery improvement in an industrial flotation circuit: A case study of Sarcheshmeh copper mine. *Energy Sources, Part A: Recovery, Utilization, and Environmental Effects,* 41**,** 761-778 DOI: https://doi.org/10.1080/15567036.2018.1520356.

ATEŞOK, G., BOYLU, F. & ÇELİK, M. S. 2001. Carrier flotation for desulfurization and deashing of difficult-to-float coals. *Minerals Engineering,* 14**,** 661-670 DOI: https://doi.org/10.1016/S0892-6875(01)00058-9.

ATLURI, V., GAO, Y., WANG, X., PAN, L. & MILLER, J. D. 2019. The Influence of Polysaccharides on Film Stability and Bubble Attachment at the Talc Surface. *Mining, Metallurgy & Exploration,* 36**,** 71-80 DOI: https://doi.org/10.1007/s42461-018-0028-4.

AZEVEDO, A., ETCHEPARE, R., CALGAROTO, S. & RUBIO, J. 2016. Aqueous dispersions of nanobubbles: Generation, properties and features. *Minerals Engineering,* 94**,** 29-37 DOI: https://doi.org/10.1016/j.mineng.2016.05.001.

AZEVEDO, A., OLIVEIRA, H. & RUBIO, J. 2019. Bulk nanobubbles in the mineral and environmental areas: Updating research and applications. *Advances in Colloid and Interface Science,* 271**,** 101992 DOI: https://doi.org/10.1016/j.cis.2019.101992.

BAGSTER, D. F. & MCILVENNY, J. D. 1985. Studies in the selective flocculation of hematite from gangue using high molecular weight polymers. Part 1: Chemical factors. *International Journal of Mineral Processing,* 14**,** 1-20 DOI: https://doi.org/10.1016/0301-7516(85)90010-9.

BENSLEY, C. N., SWANSON, A. R. & NICOL, S. K. 1977. The effect of emulsification on the selective agglomeration of fine coal. *International Journal of Mineral Processing,* 4**,** 173-184 DOI: https://doi.org/10.1016/0301-7516(77)90024-2.

BHASKAR RAJU, G. & KHANGAONKAR, P. R. 1982. Electro-flotation of chalcopyrite fines. *International Journal of Mineral Processing,* 9**,** 133-143 DOI: https://doi.org/10.1016/0301-7516(82)90022-9.

BILGEN, S. & WILLS, B. A. 1991. Shear flocculation — A review. *Minerals Engineering,* 4**,** 483-487 DOI: https://doi.org/10.1016/0892-6875(91)90148-O.

BOS, J. L. & QUAST, K. B. 2000. Effects of oils and lubricants on the flotation of copper sulphide minerals. *Minerals Engineering,* 13**,** 1623-1627 DOI: https://doi.org/10.1016/S0892-6875(00)00145-X.

BULATOVIC, S. M. 2007. 12 - Flotation of Copper Sulfide Ores. *In:* BULATOVIC, S. M. (ed.) *Handbook of Flotation Reagents.* Amsterdam: Elsevier DOI: https://doi.org/10.1016/B978-044453029-5/50021-6.

CALGAROTO, S., AZEVEDO, A. & RUBIO, J. 2015. Flotation of quartz particles assisted by nanobubbles. *International Journal of Mineral Processing,* 137**,** 64-70 DOI: https://doi.org/10.1016/j.minpro.2015.02.010.

CEBECI, Y. & SÖNMEZ, İ. 2002. The investigation of coal–pyrite/lignite concentration and their separation in the artificial mixture by oil agglomeration. *Fuel,* 81**,** 1139-1146 DOI: https://doi.org/10.1016/S0016-2361(02)00028-5.

CEBECI, Y. & SÖNMEZ, İ. 2006. Application of the Box-Wilson experimental design method for the spherical oil agglomeration of coal. *Fuel,* 85**,** 289-297 DOI: https://doi.org/10.1016/j.fuel.2005.07.017.

CHIPAKWE, V., JOLSTERÅ, R. & CHELGANI, S. C. 2021a. Nanobubble-Assisted Flotation of Apatite Tailings: Insights on Beneficiation Options. *ACS Omega,* 6**,** 13888-13894 DOI: https://doi.org/10.1021/acsomega.1c01551.

CHIPAKWE, V., SAND, A. & CHELGANI, S. C. 2021b. Nanobubble assisted flotation separation of complex Pb–Cu–Zn sulfide ore – Assessment of process readiness. *Separation Science and Technology***,** 1-8 DOI: https://doi.org/10.1080/01496395.2021.1981942.

CRAWFORD, R. & RALSTON, J. 1988. The influence of particle size and contact angle in mineral flotation. *International Journal of Mineral Processing,* 23**,** 1-24 DOI: https://doi.org/10.1016/0301-7516(88)90002-6.

DE F. GONTIJO, C., FORNASIERO, D. & RALSTON, J. 2007. The limits of fine and coarse particle flotation. *The Canadian Journal of Chemical Engineering,* 85**,** 739-747 DOI: https://doi.org/10.1002/cjce.5450850519.

DE LIMA, G. F., DE OLIVEIRA, C., DE ABREU, H. A. & DUARTE, H. A. 2011. Water Adsorption on the Reconstructed (001) Chalcopyrite Surfaces. *The Journal of Physical Chemistry C,* 115**,** 10709-10717 DOI: https://doi.org/10.1021/jp201106e.

DIANZUO, W., GUANZHOU, Q. & WEIBAI, H. 1988. The effect of carrier — promoting aggregation of coarse particles in fine particle flotation. *In:* PLUMPTON, A. J. (ed.) *Production and Processing of Fine Particles.* Amsterdam: Pergamon DOI: https://doi.org/10.1016/B978-0-08-036448-3.50037-2.

DUAN, J., FORNASIERO, D. & RALSTON, J. 2003. Calculation of the flotation rate constant of chalcopyrite particles in an ore. *International Journal of Mineral Processing,* 72**,** 227-237 DOI: https://doi.org/10.1016/S0301-7516(03)00101-7.

FAN, M., TAO, D., HONAKER, R. & LUO, Z. 2010a. Nanobubble generation and its applications in froth flotation (part II): fundamental study and theoretical analysis. *Mining Science and Technology (China),* 20**,** 159-177 DOI: https://doi.org/10.1016/S1674-5264(09)60179-4.

FAN, M., TAO, D., HONAKER, R. & LUO, Z. 2010b. Nanobubble generation and its applications in froth flotation (part III): specially designed laboratory scale column flotation of phosphate. *Mining Science and Technology (China),* 20**,** 317-338 DOI: https://doi.org/10.1016/S1674-5264(09)60205-2.

FARROKHPAY, S., FILIPPOVA, I., FILIPPOV, L., PICARRA, A., RULYOV, N. & FORNASIERO, D. 2020. Flotation of fine particles in the presence of combined microbubbles and conventional bubbles. *Minerals Engineering,* 155**,** 106439 DOI: https://doi.org/10.1016/j.mineng.2020.106439.

FINCH, J. A. 1995. Column flotation: A selected review— part IV: Novel flotation devices. *Minerals Engineering,* 8**,** 587-602 DOI: https://doi.org/10.1016/0892-6875(95)00023-J.

FUERSTENAU, M. C., JAMESON, G. J. & YOON, R.-H. 2007. *Froth flotation: a century of innovation*, SME.

GAO, J., BU, X., ZHOU, S., WANG, X., BILAL, M., HASSAN, F. U., HASSANZADEH, A., XIE, G. & CHELGANI, S. C. 2022. Pickering emulsion prepared by nano-silica particles – A comparative study for exploring the effect of various mechanical methods. *Ultrasonics Sonochemistry,* 83**,** 105928 DOI: https://doi.org/10.1016/j.ultsonch.2022.105928.

GRAY, M. L., CHAMPAGNE, K. J., SOONG, Y. & FINSETH, D. H. 2001. Parametric study of the column oil agglomeration of fly ash. *Fuel,* 80**,** 867-871 DOI: https://doi.org/10.1016/S0016-2361(00)00151-4.

HAN, B., ALTANSUKH, B., HAGA, K., STEVANOVIĆ, Z., JONOVIĆ, R., AVRAMOVIĆ, L., UROSEVIĆ, D., TAKASAKI, Y., MASUDA, N., ISHIYAMA, D. & SHIBAYAMA, A. 2018. Development of copper recovery process from flotation tailings by a combined method of high–pressure leaching–solvent extraction. *Journal of Hazardous Materials,* 352**,** 192-203 DOI: https://doi.org/10.1016/j.jhazmat.2018.03.014.

HAN, H., LIU, A. & WANG, H. 2020. Effect of Hydrodynamic Cavitation Assistance on Different Stages of Coal Flotation. *Minerals,* 10 DOI: https://doi.org/10.3390/min10030221.

HANSEN, H. K., YIANATOS, J. B. & OTTOSEN, L. M. 2005. Speciation and leachability of copper in mine tailings from porphyry copper mining: Influence of particle size. *Chemosphere,* 60**,** 1497-1503 DOI: https://doi.org/10.1016/j.chemosphere.2005.01.086.

HOGG, R. 2000. Flocculation and dewatering. *International Journal of Mineral Processing,* 58**,** 223-236 DOI: https://doi.org/10.1016/S0301-7516(99)00023-X.

HORNN, V., ITO, M., SHIMADA, H., TABELIN, B. C., JEON, S., PARK, I. & HIROYOSHI, N. 2020a. Agglomeration-Flotation of Finely Ground Chalcopyrite and Quartz: Effects of Agitation Strength during Agglomeration Using Emulsified Oil on Chalcopyrite. *Minerals,* 10 DOI: 10.3390/min10040380.

HORNN, V., ITO, M., SHIMADA, H., TABELIN, C. B., JEON, S., PARK, I. & HIROYOSHI, N. 2020b. Agglomeration-Flotation of Finely Ground Chalcopyrite and Quartz: Effects of Agitation Strength during Agglomeration Using Emulsified Oil on Chalcopyrite. *Minerals,* 10 DOI: https://doi.org/10.3390/min10040380.

HORNN, V., ITO, M., SHIMADA, H., TABELIN, C. B., JEON, S., PARK, I. & HIROYOSHI, N. 2020c. Agglomeration–Flotation of Finely Ground Chalcopyrite Using Emulsified Oil Stabilized by Emulsifiers: Implications for Porphyry Copper Ore Flotation. *Metals,* 10 DOI: https://doi.org/10.3390/met10070912.

HORNN, V., ITO, M., YAMAZAWA, R., SHIMADA, H., TABELIN, C. B., JEON, S., PARK, I. & HIROYOSHI, N. 2020d. Kinetic Analysis for Agglomeration-Flotation of Finely Ground Chalcopyrite: Comparison of First Order Kinetic Model and Experimental Results. *MATERIALS TRANSACTIONS,* 61**,** 1940-1948 DOI: https://doi.org/10.2320/matertrans.M-M2020843.

HU, W., WANG, D. & JIN, H. Flotation of Wolframite slime-practice and technological innovation. CIM BULLETIN, 1982. CANADIAN INST MINING METALLURGY PETROLEUM 101 6TH AVE SW, STE 320, CALGARY …, 78-78.

HU, W., WANG, D. & QU, G. Autogenous carrier flotation. Proceding of International mineral processing Congress, 1988. 445-452.

HU, Y., QIU, G. & MILLER, J. D. 2003. Hydrodynamic interactions between particles in aggregation and flotation. *International Journal of Mineral Processing,* 70**,** 157-170 DOI: https://doi.org/10.1016/S0301-7516(03)00023-1.

JAMESON, G. J. 2012. The effect of surface liberation and particle size on flotation rate constants. *Minerals Engineering,* 36-38**,** 132-137 DOI: https://doi.org/10.1016/j.mineng.2012.03.011.

JIANGANG, F., KAIDA, C., HUI, W., CHAO, G. & WEI, L. 2012. Recovering molybdenite from ultrafine waste tailings by oil agglomerate flotation. *Minerals Engineering,* 39**,** 133-139 DOI: https://doi.org/10.1016/j.mineng.2012.07.006.

KAPUR, A. & GRAEDEL, T. E. 2006. Copper Mines Above and Below the Ground. *Environmental Science & Technology,* 40**,** 3135-3141 DOI: https://doi.org/10.1021/es0626887.

KIRSTEN HUND, D. L. P., THAO P. FABREGAS, TIM LAING, JOHN DREXHAGE 2020. Minerals for Climate Action: The Mineral Intensity of the Clean Energy Transition. Washington, DC.

KUSAKA, E. 2014. Microbubble flotation of ultrafine divided sulfide mineral. *The mining and materials processing institute of Japan,* 1.

LANGE, A. G., SKINNER, W. M. & SMART, R. S. C. 1997. Fine: Coarse particle interactions and aggregation in sphalerite flotation. *Minerals Engineering,* 10**,** 681-693 DOI: https://doi.org/10.1016/S0892-6875(97)00048-4.

LASKOWSKI, J. S. & YU, Z. 2000. Oil agglomeration and its effect on beneficiation and filtration of low-rank/oxidized coals. *International Journal of Mineral Processing,* 58**,** 237-252 DOI: https://doi.org/10.1016/S0301-7516(99)90040-6.

LEISTNER, T., EMBRECHTS, M., LEIßNER, T., CHEHREH CHELGANI, S., OSBAHR, I., MÖCKEL, R., PEUKER, U. A. & RUDOLPH, M. 2016. A study of the reprocessing of fine and ultrafine cassiterite from gravity tailing residues by using various flotation techniques. *Minerals Engineering,* 96-97**,** 94-98 DOI: https://doi.org/10.1016/j.mineng.2016.06.020.

LEISTNER, T., PEUKER, U. A. & RUDOLPH, M. 2017. How gangue particle size can affect the recovery of ultrafine and fine particles during froth flotation. *Minerals Engineering,* 109**,** 1-9 DOI: https://doi.org/10.1016/j.mineng.2017.02.005.

LI, C. & ZHANG, H. 2022. A review of bulk nanobubbles and their roles in flotation of fine particles. *Powder Technology,* 395**,** 618-633 DOI: https://doi.org/10.1016/j.powtec.2021.10.004.

LI, D., YIN, W., LIU, Q., CAO, S., SUN, Q., ZHAO, C. & YAO, J. 2017. Interactions between fine and coarse hematite particles in aqueous suspension and their implications for flotation. *Minerals Engineering,* 114**,** 74-81 DOI: https://doi.org/10.1016/j.mineng.2017.09.012.

LIU, Q. & WANNAS, D. THE ROLE OF POLYMERIC-DEPRESSANT-INDUCED FLOCCULATION IN FINE PARTICLE FLOTATION, IN. 2004. PROCEEDINGS OF THE UBC MCGILL BIENNIAL INTERNATIONAL SYMPOSIUM ON ….

MANDRE, N. R. & PANIGRAHI, D. 1997. Studies on selective flocculation of complex sulphides using cellulose xanthate. *International Journal of Mineral Processing,* 50**,** 177-186 DOI: https://doi.org/10.1016/S0301-7516(97)00013-6.

MANKOSA, M. J., KOHMUENCH, J. N., CHRISTODOULOU, L. & LUTTRELL, G. H. Recovery of values from a porphory copper tailings stream. Proceedings, XXVIII International Mineral Processing Congress, September, 2016. 11-15.

MANKOSA, M. J., KOHMUENCH, J. N., CHRISTODOULOU, L. & YAN, E. S. 2018. Improving fine particle flotation using the StackCell™ (raising the tail of the elephant curve). *Minerals Engineering,* 121**,** 83-89 DOI: https://doi.org/10.1016/j.mineng.2018.03.012.

MEHROTRA, V. P., SASTRY, K. V. S. & MOREY, B. W. 1983. Review of oil agglomeration techniques for processing of fine coals. *International Journal of Mineral Processing,* 11**,** 175-201 DOI: https://doi.org/10.1016/0301-7516(83)90025-X.

MIETTINEN, T., RALSTON, J. & FORNASIERO, D. 2010. The limits of fine particle flotation. *Minerals Engineering,* 23**,** 420-437 DOI: https://doi.org/10.1016/j.mineng.2009.12.006.

MOSES, L. B. & PETERSEN, F. W. 2000. Flotation as a separation technique in the coal gold agglomeration process. *Minerals Engineering,* 13**,** 255-264 DOI: https://doi.org/10.1016/S0892-6875(00)00005-4.

MURAO, K. 2014. Fundamental study on the collectorless microbubble flotation using sodium hydrosulfide. *The mining and materials processing institute of Japan,* 1.

NGUYEN-VAN, A. 1994. The Collision between Fine Particles and Single Air Bubbles in Flotation. *Journal of Colloid and Interface Science,* 162**,** 123-128 DOI: https://doi.org/10.1006/jcis.1994.1016.

NGUYEN, A. & SCHULZE, H. J. 2003. *Colloidal science of flotation*, CRC Press.

OBER, J. A. 2018. Mineral commodity summaries 2018. *Mineral Commodity Summaries.* Reston, VA.

PARK, I. 2022. Advances in Selective Flotation and Leaching Process in Metallurgy. *Metals,* 12 DOI: https://doi.org/10.3390/met12010144.

PARK, I., HONG, S., JEON, S., ITO, M. & HIROYOSHI, N. 2020a. Flotation Separation of Chalcopyrite and Molybdenite Assisted by Microencapsulation Using Ferrous and Phosphate Ions: Part I. Selective Coating Formation. *Metals,* 10 DOI: https://doi.org/10.3390/met10121667.

PARK, I., HONG, S., JEON, S., ITO, M. & HIROYOSHI, N. 2020b. A Review of Recent Advances in Depression Techniques for Flotation Separation of Cu–Mo Sulfides in Porphyry Copper Deposits. *Metals,* 10 DOI: https://doi.org/10.3390/met10091269.

PARK, I., HONG, S., JEON, S., ITO, M. & HIROYOSHI, N. 2021a. Flotation Separation of Chalcopyrite and Molybdenite Assisted by Microencapsulation Using Ferrous and Phosphate Ions: Part II. Flotation. *Metals,* 11 DOI: https://doi.org/10.3390/met11030439.

PARK, I., KANAZAWA, Y., SATO, N., GALTCHANDMANI, P., JHA, M. K., TABELIN, C. B., JEON, S., ITO, M. & HIROYOSHI, N. 2021b. Beneficiation of Low-Grade Rare Earth Ore from Khalzan Buregtei Deposit (Mongolia) by Magnetic Separation. *Minerals,* 11 DOI: https://doi.org/10.3390/min11121432.

PARK, I., TABELIN, C. B., JEON, S., LI, X., SENO, K., ITO, M. & HIROYOSHI, N. 2019. A review of recent strategies for acid mine drainage prevention and mine tailings recycling. *Chemosphere,* 219**,** 588-606 DOI: https://doi.org/10.1016/j.chemosphere.2018.11.053.

PARKER, J. L., CLAESSON, P. M. & ATTARD, P. 1994. Bubbles, cavities, and the long-ranged attraction between hydrophobic surfaces. *The Journal of Physical Chemistry,* 98**,** 8468-8480 DOI: https://doi.org/10.1021/j100085a029.

PATIL, D. P., ANDREWS, J. R. G. & UHLHERR, P. H. T. 2001. Shear flocculation—kinetics of floc coalescence and breakage. *International Journal of Mineral Processing,* 61**,** 171-188 DOI: https://doi.org/10.1016/S0301-7516(00)00036-3.

PEARSE, M. J. 2003. Historical use and future development of chemicals for solid–liquid separation in the mineral processing industry. *Minerals Engineering,* 16**,** 103-108 DOI: https://doi.org/10.1016/S0892-6875(02)00288-1.

PHIRI, T., TEPA, C. & NYATI, R. 2019. Effect of Desliming on Flotation Response of Kansanshi Mixed Copper Ore %J Journal of Minerals and Materials Characterization and Engineering. Vol.07No.04**,** 20 DOI: https://doi.org/10.4236/jmmce.2019.74015.

PYECHA, J., LACOUTURE, B., SIMS, S., HOPE, G. & STRADLING, A. 2006. Evaluation of a MicrocelTM sparger in the Red Dog column flotation cells. *Minerals Engineering,* 19**,** 748-757 DOI: https://doi.org/10.1016/j.mineng.2005.09.044.

PYKE, B., FORNASIERO, D. & RALSTON, J. 2003. Bubble particle heterocoagulation under turbulent conditions. *Journal of Colloid and Interface Science,* 265**,** 141-151 DOI: https://doi.org/10.1016/S0021-9797(03)00345-X.

RALSTON, J. & DUKHIN, S. S. 1999. The interaction between particles and bubbles. *Colloids and Surfaces A: Physicochemical and Engineering Aspects,* 151**,** 3-14 DOI: https://doi.org/10.1016/S0927-7757(98)00642-6.

RODRIGUES, R. T. & RUBIO, J. 2007. DAF–dissolved air flotation: Potential applications in the mining and mineral processing industry. *International Journal of Mineral Processing,* 82**,** 1-13 DOI: https://doi.org/10.1016/j.minpro.2006.07.019.

RUBIO, J. & HOBERG, H. 1993. The process of separation of fine mineral particles by flotation with hydrophobic polymeric carrier. *International Journal of Mineral Processing,* 37**,** 109-122 DOI: https://doi.org/10.1016/0301-7516(93)90008-X.

SAHINOGLU, E. & USLU, T. 2008. Amenability of Muzret bituminous coal to oil agglomeration. *Energy Conversion and Management,* 49**,** 3684-3690 DOI: https://doi.org/10.1016/j.enconman.2008.06.026.

SAHINOGLU, E. & USLU, T. 2013. Use of ultrasonic emulsification in oil agglomeration for coal cleaning. *Fuel,* 113**,** 719-725 DOI: https://doi.org/10.1016/j.fuel.2013.06.046.

SCHLESINGER, M. E., KING, M. J., SOLE, K. C. & DAVENPORT, W. G. 2011a. Chapter 1 - Overview. *In:* SCHLESINGER, M. E., KING, M. J., SOLE, K. C. & DAVENPORT, W. G. (eds.) *Extractive Metallurgy of Copper (Fifth Edition).* Oxford: Elsevier DOI: https://doi.org/10.1016/B978-0-08-096789-9.10001-0.

SCHLESINGER, M. E., KING, M. J., SOLE, K. C. & DAVENPORT, W. G. 2011b. Chapter 2 - Production and Use. *In:* SCHLESINGER, M. E., KING, M. J., SOLE, K. C. & DAVENPORT, W. G. (eds.) *Extractive Metallurgy of Copper (Fifth Edition).* Oxford: Elsevier DOI: https://doi.org/10.1016/B978-0-08-096789-9.10002-2.

SCHLESINGER, M. E., KING, M. J., SOLE, K. C. & DAVENPORT, W. G. 2011c. Chapter 4 - Production of Cu Concentrate from Finely Ground Cu Ore. *In:* SCHLESINGER, M. E.,

KING, M. J., SOLE, K. C. & DAVENPORT, W. G. (eds.) *Extractive Metallurgy of Copper (Fifth Edition).* Oxford: Elsevier DOI: https://doi.org/10.1016/B978-0-08-096789-9.10004-6.

SCHUBERT, H. 2008. On the optimization of hydrodynamics in fine particle flotation. *Minerals Engineering,* 21**,** 930-936 DOI: https://doi.org/10.1016/j.mineng.2008.02.012.

SEN, S., SEYRANKAYA, A. & CILINGIR, Y. 2005. Coal–oil assisted flotation for the gold recovery. *Minerals Engineering,* 18**,** 1086-1092 DOI: https://doi.org/10.1016/j.mineng.2005.03.007.

SHERGOLD, H. 1984. Flotation in mineral processing. *The Scientific Basis of Flotation.* Springer DOI: https://doi.org/10.1007/978-94-009-6926-1_7.

SIVAMOHAN, R. 1990. The problem of recovering very fine particles in mineral processing — A review. *International Journal of Mineral Processing,* 28**,** 247-288 DOI: https://doi.org/10.1016/0301-7516(90)90046-2.

SLAGHUIS, J. H. & FERREIRA, L. C. 1987. Selective spherical agglomeration of coal: An amended mechanism of agglomerate formation and growth and its effect on product quality. *Fuel,* 66**,** 1427-1430 DOI: https://doi.org/10.1016/0016-2361(87)90191-8.

SOBHY, A. & TAO, D. 2013. Nanobubble column flotation of fine coal particles and associated fundamentals. *International Journal of Mineral Processing,* 124**,** 109-116 DOI: https://doi.org/10.1016/j.minpro.2013.04.016.

SONG, S., LOPEZ-VALDIVIESO, A., REYES-BAHENA, J. L. & LARA-VALENZUELA, C. 2001. Floc flotation of galena and sphalerite fines. *Minerals Engineering,* 14**,** 87-98 DOI: https://doi.org/10.1016/S0892-6875(00)00162-X.

SRIPRIYA, R., RAO, P. V. T. & CHOUDHURY, B. R. 2003. Optimisation of operating variables of fine coal flotation using a combination of modified flotation parameters and statistical techniques. *International Journal of Mineral Processing,* 68**,** 109-127 DOI: https://doi.org/10.1016/S0301-7516(02)00063-7.

SUBRAHMANYAM, T. V. & FORSSBERG, K. S. E. 1990. Fine particles processing: shear-flocculation and carrier flotation — a review. *International Journal of Mineral Processing,* 30**,** 265-286 DOI: https://doi.org/10.1016/0301-7516(90)90019-U.

SUPPES, R. & HEUSS-AßBICHLER, S. 2021. Resource potential of mine wastes: A conventional and sustainable perspective on a case study tailings mining project. *Journal of Cleaner Production,* 297**,** 126446 DOI: https://doi.org/10.1016/j.jclepro.2021.126446.

SUTHERLAND, K. L. 1948. Physical Chemistry of Flotation. XI. Kinetics of the Flotation Process. *The Journal of Physical and Colloid Chemistry,* 52**,** 394-425 DOI: https://doi.org/10.1021/j150458a013.

TABELIN, C. B., PARK, I., PHENGSAART, T., JEON, S., VILLACORTE-TABELIN, M., ALONZO, D., YOO, K., ITO, M. & HIROYOSHI, N. 2021. Copper and critical metals production from porphyry ores and E-wastes: A review of resource availability, processing/recycling challenges, socio-environmental aspects, and sustainability issues. *Resources, Conservation and Recycling,* 170**,** 105610 DOI: https://doi.org/10.1016/j.resconrec.2021.105610.

TABOSA, E. & RUBIO, J. 2010. Flotation of copper sulphides assisted by high intensity conditioning (HIC) and concentrate recirculation. *Minerals Engineering,* 23**,** 1198-1206 DOI: https://doi.org/10.1016/j.mineng.2010.08.004.

TERASAKA, K. 2014. Leading edge in fine bubble technology. *Journal of the Japan Institute of Energy,* 93**,** 1022-1024.

TORTORELLI, J. P., CRAVEN, J. W., TOGURI, J. M., DOBBY, G. S. & AGAR, G. E. 1997. The effect of external gas/slurry contact on the flotation of fine particles. *Minerals Engineering,* 10**,** 1127-1138 DOI: https://doi.org/10.1016/S0892-6875(97)00099-X.

TRAHAR, W. J. 1981. A rational interpretation of the role of particle size in flotation. *International Journal of Mineral Processing,* 8**,** 289-327 DOI: https://doi.org/10.1016/0301-7516(81)90019-3.

TRAHAR, W. J. & WARREN, L. J. 1976. The flotability of very fine particles — A review. *International Journal of Mineral Processing,* 3**,** 103-131 DOI: https://doi.org/10.1016/0301-7516(76)90029-6.

TRAN, T. Q., CHINNAPPAN, A., LEE, J. K., LOC, N. H., TRAN, L. T., WANG, G., KUMAR, V. V., JAYATHILAKA, W. A. D. M., JI, D., DODDAMANI, M. & RAMAKRISHNA, S. 2019. 3D Printing of Highly Pure Copper. *Metals,* 9 DOI: https://doi.org/10.3390/met9070756.

UCHIDA, T., OSHITA, S., OHMORI, M., TSUNO, T., SOEJIMA, K., SHINOZAKI, S., TAKE, Y. & MITSUDA, K. 2011. Transmission electron microscopic observations of nanobubbles and their capture of impurities in wastewater. *Nanoscale Research Letters,* 6**,** 295 DOI: https://doi.org/10.1186/1556-276X-6-295.

USHER, S. P., SPEHAR, R. & SCALES, P. J. 2009. Theoretical analysis of aggregate densification: Impact on thickener performance. *Chemical Engineering Journal,* 151**,** 202-208 DOI: https://doi.org/10.1016/j.cej.2009.02.027.

VALDERRAMA, L. & RUBIO, J. 1998. High intensity conditioning and the carrier flotation of gold fine particles. *International Journal of Mineral Processing,* 52**,** 273-285 DOI: https://doi.org/10.1016/S0301-7516(97)00068-9.

VAN NETTEN, K., MORENO-ATANASIO, R. & GALVIN, K. P. 2014. Fine Particle Beneficiation through Selective Agglomeration with an Emulsion Binder. *Industrial & Engineering Chemistry Research,* 53**,** 15747-15754 DOI: https://doi.org/10.1021/ie5027502.

VOTHY, H. 2020. *Development of Agglomeration-Flotation for Finely Ground Copper Sulfides.* 北海道大学.

WANG, Q., ZHAO, H., QI, N., QIN, Y., ZHANG, X. & LI, Y. 2019. Generation and Stability of Size-Adjustable Bulk Nanobubbles Based on Periodic Pressure Change. *Scientific Reports,* 9**,** 1118 DOI: https://doi.org/10.1038/s41598-018-38066-5.

WARREN, L. J. 1975a. Shear-flocculation of ultrafine scheelite in sodium oleate solutions. *Journal of Colloid and Interface Science,* 50**,** 307-318 DOI: https://doi.org/10.1016/0021-9797(75)90234-9.

WARREN, L. J. T. I. M. M., SECT. C. MIN. PROC. EXT. METALL. 1975b. Slime coating and shear flocculation in the scheelite-sodium oleate system. 84**,** 99-104.

WATERS, K. E., HADLER, K. & CILLIERS, J. J. 2008. The flotation of fine particles using charged microbubbles. *Minerals Engineering,* 21**,** 918-923 DOI: https://doi.org/10.1016/j.mineng.2008.04.011.

WHEELOCK, T. D., MILANA, G. & VETTOR, A. 1994. The role of air in oil agglomeration of coal at a moderate shear rate. *Fuel,* 73**,** 1103-1107 DOI: https://doi.org/10.1016/0016-2361(94)90245-3.

WILLS, B. A. & FINCH, J. A. 2016. Chapter 12 - Froth Flotation. *In:* WILLS, B. A. & FINCH, J. A. (eds.) *Wills' Mineral Processing Technology (Eighth Edition).* Boston: Butterworth-Heinemann DOI: https://doi.org/10.1016/B978-0-08-097053-0.00012-1.

WU, X. Q., MONHEMIUS, A. J. & GOCHIN, R. J. 2005. Quantitative assessment of hydrophobic agglomeration performance. *Minerals Engineering,* 18**,** 567-573 DOI: https://doi.org/10.1016/j.mineng.2004.09.005.

YOON, R. H. 1993. Microbubble flotation. *Minerals Engineering,* 6**,** 619-630 DOI: https://doi.org/10.1016/0892-6875(93)90116-5.

YOON, R. H. 2000. The role of hydrodynamic and surface forces in bubble–particle interaction. *International Journal of Mineral Processing,* 58**,** 129-143 DOI: https://doi.org/10.1016/S0301-7516(99)00071-X.

YUAN, X. M., PALSSON, B. I. & FORSSBERG, K. S. E. 1996. Statistical interpretation of flotation kinetics for a complex sulphide ore. *Minerals Engineering,* 9**,** 429-442 DOI: https://doi.org/10.1016/0892-6875(96)00028-3.

ZHANG, Q., NIU, C., BU, X., BILAL, M., NI, C. & PENG, Y. 2021. Enhancement of Flotation Performance of Oxidized Coal by the Mixture of Laurylamine Dipropylene Diamine and Kerosene. *Minerals,* 11 DOI: https://doi.org/10.3390/min11111271.

ZHOU, H., GENG, L., ZHANG, Y., YANG, Z., HE, K. & XIE, F. 2021. Selective flotation separation of chalcopyrite and sphalerite by thermal pretreatment under air

atmosphere. *Physicochemical Problems of Mineral Processing,* 57**,** 305-314 DOI: https://doi.org/10.37190/ppmp/131667.

ZHOU, S., WANG, X., BU, X., WANG, M., AN, B., SHAO, H., NI, C., PENG, Y. & XIE, G. 2020. A novel flotation technique combining carrier flotation and cavitation bubbles to enhance separation efficiency of ultra-fine particles. *Ultrasonics Sonochemistry,* 64**,** 105005 DOI: https://doi.org/10.1016/j.ultsonch.2020.105005.

ZIMMERMAN, W. B., TESAŘ, V. & BANDULASENA, H. C. H. 2011. Towards energy efficient nanobubble generation with fluidic oscillation. *Current Opinion in Colloid & Interface Science,* 16**,** 350-356 DOI: https://doi.org/10.1016/j.cocis.2011.01.010.

# CHAPTER 3: Autogenous carrier flotation using coarse chalcopyrite particles as carriers

## 3.1 Introduction

As discussed in the previous chapter, carrier flotation can be a suitable option to recover fine copper sulfide particles. In the case of the heterogenous carrier flotation technique, separation of fines and carrier is necessary after the flotation process. Using the same minerals as a carrier for fines (autogenous carrier flotation) will eliminate the post-separation step making the process simpler. Therefore, autogenous carrier flotation is preferred.

Even in the usual flotation process for copper minerals like chalcopyrite, the pulp contains both fine and coarse particles, and autogenous carrier flotation may occur to some extent automatically. However, the effect of coarse copper sulfide particles on the flotation behavior of fine copper sulfide particles is not documented so far, therefore no literature is available. To design an optimized autogenous carrier flotation process for fine copper sulfides, the effects of size and mass of carrier (coarse copper sulfides) on the recovery of fine copper sulfides must be investigated.

In this chapter, specially designed flotation experiments were conducted to study the autogenous carrier flotation for the recovery of finely ground chalcopyrite. Coarse chalcopyrite was used as the carrier and the effects of carrier size and amount on fine chalcopyrite recovery were investigated. To confirm the attachment of fines to coarse carrier particles, particle size analysis, and SEM observation were conducted. Moreover, to elucidate the mechanism, calculations were done based on the extended Derjaguin-Landau-Verwey-Overbeek (EDLVO) theory.

## 3.2 Materials and reagents

### *3.2.1 Materials*

Two samples (chalcopyrite and quartz) were used in this study. A chalcopyrite sample was acquired from Copper Queen Mine, Arizona USA, while the quartz sample (99% purity) was obtained from Wako Pure Chemical Industries Co., Ltd., Osaka, Japan. The chalcopyrite sample was characterized by X-ray fluorescence (XRF) (EDXL300, Rigaku Corporation, Tokyo, Japan) and X-ray powder diffraction (XRD, Multiplex, Rigaku Corporation, Tokyo, Japan), indicating that it is mainly composed of chalcopyrite (76%) with pyrite (3%) and silicate minerals (quartz and actinolite; 21%) as impurities.

*3.2.2 Reagents*

Potassium amyl xanthate (KAX, $C_5H_{11}OCSSK$) (Tokyo Chemical Industry Co., Ltd., Japan) and methyl isobutyl carbinol (MIBC, $C_6H_{14}O$) were purchased from Wako Pure Chemical Industries, Ltd., Japan, were used as collector and frother, respectively.

## 3.3 Methods

*3.3.1 Sample preparation*

Two size fraction ranges of chalcopyrite were selected as the carrier, i.e., –106+75 µm and –75+38 µm. The samples were crushed and ground by a jaw crusher (1023-A, Yoshida Manufacturing Co., Ltd, Sapporo, Japan) and disc mill (RS100, Retsch Inc., Haan, Germany) respectively. Screens sizes of 106 µm, 75 µm, and 38 µm were used, and –38 µm particles were further subjected to grinding to obtain a particle size of $D_{50}$ = 2.3 µm determined by Microtrac (MT3300SX, Nikkiso Co., Ltd., Tokyo, Japan). The quartz sample was subjected to crushing and grinding in the same manner as described above. The $D_{50}$ of the quartz sample was 3.6 µm. The particle size distribution of fine chalcopyrite and quartz used in this study is presented in Fig. 3-1.

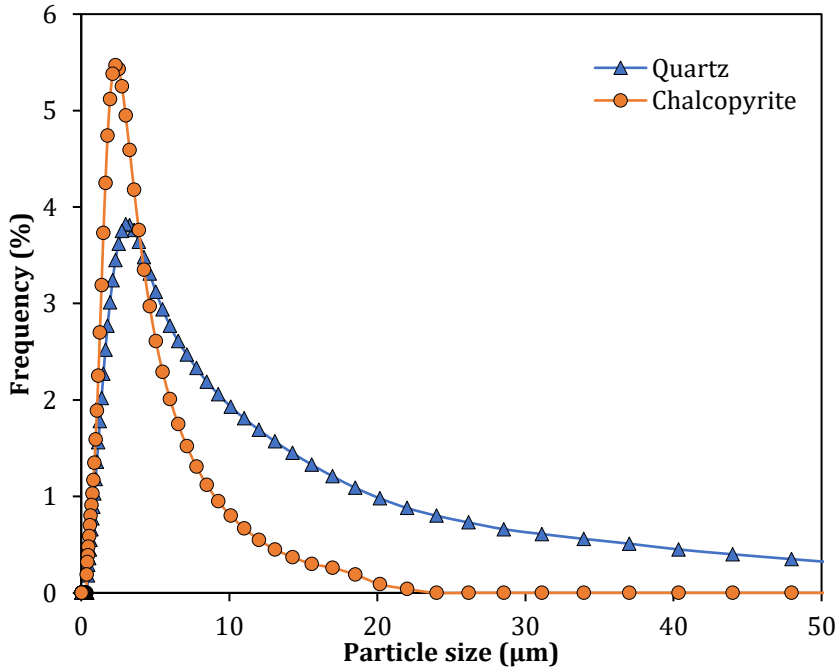


Fig. 3-1. Particle size distribution of quartz and chalcopyrite samples.

*3.3.2 Conventional flotation*

Single-stage flotation experiments were performed using an agitator-type flotation machine (FT-1000, Heiko, Japan) in a 0.5 L square flotation cell with an impeller speed of 1000 rpm and 1 L/min of airflow rate. The sample was ultrasonicated before conditioning with the collector and frother. The sample was conditioned with the collector (KAX) for 3

minutes and with frother (MIBC) for another 3 minutes before introducing air into the flotation chamber. Flotation concentrates were collected at intervals 1, 4, 7, and 10 min. Tailings and concentrates were dried at 105 °C for 24 hours and weighed. Representative samples were taken and were used for XRF analysis to determine the Cu recovery using the following equation:

$$R = \frac{Cc}{Ff} \times 100, \tag{3.1}$$

where $F$ and $C$ are the % weights of the feed and concentrate, respectively; and $f$ and $c$ are the assays of the feed and concentrate.

*3.3.3 Carrier flotation*

To perform carrier flotation, carrier particles of different size fractions were mixed with ultra-fine particles ($D_{50}$ = 2.3 µm). The carrier particles were mixed in different ratios to observe the effect of carrier particles on the flotation of fine particles. $SiO_2$ was also added to the mixture of coarse and fine chalcopyrite to observe the effect of the gangue mineral. The rest of the parameters were kept the same as mentioned above except the froth and tailings were immediately sieved (using 75 and 38 µm sieves) after collection and then kept in the oven to let the samples dry. The dried concentrates and tailings were subjected to XRF analysis to calculate Cu recovery.

*3.3.4 Particle size analysis*

The fine and coarse fractions were analyzed using Microtrac (Microtrac® MT3300SX, Nikkiso Co., Ltd., Tokyo, Japan). In the case of mixtures of carrier and fines, particle size distribution measurements were carried out after conditioning the mixture (before flotation) with the collector. The same sample (mixture of carrier and fines after conditioning with collector) was used for scanning electron microscopy analysis (SEM, JSM-IT200, JEOL Ltd., Tokyo, Japan).

## 3.4 Results and discussion

*3.4.1 Effects of particle size on flotation behavior*

In flotation, fine particles do not collide with air bubbles hence the low recovery of fines to froth. Fig. 3-2 shows the experimental results of flotation vs model calculation results for fine chalcopyrite ($D_{50}$ = 2.3 µm) and coarse chalcopyrite (size: –106+75 µm). The results show that recovery of fine chalcopyrite was much lower than that of coarse chalcopyrite, i.e., around 27% for fines and around 96% for coarse particles after 10 min flotation.

To confirm that the low recovery of fine chalcopyrite is due to the low collision probability of fine particles and an air bubble, the experimental results were compared with a first-order kinetic model assuming that flotation efficiency is mainly dependent on particle-bubble collision probability ($P_c$) and is given by the following equation (Yoon, 2000, Hornn et al., 2020):

$$P_c = \left[\frac{3}{2} + \frac{4Re_b{}^{0.72}}{15}\right]\left(\frac{D_p}{D_b}\right)^2, \quad 3.2$$

where $Re_b$ is Reynold number of the air bubbles, while $D_p$ and $D_b$ are diameters of particle and air bubble respectively. Eq. (3.3) shows the recovery $R$ using a first-order kinetic equation developed by (Hornn et al., 2020):

$$R = \Sigma\eta_i \, R_i = \Sigma\eta_i\left(1 - e^{-kit}\right) \quad 3.3$$

where $R_i$ is the recovery of target particles having a size distribution $\eta_i$, and $k_i$ is the kinetic constant, calculated as (Hornn et al., 2020):

$$k_i = n_b \times \frac{\pi}{4}\left(D_b + D_{pi}\right)^2 (v_b + v_i) \times P_{ci} \quad 3.4$$

The nomenclature used in the above equation is as follows:

$n_b$: Number of bubbles

$D_{pi}$: Diameter of particle

$D_b$: Diameter of bubble

$v_b$: Bubble rising velocity

$v_i$: Particle settling velocity

Overall, in this model calculation, collision probability determined by particle size is the only parameter to determine the flotation recovery. This model assumes that the attachment probability of a particle to an air bubble is 1, and the detachment probability of a particle from an air bubble is 0. These assumptions are true for hydrophobic particles.

The calculated results are shown in Fig. 3-2 with solid lines. The calculated results fit well with the experimental results for both fine and coarse chalcopyrite. As collision probability is the only parameter to determine the flotation recovery in the model

calculation, the match between model and experimental results confirms that low collision probability for fine particles with air bubbles is the major cause of the low recovery of fine particles in the flotation experiments.

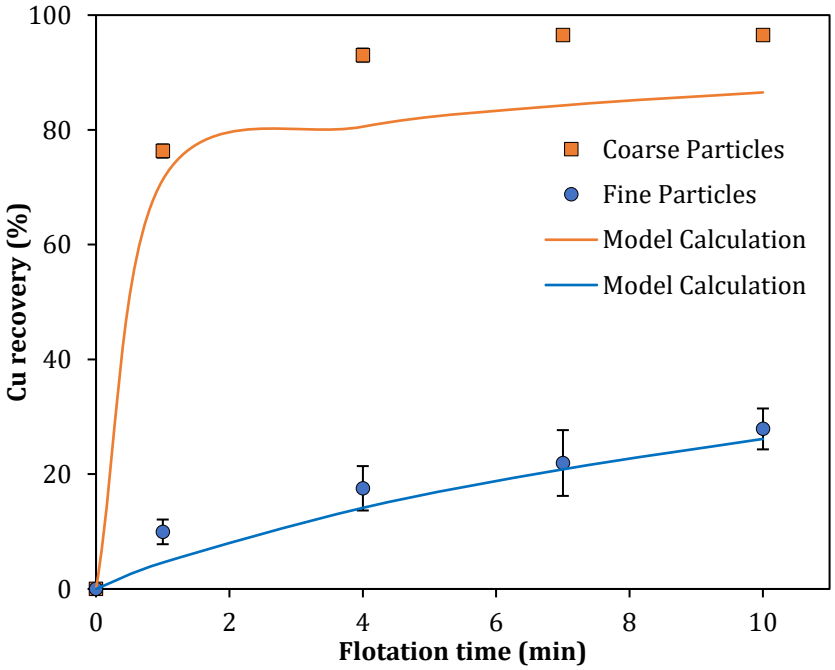


Fig. 3-2. Effects of particle size on flotation recovery (experimental results and model calculation), Test conditions: [KAX] = 200 g/t; [MIBC] = 25 µL/L; [Fine particle] = $D_{50}$ = 2.3 µm; [Coarse particles size] = –106+75 µm.

*3.4.2 Attachment of fine particles to the carrier*

When fine particles are attached to the surface of coarse particles in the mixture of fine and coarse particles, the particle size distribution of the mixture is not the same as the simple sum of the distributions of fine and coarse particles. Particle size distribution for 10 g fine particles, 10 g coarse particles, and the mixture of 10 g fine and 10 g coarse particles suspended in a 400 mL- flotation cell after conditioning with KAX were analyzed using Microtrac and SEM-EDX. Fig. 3-3 shows the particle size distribution (volumetric frequency vs. particle diameter) of fine and coarse particles suspended in water. The peaks of the curves are observed at 3.5 µm for fine particles and 57 µm for coarse particles. The solid line in Fig. 3-4 shows the measured frequency of the mixture of fine and coarse particles. For comparison, a calculated size distribution curve, $\eta_{cal}$, obtained through Eq. (3.5) assuming negligible attachment of fine particles on coarse particles, for the mixture, was also plotted as a dotted line in Fig. 3-4.

$$\eta_{cal} = (\eta_{fine} + \eta_{coarse})/2\,, \qquad 3.5$$

where $\eta_{fine}$ and $\eta_{coarse}$ are volumetric frequencies of fine and coarse particles shown in Fig. 3-3.

As shown in Fig. 3-4, the comparison of the measured result (solid lines) with the calculated results (dotted line) shows the measured frequencies were smaller at the peak position of fine particles (3.5 μm) and larger at the peak for coarse (57 μm). This suggests that fine chalcopyrite particles were attached to the surface of coarse chalcopyrite particles before flotation when they were agitated together in the flotation cell after conditioning with KAX. The SEM microphotograph (Fig. 3-5) for the mixture of fine and coarse particles also confirmed that the fine particles were attached to the surface of coarse particles.

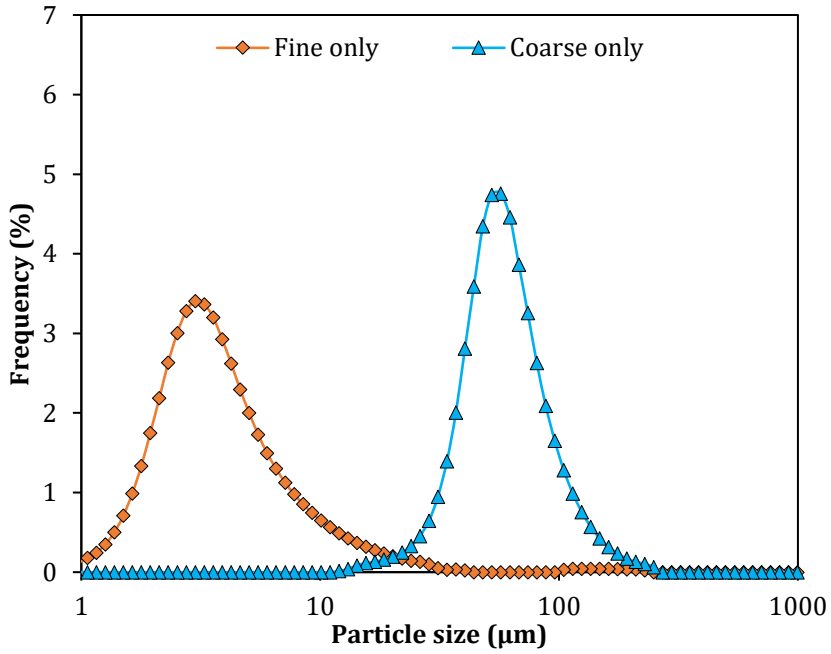


Fig. 3-3. Particle size distribution of coarse or fine chalcopyrite after conditioning with the collector.

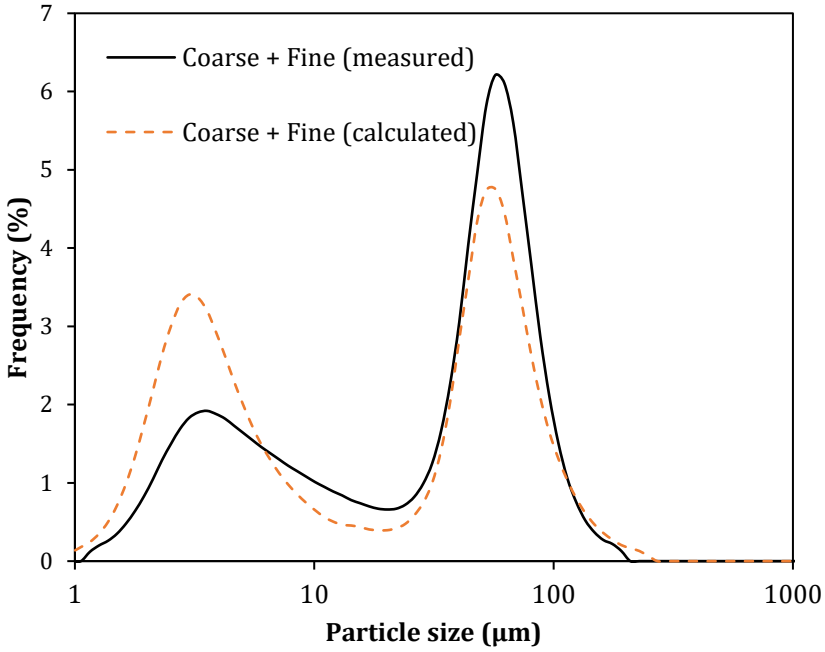


Fig. 3-4. Particle size distribution of the mixture of coarse and fine chalcopyrite after conditioning with the collector (measured vs calculated).

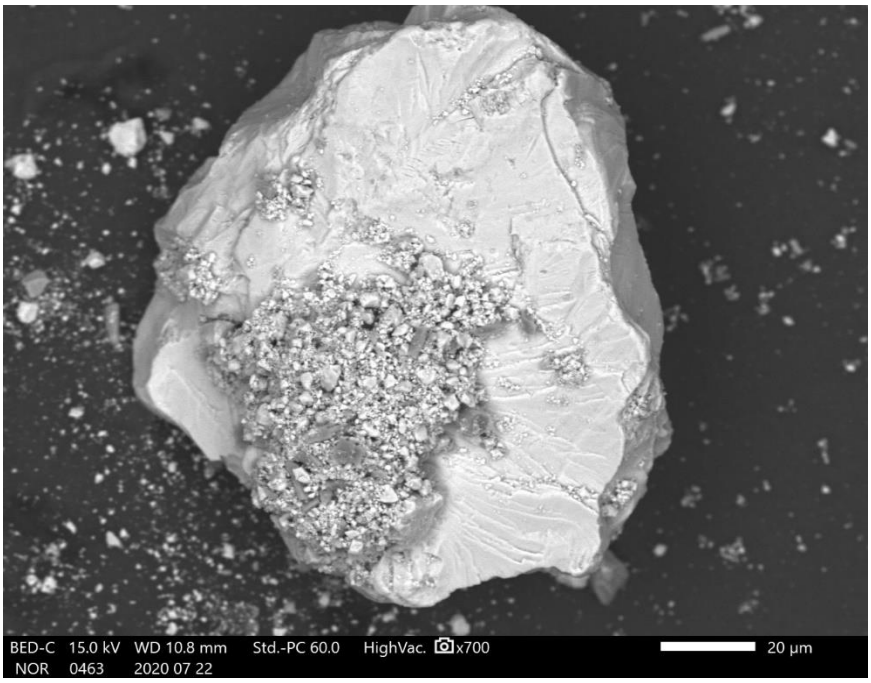


Fig. 3-5. SEM image of the mixture of fine and coarse chalcopyrite after conditioning with the collector in the flotation cell.

To identify the forces causing the attachment of fine chalcopyrite to coarse chalcopyrite (carrier), the theoretical calculation was done. According to the extended Derjaguin-Landau-Verwey-Overbeek (EDLVO) theory, van der Waals interaction and hydrophobic interaction act as attractive forces between two hydrophobic particles of the same mineral suspended in aqueous solutions, and electrostatic interaction acts as a repulsive

force between them. Fig. 3-6, 7, and 8 show the calculated values of potential energy for electrostatic, van der Waals, and hydrophobic interactions as a function of the separation distance between two individual particles. The van der Waals interaction energy ($V_W$) is calculated according to the following equation:

$$V_W = -\left(\frac{AR_fR_c}{6H(R_f + R_c)}\right), \quad 3.6$$

where $H$ represents the distance between two spherical particles, $R_f$ and $R_c$ represent the radius of fine and coarse particles, and $A$ is the Hamaker constant, calculated by:

$$A = \left(\sqrt{A_{11}} - \sqrt{A_{22}}\right)^2, \quad 3.7$$

where, $A_{11}$and $A_{22}$ are Hamaker constants for chalcopyrite ($3.25 \times 10^{-20}$ J) and water ($4.0 \times 10^{-20}$J), respectively (Li et al., 2018, Lu et al., 2015).

Electrostatic interactions ( $V_E$) between coarse-fine and fine-fine chalcopyrite is calculated according to the following equation:

$$V_E = 4\pi\varepsilon_0\varepsilon_r \frac{RfRc}{R1 + R2}\psi^2 ln\,[1 + exp(-\mathcal{K}H)] \quad 3.8$$

$\mathcal{K}$ is Debye constant and is calculated by

$$\mathcal{K} = \left(\frac{2e^2N_Acz^2}{\varepsilon_0\varepsilon_r kT}\right)^{1/2} \quad 3.9$$

The nomenclature used in Eqs. (3.8) and (3.9) are as follows:

$\varepsilon_0$: permittivity of vacuum ($8.854 \times 10^{-12}$ F m $^{-1}$)

$\varepsilon_r$: relative permittivity for water ($\varepsilon_r = 81$)

$\psi$: zeta potential of chalcopyrite particles

$e$: electronic charge ($1.602 \times 10^{-19}$ C)

$N_A$: Avogadro number ($6.023 \times 10^{23}$ mol$^{-1}$)

$c$: concentration (mol m$^{-3}$)

$z$: valence of the ion

$k$: Boltzmann constant ($1.381 \times 10^{-23}$ J)

$T$: temperature (K)

Hydrophobic interaction ($V_H$) is calculated by the following equation (Hu and Dai, 2003, Yao et al., 2016):

$$V_H = 2\pi \frac{R_f Rc}{R1 + R2} \, ho V_H^0 \, exp\left(\frac{Ho - H}{ho}\right), \tag{3.10}$$

where $Ho$ and $ho$ are the minimum equilibrium distance between the particles and decay length, respectively. In the calculation, $Ho$ and $ho$ were assumed to be 0.2 nm and 1 nm, respectively (Yao et al., 2016, Li et al., 2017). The value of $V_H^0$ is calculated using the following equation:

$$V_H^0 = -4\left(\sqrt{\gamma_L^+ \gamma_L^-} - \sqrt{\gamma_L^+ \gamma_S^-}\right), \tag{3.11}$$

where $\gamma^+$ and $\gamma^-$ represent surface energy values, and subscript S and L represent solid and liquid. In the calculation, reported values of the surface energies for water and chalcopyrite, listed in Table 3-1, were used.

Table 3-1. Surface energy values of water and chalcopyrite (Vilinska and Rao, 2009, Yao et al., 2016).

| $\gamma_L^+$ (mJ m$^{-2}$) | $\gamma_L^-$ (mJ m$^{-2}$) | $\gamma_S^-$ (mJ m$^{-2}$) |
|---|---|---|
| 25.5 | 25.5 | 6.34 |

Based on Eqs. (3.6), (3.8), and (3.10), van der Waals, electrostatic and hydrophobic interaction energies between coarse-fine particles and fine-fine particles are calculated, and the results are shown in Fig. 3-6, Fig. 3-7, and Fig. 3-8 respectively. As shown in Fig. 3-8, as compared to electrostatic and van der Waals interactions (Fig. 3-6 and Fig. 3-7), the potential energy of hydrophobic interaction is much larger, indicating that hydrophobic interaction is the dominant factor causing the attachment of particles.

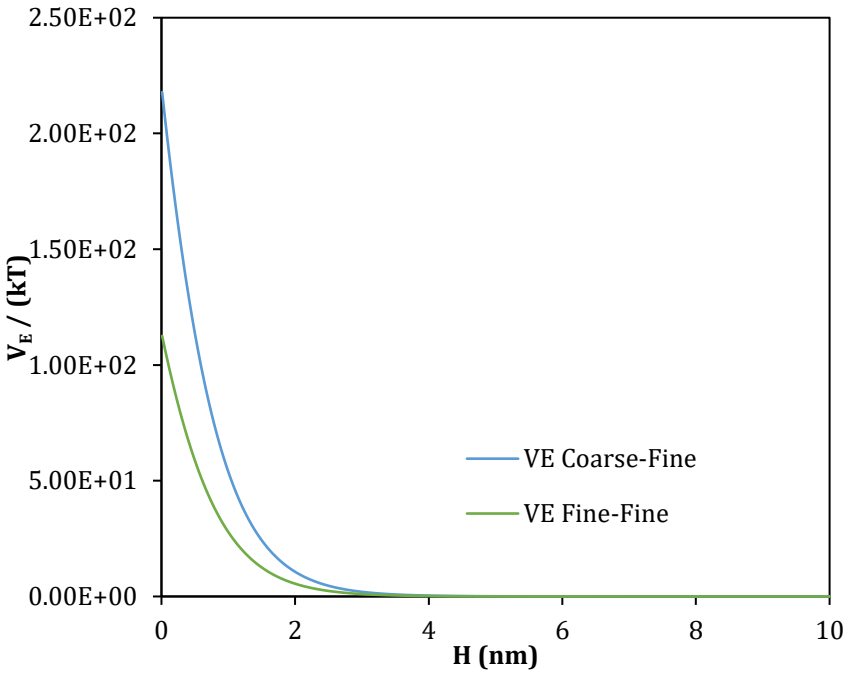


Fig. 3-6. Electrostatic interactions ($V_E$) between particles.

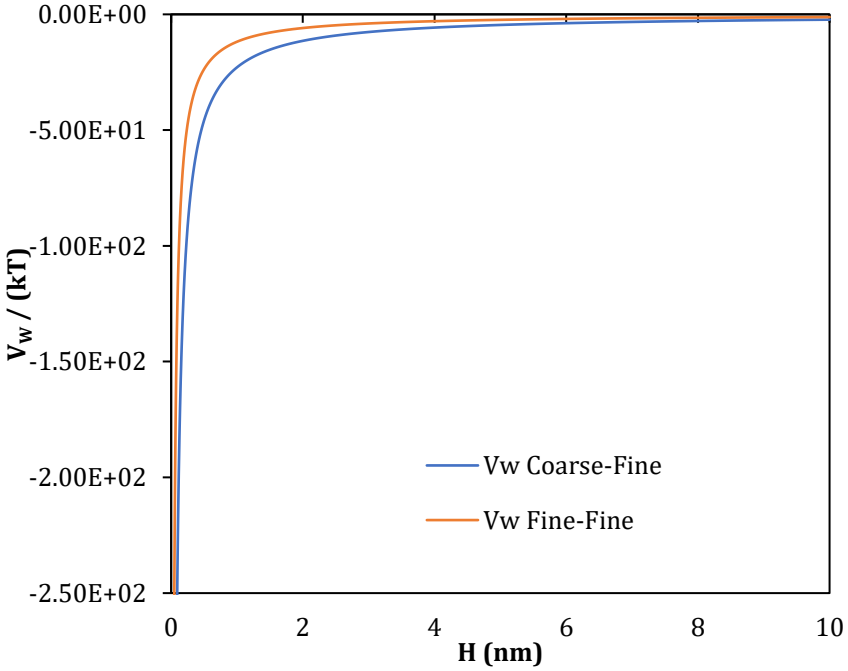


Fig. 3-7. van der Waals interactions ($V_W$) between particles.

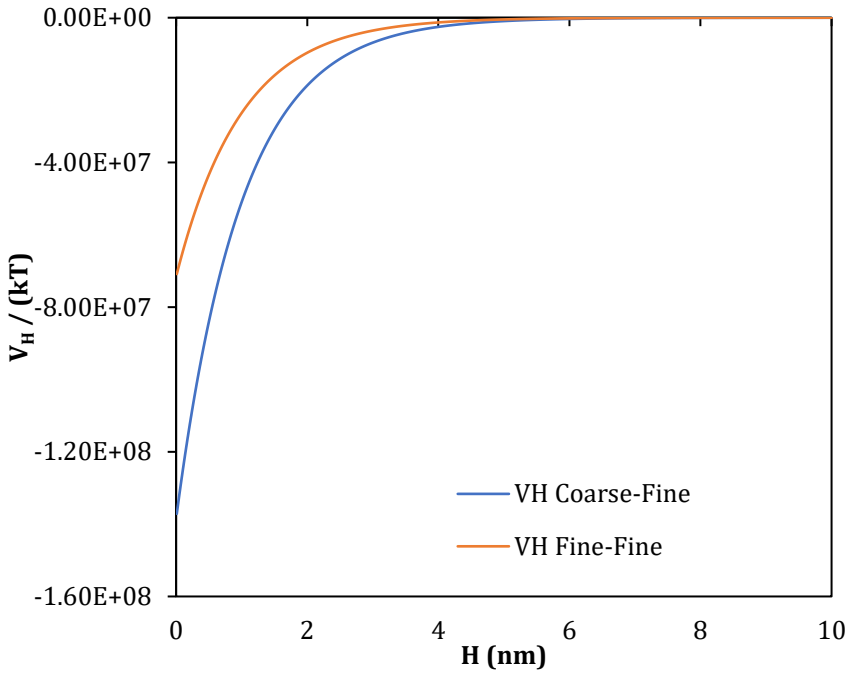

Fig. 3-8. Hydrophobic interactions ($V_H$) between particles.

Fig. 3-8 shows that the hydrophobic interaction between coarse and fine particles is greater than that for fine-fine particles: at a distance of 2 nm, $V_H$ is $-1\times10^7$ for fine-fine particles and $-2\times10^7$ for coarse-fine particles. Although the values of $V_H$ for coarse-fine particles were larger than that for fine-fine particles, the difference was not so significant: the values for fine-fine particles were about half of that for coarse-fine particles. This suggests that the attraction between coarse and fine particles is stronger than between fine-fine particles and this may cause enhanced attachment between fine and coarse particles, but the possibility of fine-fine attachment cannot be ruled out. This is in line with the SEM-EDX result, which shows aggregates of fine particles attached to coarse particles.

*3.4.3 Effects of carrier addition on flotation behavior of fines*

Fig. 3-9 shows the recovery of fine particles with and without 10 g carrier (–106+75 μm) as a function of time. The recovery of fine chalcopyrite increased significantly when coarse particles were introduced. These coarse particles acting as a carrier enhanced the recovery of the fine particles attached to their surface. Overall, the recovery after 10 minutes of flotation increased from 27% without a carrier to 65% with 10 g of coarse chalcopyrite as a carrier.

The effects of fines on the recovery of coarse particles were also investigated. Fig. 3-10 shows the recovery of coarse particles (–106+75 μm) to the froth in the flotation experiments with and without fine chalcopyrite. The recovery of coarse chalcopyrite in

the froth decreased with fines, but this suppressive effect was not so significant: recovery at 10 minutes of flotation was 96% without fines and 91% with fines. In both cases, the recovery of coarse chalcopyrite was over 90%.

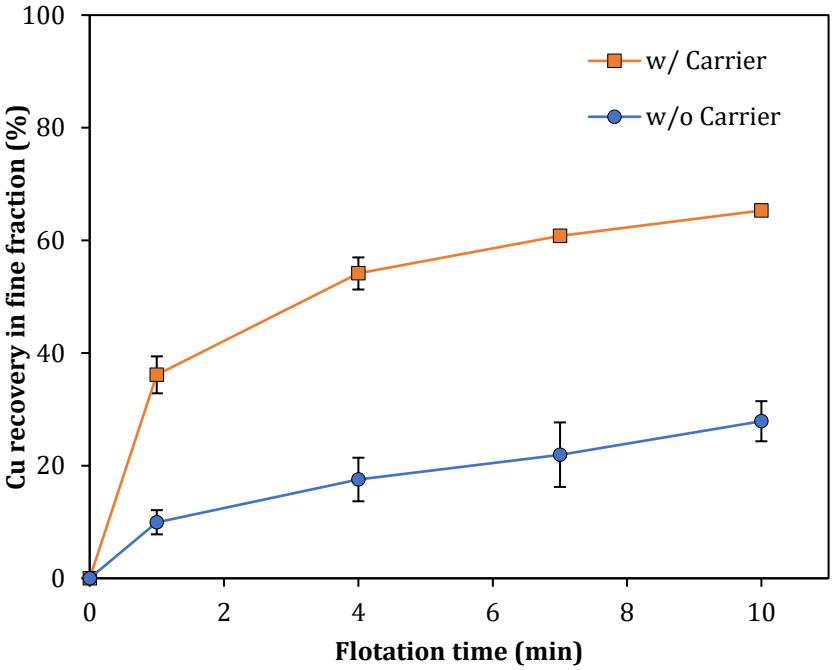


Fig. 3-9. Cu Recovery% of fines, Test conditions: [KAX] = 200 g/t of fines; [MIBC] = 25 µL/L; [Carrier size] = –106+75 µm; [Carrier amount] = 10 g.

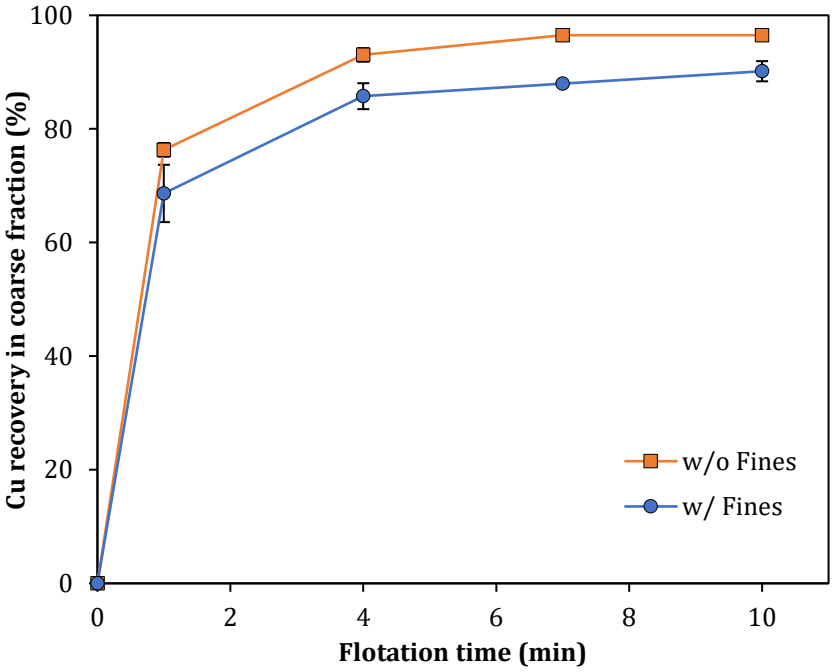


Fig. 3-10. Effect of fines on recovery of coarse particles, Test conditions: [KAX] = 200 g/t of fines; [MIBC] = 25 µL/L; [Carrier Size] = –106+75 µm.

*3.4.4 Effects of carrier amount and size*

To investigate the effects of carrier size and amount, flotation experiments for fine chalcopyrite were conducted with varying amounts of the carriers of two different size fractions, i.e., –106+75 µm and –75+38 µm chalcopyrite. Fig. 3-11 and Fig. 3-12 show the recovery of fine chalcopyrite and total Cu recovery to the froth respectively, after 10 min of flotation experiments as a function of carrier amount. The recovery of fines increased with increasing carrier amount, however, there was no significant effect of carrier size on the recovery of fines. Regardless of the carrier size, the recovery of the fines increased from 25% without a carrier to more than 75% with the maximum amount of carrier (20 g). Similarly, total Cu recovery was around 85% using a 20 g carrier.

In carrier flotation, fines are attached to the carrier (coarse particles) and the fine-loaded carrier is recovered into the froth. Considering this, the loading amount of fines on the carrier is the main factor to determine the recovery of fines to the froth in carrier flotation. The loaded amount of fine particles on the carrier (coarse particles) depends on the collision of coarse-fine particles and the detachment of fines from fine/coarse aggregate. If the agitation strength which causes the detachment is weaker than the attraction forces (hydrophobic interaction) between fines and coarse, the detachment effect can be ignored, and the collision becomes the major factor to determine the loaded amount of fines on the carrier (coarse) particles.

Under turbulent conditions, the collision frequency between fine and coarse (carrier) particles, $f_c$ $[s^{-1}m^{-3}]$ is expressed as:

$$f_c \propto \left(D_f + D_c\right)^3 n_f n_c \qquad 3.12$$

where, $D_f$ and $D_c$ are diameters of fine and coarse (carrier) particles, and $n_f$ and $n_c$ are number concentrations of fine and coarse particles in the suspension, respectively (Levich, 1962, Hu et al., 2003). If $D_f << D_c$, which is in this case, then the above expression can be written as follows:

$$f_c \propto {D_c}^3 n_f n_c \qquad 3.13$$

The concentration of coarse particles, $n_c$, is expressed by:

$$n_c = \frac{m_c/\rho_c}{V_c} = \frac{m_c/\rho_c}{\phi_c D_c^3}, \qquad 3.14$$

where, $m_c, \rho_c, and\ V_c$ are mass, density, and volume of coarse particles, respectively; $\phi_c$ is a volume shape factor and its value is $\pi/6$ when a coarse particle is a sphere. Substituting Eq. (3.14)to Eq. (3.13), the following equation is derived for the collision frequency.

$$f_c \propto \frac{m_c}{\rho_c \phi_c} n_f \qquad 3.15$$

This equation means that collision frequency is not dependent on the size of the carrier, but it increases with increasing carrier mass. This agrees with the results shown in Fig. 3-11: the recovery of fines increases when carrier amount (mass) increases, regardless of carrier size.

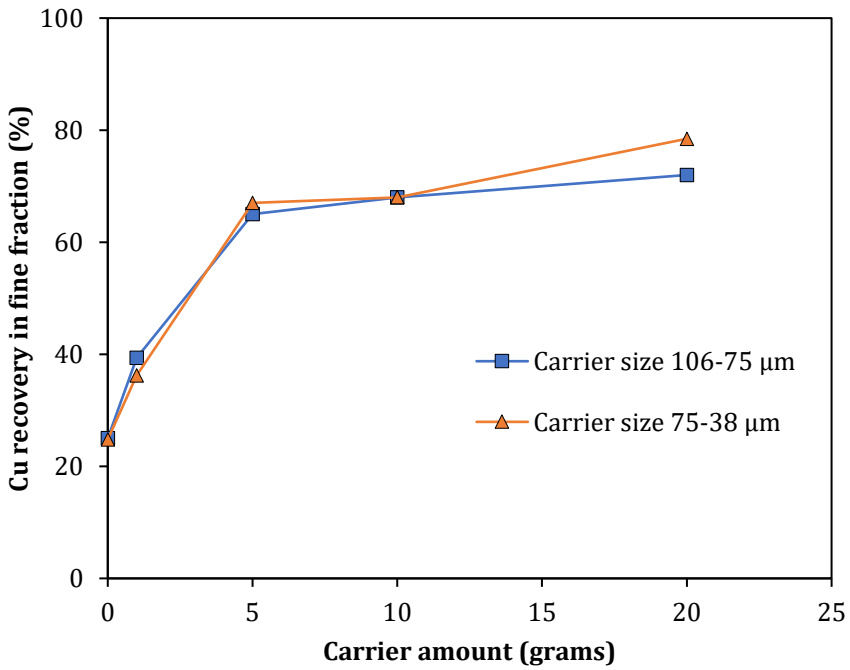


Fig. 3-11. Effect of carrier amount on recovery of fines, Test conditions: [KAX] = 200 g/t of fines; [MIBC] = 25 µL/L.

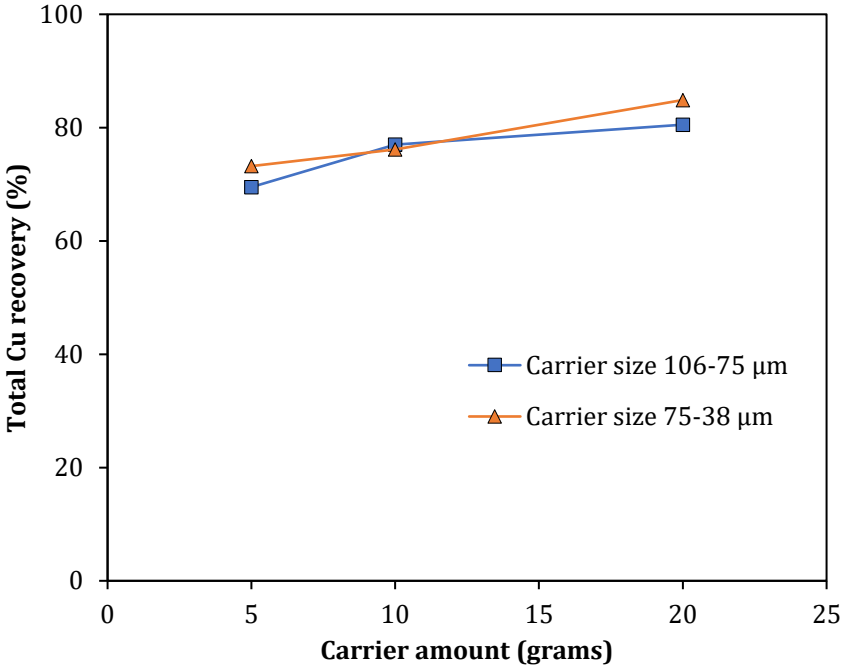

Fig. 3-12. Effect of carrier amount on overall Cu recovery, Test conditions: [KAX] = 200 g/t of fines; [MIBC] = 25 µL/L.

*3.4.5 Effects of the carrier on the separation of chalcopyrite and quartz*

In the above section, the effects of the carrier on the recovery of fine chalcopyrite during flotation were mainly discussed. The industrial operation of flotation needs to separate fine chalcopyrite and gangue minerals like quartz. This section presents the investigation of the effect of carrier addition on the separation of chalcopyrite and quartz. 20 g fine chalcopyrite and 5 g fine quartz were mixed and subjected to flotation experiments with and without 10 g of the carrier. Froth was collected and subjected to sieving to separate the coarse fraction (carrier or coarse chalcopyrite) and a fine fraction (a mixture of fine chalcopyrite/quartz). After drying, weights of coarse and fine fractions were determined and Cu and Si content in both fractions were determined by XRF. Based on the data, fine chalcopyrite recovery, fine silica recovery, as well as total copper recovery into the froth, were calculated.

Fig. 3-13 shows the effect of carrier addition on the flotation of fine chalcopyrite/quartz mixture. Fig. 3-13 and Fig. 3-14 show fine chalcopyrite recovery, as well as total copper recovery to the froth, increased when 10 g coarse chalcopyrite was used as a carrier: After 10 minutes of flotation, the recovery of fine chalcopyrite increased to 65% with a carrier from 28% without a carrier, and total copper recovery increased to 72% with a carrier from 28% without a carrier. As shown in Fig. 3-15, when the carrier was added, recovery of fine quartz to the froth increased slightly: at 10 min the recovery increased from 10%

without a carrier to 18% with a carrier, which may be due to the entrainment of fine quartz with water recovered to froth.

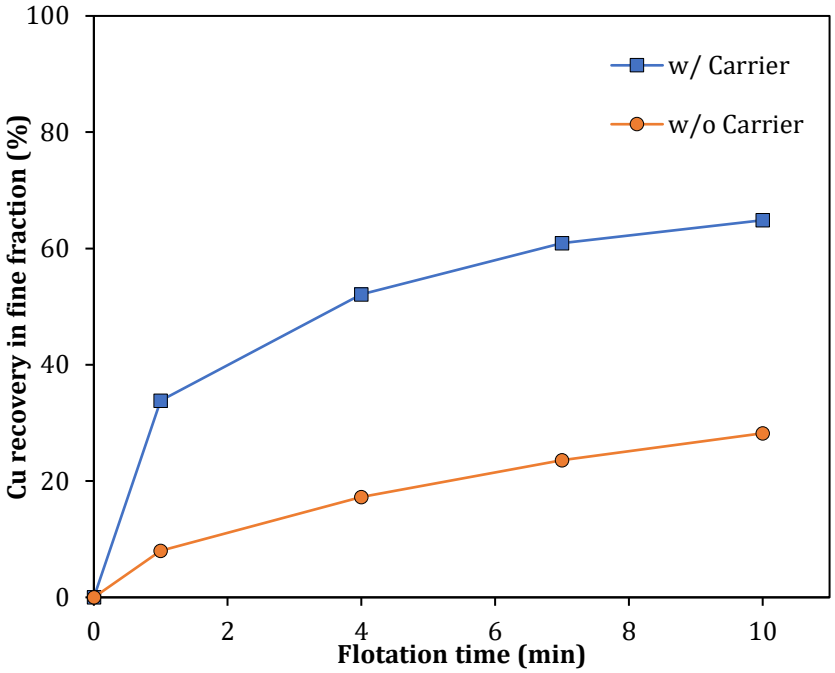


Fig. 3-13. Effect of quartz on recovery of fine chalcopyrite with and without carrier: Test conditions: [KAX] = 200 g/t of fines; [MIBC] = 25 µL/L.

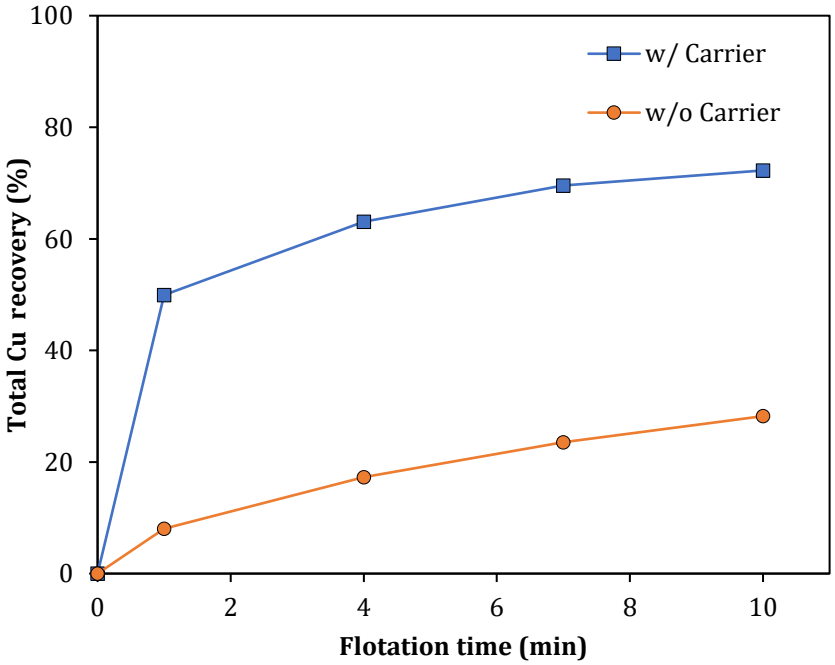


Fig. 3-14. Effect of quartz on total Cu recovery with and without addition of carrier, Test conditions: [KAX] = 200 g/t of fines; [MIBC] = 25 µL/L.

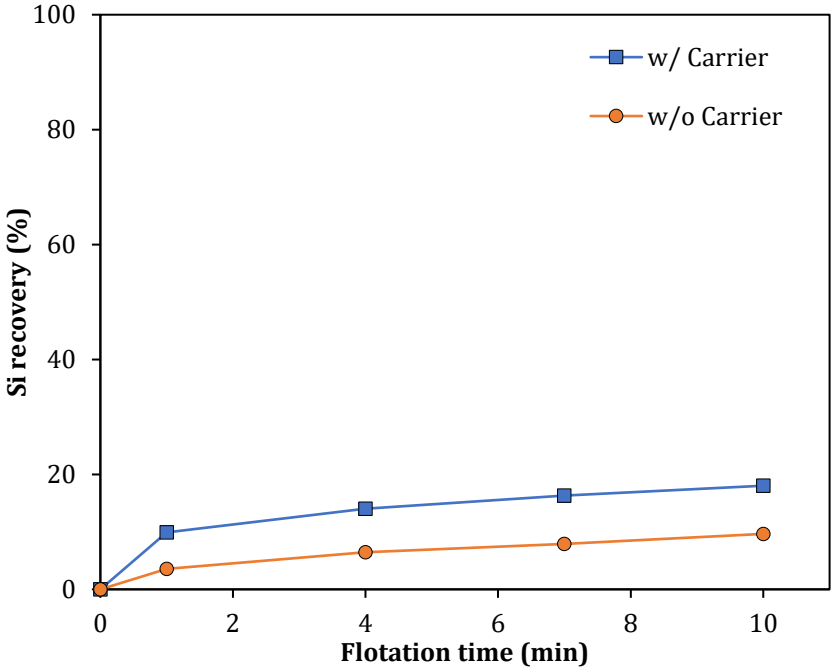


Fig. 3-15. Cumulative silica recovery% with and without carrier, Test conditions: [KAX] = 200 g/t of fines; [MIBC] = 25 µL/L.

Fig. 3-16 shows the relationship between total Cu recovery to froth and total Si recovery to tailing after 10 min of flotation with and without coarse chalcopyrite as a carrier. The separation efficiency of Si and Cu, defined by the following equation, can be evaluated from Fig. *3-16*.

$$\eta\,(\%) = R_{Cu}\,(\%) + R_{Si}\,(\%) - 100 \qquad 3.16$$

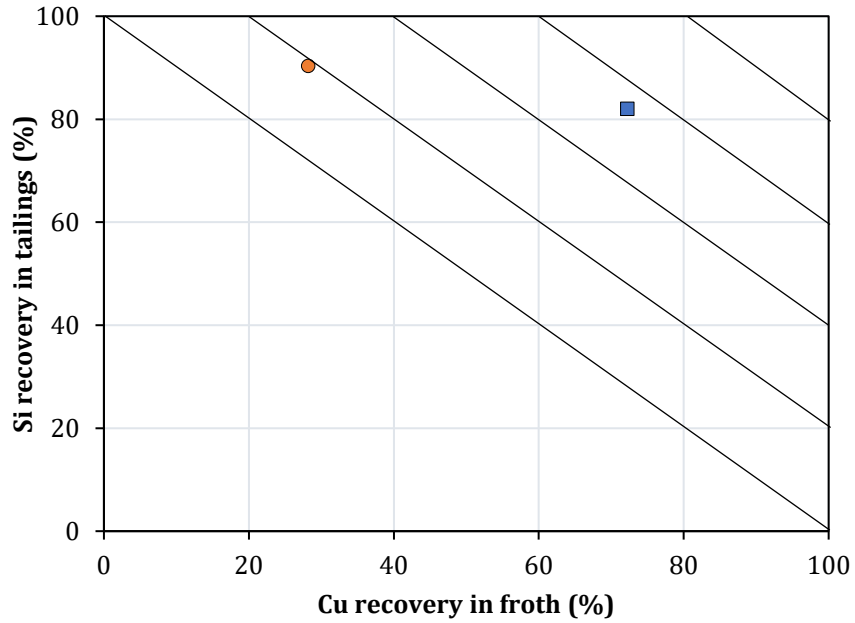


Fig. 3-16. Relationship between total Cu% recovery in froth and total silica % recovery in tailings of chalcopyrite and Silica mixture with and without the addition of carrier, Test conditions: [KAX] = 200 g/t of fines; [MIBC] = 25 µL/L.

where, $R_{Cu}$ and $R_{Si}$ is the recovery of Cu to froth and Si to tailing. From the inclined lines in Fig. 16 separation efficiency can be determined. Without a carrier, separation efficiency was less than 20% while it was improved to around 55% with a 10 g carrier. This suggests that the addition of coarse chalcopyrite as a carrier is effective to improve fine chalcopyrite recovery as well as Cu/Si separation efficiency.

### 3.5 Conclusions

In this chapter, the effects of coarse chalcopyrite (as a carrier) on the flotation behavior of fine chalcopyrite were investigated. From size distribution data for the mixture of fine/coarse chalcopyrite suspended in the flotation pulp, attachment of fine chalcopyrite to the carrier (coarse chalcopyrite) was confirmed. The theoretical calculation for the interaction between the particles showed that hydrophobic interaction was the dominant factor that causes the attachment of fines to the carrier. The results of flotation experiments showed that the recovery of fine chalcopyrite to the froth increased with increasing carrier amounts. The results of the flotation experiments for fine chalcopyrite/silica mixture showed that the addition of coarse chalcopyrite as a carrier promoted the overall Cu recovery as well as separation efficiency.

This chapter was modified from **Bilal, M.;** Ito, M.; Koike, K.; Hornn, V.; Ul Hassan, F.; Jeon, S.; Park, I.; Hiroyoshi, N. Effects of coarse chalcopyrite on flotation behavior of fine chalcopyrite. Miner. Eng. **2021**, 163, 106776.

### References


HORNN, V., ITO, M., YAMAZAWA, R., SHIMADA, H., TABELIN, C. B., JEON, S., PARK, I. & HIROYOSHI, N. 2020. Kinetic Analysis for Agglomeration-Flotation of Finely Ground Chalcopyrite: Comparison of First Order Kinetic Model and Experimental Results. *MATERIALS TRANSACTIONS,* 61**,** 1940-1948 DOI: https://doi.org/10.2320/matertrans.M-M2020843.

HU, Y. & DAI, J. 2003. Hydrophobic aggregation of alumina in surfactant solution. *Minerals Engineering,* 16**,** 1167-1172 DOI: https://doi.org/10.1016/j.mineng.2003.07.018.

HU, Y., QIU, G. & MILLER, J. D. 2003. Hydrodynamic interactions between particles in aggregation and flotation. *International Journal of Mineral Processing,* 70**,** 157-170 DOI: https://doi.org/10.1016/S0301-7516(03)00023-1.

LEVICH, V. G. E. 1962. Physicochemical hydrodynamics.

LI, D., YIN, W., LIU, Q., CAO, S., SUN, Q., ZHAO, C. & YAO, J. 2017. Interactions between fine and coarse hematite particles in aqueous suspension and their implications for

flotation. *Minerals Engineering,* 114**,** 74-81 DOI: https://doi.org/10.1016/j.mineng.2017.09.012.

LI, W., LI, Y., XIAO, Q., WEI, Z. & SONG, S. 2018. The Influencing Mechanisms of Sodium Hexametaphosphate on Chalcopyrite Flotation in the Presence of MgCl2 and CaCl2. *Minerals,* 8 DOI: https://doi.org/10.3390/min8040150.

LU, J., YUAN, Z., LIU, J., LI, L. & ZHU, S. 2015. Effects of magnetite on magnetic coating behavior in pentlandite and serpentine system. *Minerals Engineering,* 72**,** 115-120 DOI: https://doi.org/10.1016/j.mineng.2014.12.038.

VILINSKA, A. & RAO, K. H. J. T. O. C. S. J. 2009. Surface thermodynamics and extended DLVO theory of Acidithiobacillus ferrooxidans cells adhesion on pyrite and chalcopyrite. 2.

YAO, J., YIN, W. & GONG, E. 2016. Depressing effect of fine hydrophilic particles on magnesite reverse flotation. *International Journal of Mineral Processing,* 149**,** 84-93 DOI: https://doi.org/10.1016/j.minpro.2016.02.013.

YOON, R. H. 2000. The role of hydrodynamic and surface forces in bubble–particle interaction. *International Journal of Mineral Processing,* 58**,** 129-143 DOI: https://doi.org/10.1016/S0301-7516(99)00071-X.

# CHAPTER 4: Heterogenous carrier flotation using coarse pyrite particles as carriers

## 4.1 Introduction

In the previous chapter, we studied the effects of coarse chalcopyrite as a carrier on the flotation behavior of finely ground chalcopyrite particles ($D_{50}$ ~3 µm), and it was confirmed that fine chalcopyrite recovery was significantly improved using coarse chalcopyrite particles as carriers.

Considering tailings as future resources, which have mostly fine chalcopyrite particles, an autogenous carrier flotation technique using coarse chalcopyrite particles as carriers may not be applicable. Thus, because coarse chalcopyrite particles are not available at the tailings site, an alternate carrier is required. Pyrite ($FeS_2$) is a suitable choice as a carrier for fine chalcopyrite particles because of its abundance at mine sites. The effects of coarse pyrite particles as a carrier for finely ground chalcopyrite particles have not yet been reported; therefore, no literature is available on this topic.

In this chapter, specially designed flotation tests were conducted to study a heterogeneous carrier flotation technique using coarse pyrite particles as a carrier for the recovery of finely ground chalcopyrite particles.

## 4.2 Materials and reagents

### *4.2.1 Materials*

The chalcopyrite and pyrite samples (run of mine) used in this study were acquired from the Copper Queen Mine (Arizona, USA) and the Huanzala Mine (Peru), respectively. The samples were hammered, and visible impurities were removed by hand-picking. Mineralogical and chemical characterizations of chalcopyrite and pyrite were carried out using X-ray fluorescence (XRF) (EDXL300, Rigaku Corporation, Tokyo, Japan) and X-ray powder diffraction (XRD, Multiplex, Rigaku Corporation, Tokyo, Japan) techniques. The chemical compositions and mineralogical analyses of these samples are presented in Table 4-1 and Fig. 4-1, respectively.

Table 4-1. Chemical compositions of pyrite and chalcopyrite samples.

| Mineral | Mass (%) | | | | | |
|---|---|---|---|---|---|---|
| | Cu | Fe | S | Zn | Si | Ca |
| **Chalcopyrite** | 30.0 | 32.0 | 18.0 | 0.6 | 5.0 | 4.0 |
| **Pyrite** | 0.05 | 45.3 | 48.5 | - | 1.0 | - |

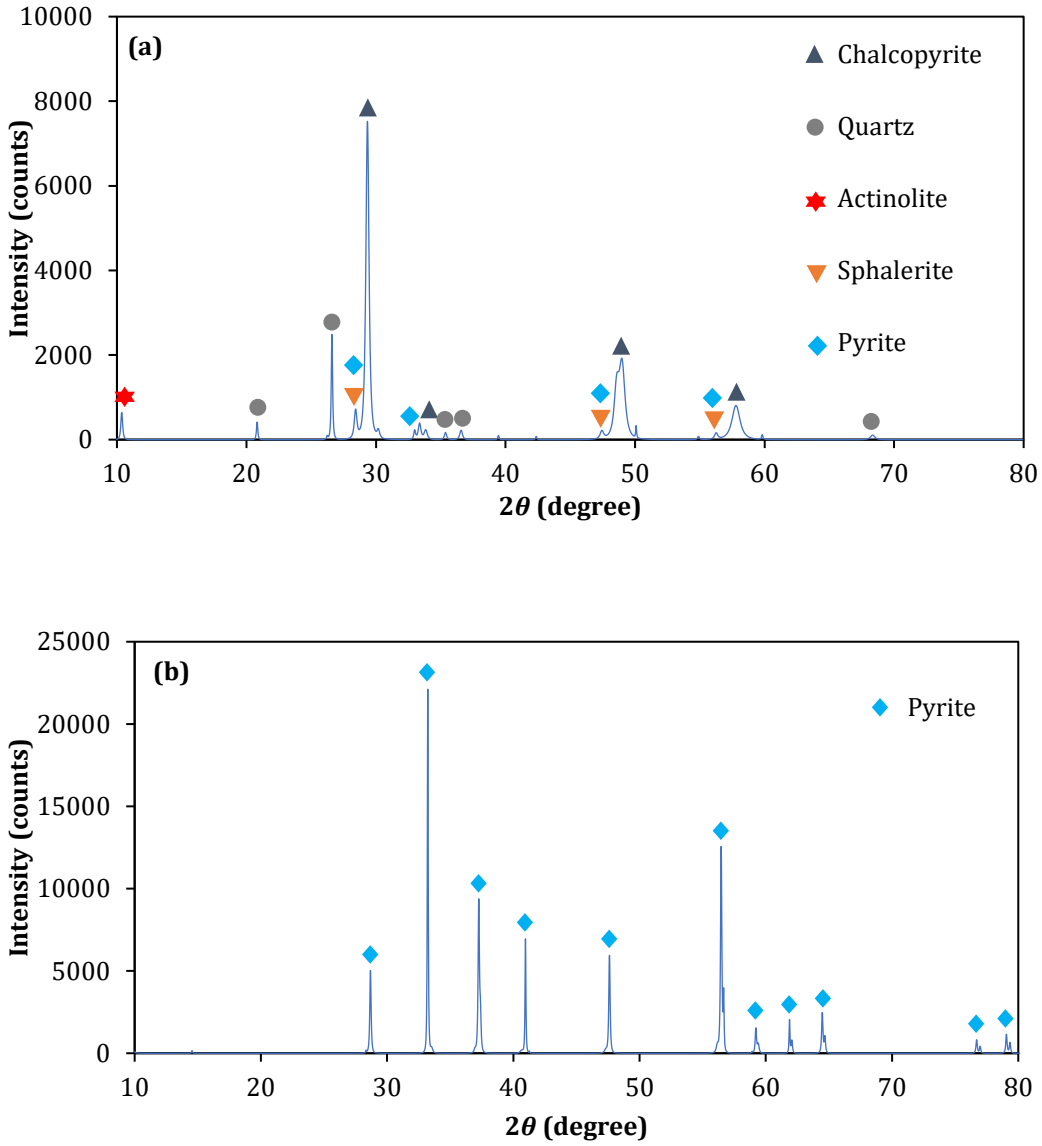


Fig. 4-1. X-ray diffraction (XRD) patterns of (a) chalcopyrite ($CuFeS_2$) and (b) pyrite ($FeS_2$).

*4.2.2 Reagents*

Potassium amyl xanthate (KAX, $C_5H_{11}OCSSK$) (Tokyo Chemical Industry Co., Ltd., Japan) and methyl isobutyl carbinol (MIBC, $C_6H_{14}O$) (Wako Pure Chemical Industries, Ltd., Japan) were used as the collector and frother reagents, respectively. Copper sulfate pentahydrate ($CuSO_45H_2O$) (Wako Pure Chemical Industries, Ltd., Japan) was used as the source of $Cu^{2+}$ for pyrite activation.

## 4.3 Methods

*4.3.1 Sample preparation*

For pyrite, the –125+106 μm ($D_{50}$ = 114 μm) size fraction was selected as the carrier. A jaw crusher (1023-A, Yoshida Manufacturing Co., Ltd, Sapporo, Japan) and disc mill (RS200, Retsch Inc., Haan, Germany) were used to crush and grind the samples,

respectively. Screens of 125 μm and 106 μm were used for pyrite, whereas a screen of 75 μm was used for chalcopyrite. In the case of chalcopyrite, particles smaller than 75 μm were further ground using a disc mill to obtain a particle size of $D_{50}$ = 3–3.5 μm, as determined by Microtrac (MT3300SX, Nikkiso Co., Ltd., Tokyo, Japan). The particle size distributions of coarse pyrite and fine chalcopyrite are shown in Fig. 4-2.

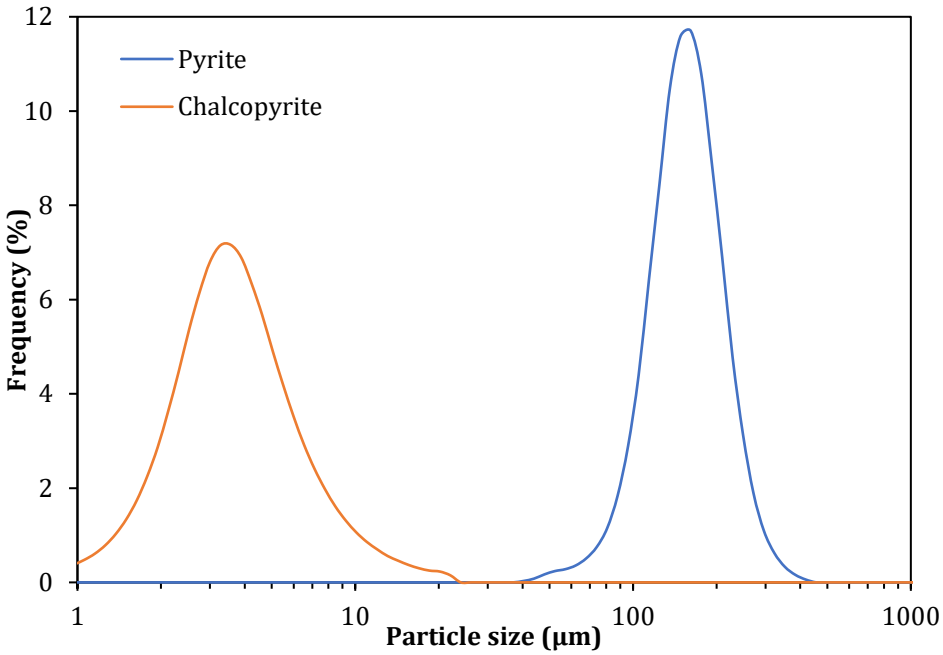


Fig. 4-2. Particle size distributions of the pyrite and chalcopyrite samples.

*4.3.2 Single mineral flotation tests*

Single mineral flotation was performed using an agitator-type flotation machine (FT-1000, Heiko, Japan) with a 0.5-L square flotation cell at an impeller speed of 1,000 rpm and an airflow rate of 1 L/min. The sample was ultrasonically treated for 5 min before conditioning with the collector (KAX) and frother (MIBC) for 5 min each. Subsequently, air bubbles were introduced into the flotation cell. The flotation time was 10 min. The flotation concentrates and tailings were oven-dried and weighed. The dried sample was analyzed by XRF, and the recoveries of Cu and Fe were calculated using Eq. (4.1):

$$R = \frac{Cc}{Ff} \times 100, \tag{4.1}$$

where $C$ and $F$ are the percentage weights of the concentrate and feed, respectively, and $c$ and $f$ are the grades of the concentrate and feed, respectively.

*4.3.3 Mixed pyrite–chalcopyrite flotation tests*

Ten grams of coarse pyrite particles (–125+106 µm size fraction) were mixed with 20 g of ultra-fine chalcopyrite particles ($D_{50}$ = 3–3.5 µm) to observe the effect of coarse pyrite particles as a carrier on the flotation of ultrafine chalcopyrite particles. The parameters here were the same as those in section *4.3.2*, except that the froth and tailings were sieved immediately with a 106 µm sieve using ethanol spray until the complete separation of coarse pyrite and fine chalcopyrite particles from each other; and their recoveries were calculated using Eq. (4.1). The ratio of finely ground chalcopyrite and coarse pyrite particles was selected based on the previous chapter.

*4.3.4 Mixed pyrite–chalcopyrite flotation tests in the presence of $Cu^{2+}$*

Ten grams of coarse pyrite particles (–125+106 µm size fraction) and 20 g of fine chalcopyrite particles were conditioned for 5, 5, and 3 min after sequentially adding $CuSO_4$ (2,000 g/t), KAX (500 g/t), and MIBC (25 µL/L), respectively. The froth and tailings were sieved immediately using the same method as mentioned in section *4.3.3*, and their recoveries were calculated using Eq. (4.1).

*4.3.5 Particle size analysis*

The coarse and fine fractions were analyzed using a particle size analyzer. For the mixture of the carrier (coarse pyrite) and fines (chalcopyrite), the particle size distribution was measured after the mixture was conditioned (before flotation) with reagents. The same sample was also analyzed using scanning electron microscopy (SEM, JSM-IT200, JEOL Ltd., Tokyo, Japan).

*4.3.6 Contact angle measurements*

The contact angles were measured to estimate the variation in the surface wettability of pyrite before and after $Cu^{2+}$ treatment. For this purpose, a small cuboid pyrite crystal (~5 mm (w) × 5 mm (d) × 10 mm (h)) was obtained by cutting the pyrite specimen with a diamond cutter. The surface was then polished with a polishing machine (SAPHIR 250 M1, ATM GmbH, Mammelzen, Germany) using a series of silicon carbide papers (P320, P600, and P1200) and diamond suspensions (3 and 1 µm). After polishing the surface of the pyrite cuboid, the contact angles of (i) untreated pyrite, (ii) $Cu^{2+}$-treated pyrite, and (iii) chalcopyrite (with the same flotation conditions) were measured using a high-magnification digital microscope (VHX-1000, Keyence Corporation, Osaka, Japan) with built-in image analysis software. Each measurement was repeated three times at various spots on the mineral surface to ascertain the statistical significance of the observations.

*4.3.7 XPS and SEM-EDX analysis*

The surface of pyrite was analyzed by Scanning electron microscopy with energy-dispersive X-ray spectroscopy (SEM-EDX, JSM-IT200, JEOL Ltd., Tokyo, Japan) and X-ray photoelectron spectroscopy (XPS, JPS-9200, JEOL Ltd., Japan) after conditioning with reagents. The XPS analysis was performed using an Al Kα X-ray source (1,486.7 eV) operated at 100 W (voltage = 10 kV; current = 10 mA) under ultra-high vacuum conditions (~$6.7 \times 10^{-7}$ Pa). The binding energies of the photoelectrons were calibrated using Fe metal (706.9 eV) as a reference for charge correction. All XPS data were analyzed using XPSPEAK version 4.1, and the spectra were deconvoluted using an 80% Gaussian–20% Lorentzian peak model and a true Shirley background (Nesbitt and Muir, 1994, Shirley, 1972, Park et al., 2020b).

## 4.4 Results and discussion

*4.4.1 Effects of coarse pyrite particles as a carrier*

Fig. 4-3 shows the recovery of 20 g of fine chalcopyrite particles with and without 10 g of coarse pyrite particles (–125+106 μm) after 10 min of flotation. The recovery of fine chalcopyrite particles did not improve when mixed with the 10 g of coarse pyrite particles. This indicates two possibilities: (1) there may be no significant attachment of fine chalcopyrite particles onto the coarse pyrite particle surfaces, or (2) fine chalcopyrite particles may have attached to the coarse pyrite particle surfaces, but pyrite did not float to the surface. The recovery of pyrite (Fig. 4-4) with and without mixing with 20 g of fine chalcopyrite particles indicated no significant difference in the recovery of pyrite. In both cases, pyrite recovery was over 90%; this is significant, as it implies that poor chalcopyrite recovery was not due to the low recovery of pyrite as a carrier. This indicates that there is no significant attachment of fine chalcopyrite particles to the surface of the coarse pyrite particles. To confirm this, the attachment of fine chalcopyrite to coarse pyrite is discussed based on particle size distribution analysis in the next section.

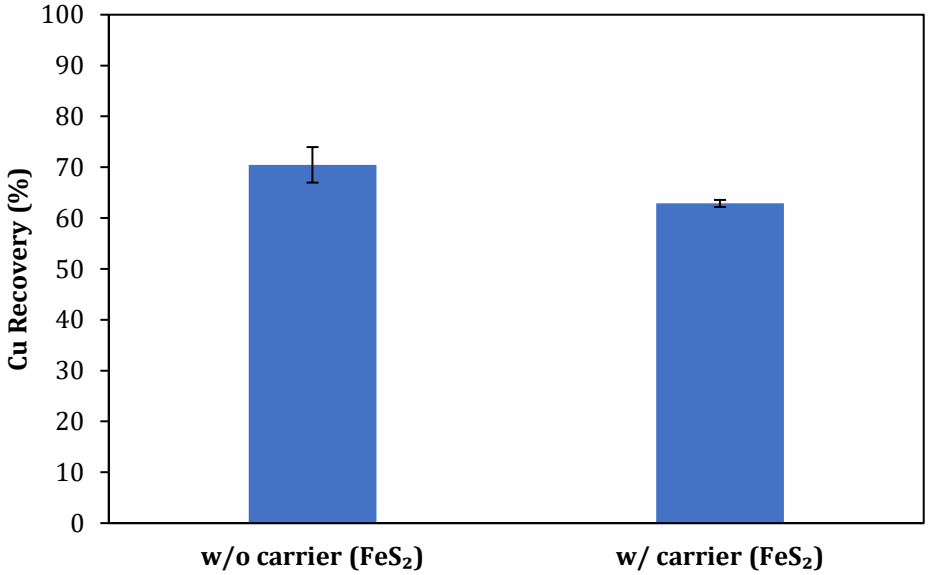


Fig. 4-3. Cu Recovery (%) from fines without (left) and with (right) pyrite as a carrier, Test conditions: [KAX] = 500 g/t; [MIBC] = 25 µL/L; [Carrier size] = –125+106 µm; [Carrier amount] = 10 g. KAX = potassium amyl xanthate; MIBC = methyl isobutyl carbinol.

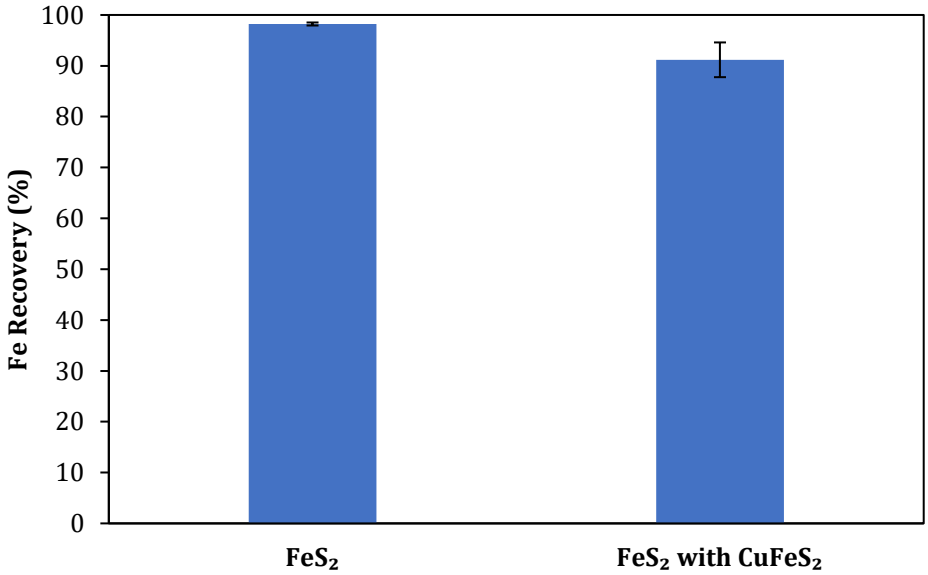


Fig. 4-4. Pyrite recovered (%) without (left) and with (right) chalcopyrite fine particles present, Test conditions: [KAX] = 500 g/t; [MIBC] = 25 µL/L; [particle size] = –125+106 µm; [$FeS_2$ amount] = 10 g; [$CuFeS_2$ amount] = 20 g.

*4.4.2 Attachment of fine particles to the carrier*

The particle size distribution of the mixture of fine and coarse particles, with the fine particles attached to the coarse particles, is not simply a sum of the individual distributions of the fine and coarse particles. Particle size distribution analysis for the mixture of 20 g of fine chalcopyrite particles and 10 g of coarse pyrite particles suspended in a 400-mL flotation cell after conditioning with KAX was carried out using Microtrac; the solid blue line in Fig. 4-5 represents the measured frequency of the mixture. For comparison, a calculated size distribution curve for the mixture, $\eta_{cal}$, was obtained using

Eq. (4.2), assuming the negligible attachment of fines to coarse particles, and was also plotted in Fig. 4-5 (dotted red line).

$$\eta_{cal} = \eta_{fine}\left(\frac{2}{3}\right) + \eta_{coarse}\left(\frac{1}{3}\right), \quad 4.2$$

where $\eta_{fine}$ and $\eta_{coarse}$ represent the volumetric frequencies of the fine and coarse particles, respectively.

Fig. 4-5 compares the measured result (solid blue line) with the calculated results (dotted red line), clearly showing that the measured frequencies are smaller at the peak position of the fine particles (approximately 3.5 μm); however, this peak never disappeared, indicating that a significant amount of unattached fine chalcopyrite remained in the suspension. It can therefore be concluded that fine chalcopyrite particles were partially attached to the surface of coarse pyrite particles, with a significant amount of fines remaining unattached in the suspension.

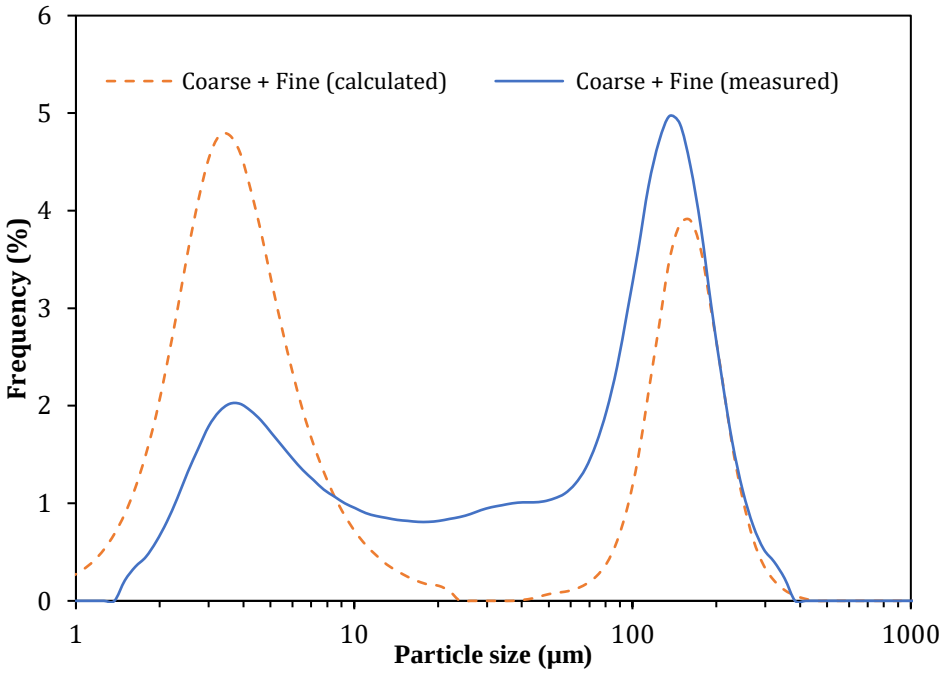


Fig. 4-5. Particle size distribution of the mixture of fine chalcopyrite and coarse pyrite particles after conditioning with the collector (measured vs. calculated).

To identify the interactions responsible for fine chalcopyrite particles attaching to coarse pyrite particles (carrier), theoretical calculations were performed. In a previous study, we compared the electrostatic, hydrophobic, and van der Waals interactions between fine chalcopyrite particles and coarse chalcopyrite carrier particles, which was based on the extended Derjaguin–Landau–Verwey–Overbeek (EDLVO) theory. In the case of fine-

chalcopyrite–coarse-chalcopyrite particles, both individual particles are negatively charged; thus, the electrostatic force between them is repulsive, while van der Waals forces and hydrophobic interactions act as attractive forces. A comparison of the two attractive forces based on theoretical calculations showed that hydrophobic interactions are the dominant attractive force for fine-chalcopyrite–coarse-chalcopyrite (Chapter 3). Similar to the fine chalcopyrite-coarse chalcopyrite particle interaction, both chalcopyrite and pyrite are negatively charged at pH values greater than 4 (Mitchell et al., 2005) and the electrostatic force acts as a repulsive force. The comparison of van der Waals forces and hydrophobic interactions based on theoretical calculations confirmed that the hydrophobic force is much stronger than the van der Waals force for fine chalcopyrite-coarse pyrite. As such, hydrophobic interactions are considered the dominant attractive force in the following discussion.

Fig. 4-6 shows calculated potential energy values for hydrophobic interactions as a function of the separation distance between two individual particles. Hydrophobic interactions ($V_H$) are calculated by Eq. (4.3) (Hu and Dai, 2003, Yao et al., 2016) as follows:

$$V_H = 2\pi \frac{R_1 R_2}{R_1 + R_2} \, ho V_H^0 \, exp\left(\frac{Ho - H}{ho}\right), \tag{4.3}$$

where $Ho$ and $ho$ are the minimum equilibrium distance between the particles and decay length, respectively. The values of $Ho$ and $ho$ were assumed to be 0.2 nm and 5 nm, respectively (Yao et al., 2016, Li et al., 2017). $R_1$ and $R_2$ represent the radii of the coarse and fine particles, respectively. The value of $V_H^0$ (acid–base free energy per unit area between the surfaces) was calculated using the following equation:

$$V_H^0 = 2[\sqrt{\gamma_3^+}(\sqrt{\gamma_1^-} + \sqrt{\gamma_2^-} - \sqrt{\gamma_3^-}) + \sqrt{\gamma_3^-}(\sqrt{\gamma_1^+} + \sqrt{\gamma_2^+} - \sqrt{\gamma_3^+}) - \sqrt{\gamma_1^+\gamma_2^-} - \sqrt{\gamma_1^-\gamma_2^+}), \tag{4.4}$$

where $\gamma_1^+$, $\gamma_2^+$ and $\gamma_1^-$, $\gamma_2^-$ are the parameters for the polar components of the surface tension of compound $S$, and $\gamma_3^+$ and $\gamma_3^-$ (for water) are both equal to $25.5 \times 10^{-3}$ J/m$^2$. $\gamma_1^+$; $\gamma_2^+$ can be calculated with Eq. (4.5) as follows:

$$(1 + cos\theta)\gamma_L = 2(\sqrt{\gamma_S^d \gamma_L^d} + \sqrt{\gamma_S^+ \gamma_L^-} + \sqrt{\gamma_S^- \gamma_L^+}) \tag{4.5}$$

Here, subscripts $S$ and $L$ represent solid and liquid, respectively, and superscript $d$ denotes the dispersive component. For water, $\gamma_L$ = $72.8 \times 10^{-3}$ J/m$^2$ and $\gamma_L^d$ = $21.8 \times 10^{-3}$ J/m$^2$. Additionally, $\theta$ represents the contact angle between the solid surface and liquid.

The mineral contact angles measured in deionized (DI) water, glycerol, and formaldehyde are presented in Table 4-2.

Table 4-2. Average contact angle values (θ°) at a pH of 8 in different solutions.

| Liquid Name/Mineral | Chalcopyrite | $Cu^{2+}$-treated pyrite | Untreated pyrite |
|---|---|---|---|
| Water | 78 | 73 | 72 |
| Glycerol | 64 | 73 | 55 |
| Formaldehyde | 52 | 68 | 66 |

The $\gamma_L$, $\gamma_L^d$, $\gamma_L^+$, and $\gamma_L^-$ values for glycerin and formaldehyde are listed in Table 3. The values of $\gamma_S^d$, $\gamma_S^+$, and $\gamma_S^-$ can be determined using Eq. (4.5). In the calculation, the reported surface energy values of glycerol and formaldehyde, listed in Table 4-3, were used.

Table 4-3. Surface energy parameters of glycerol and formaldehyde (Cheng et al., 2020).

| Liquid Name | $\gamma_L$(mJ m$^{-2}$) | $\gamma_L^d$(mJ m$^{-2}$) | $\gamma_L^+$ (mJ m$^{-2}$) | $\gamma_L^-$(mJ m$^{-2}$) |
|---|---|---|---|---|
| Glycerol | 64 | 34 | 3.92 | 57.4 |
| Formaldehyde | 58 | 39 | 2.28 | 39.6 |

Based on Eq. (4.3), the hydrophobic interaction energies between the coarse pyrite and fine chalcopyrite particles were calculated and compared to those of coarse-fine chalcopyrite particles (Fig. 4-6). As shown in Fig. 4-6, the hydrophobic interaction between coarse and fine chalcopyrite particles was much larger than that between coarse pyrite-fine chalcopyrite particles. In a previous study on the carrier flotation of fine chalcopyrite using coarse chalcopyrite as a carrier, it was found that almost all fine chalcopyrite was attached to the carrier (coarse chalcopyrite) and its flotation recovery to froth was significantly improved. On the contrary, as already discussed, the attachment of fine chalcopyrite to coarse pyrite was limited (Fig. 4-5) and flotation recovery of fine chalcopyrite did not improve even when coarse pyrite was used as a carrier (Fig. 4-3). This is in line with the calculation result shown in Fig. 4-6: a weak hydrophobic interaction may cause an imperfect attachment of fine chalcopyrite to coarse pyrite and a low chalcopyrite recovery.

The contact angle of the KAX-treated pyrite was smaller than that of chalcopyrite, causing weaker hydrophobic interactions between chalcopyrite and pyrite particles compared with chalcopyrite-chalcopyrite, as shown in Fig. 4-6. If the hydrophobicity or contact angle of pyrite is improved, coarse pyrite can be used as a carrier to improve fine chalcopyrite recovery in flotation. An idea based on the above argument is discussed in the next section.

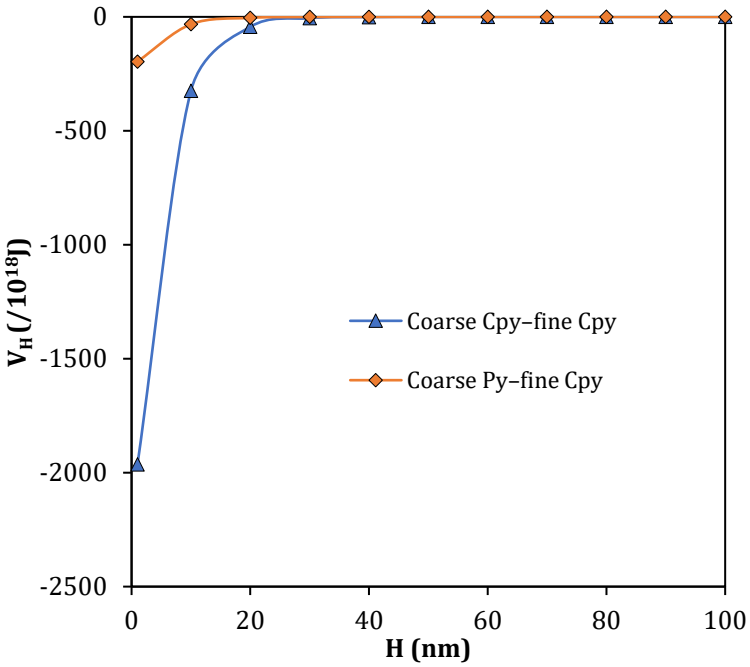


Fig. 4-6. Hydrophobic interactions ($V_H$) between coarse chalcopyrite and fine chalcopyrite particles, and those between coarse pyrite and fine chalcopyrite particles. Cpy = chalcopyrite; Py = pyrite; H = separation distance.

### *4.4.3 Effects of coarse $Cu^{2+}$-activated pyrite as a carrier*

#### 4.4.3.1 Surface characterization of $Cu^{2+}$-activated pyrite

The effects of $Cu^{2+}$ activation on the hydrophobicity of pyrite were investigated based on the discussion in the previous section. It has been well reported that surface modification is an effective way to control the hydrophobicity of minerals (Aikawa et al., 2021, Park et al., 2020a, Park et al., 2021b). For example, if a CuS-like layer or its oxidized product, such as $Cu(OH)_2$, can be formed on the pyrite surface, KAX adsorption becomes easier (Yang et al., 2016). This would enhance the hydrophobicity of the pyrite particles, making them more efficient carriers for fine chalcopyrite particles in flotation. It has been previously reported in the literature (Boulton et al., 2003) that pyrite could be activated by $Cu^{2+}$, which consequently improved its hydrophobicity. Thus, $Cu^{2+}$-treated pyrite was prepared, and its surface properties were analyzed by SEM-EDX. As can be seen in Fig. 4-7, a Cu signal was detected on the surface of the $Cu^{2+}$-treated pyrite, indicating that Cu-containing compound(s) were formed after the activation of pyrite.

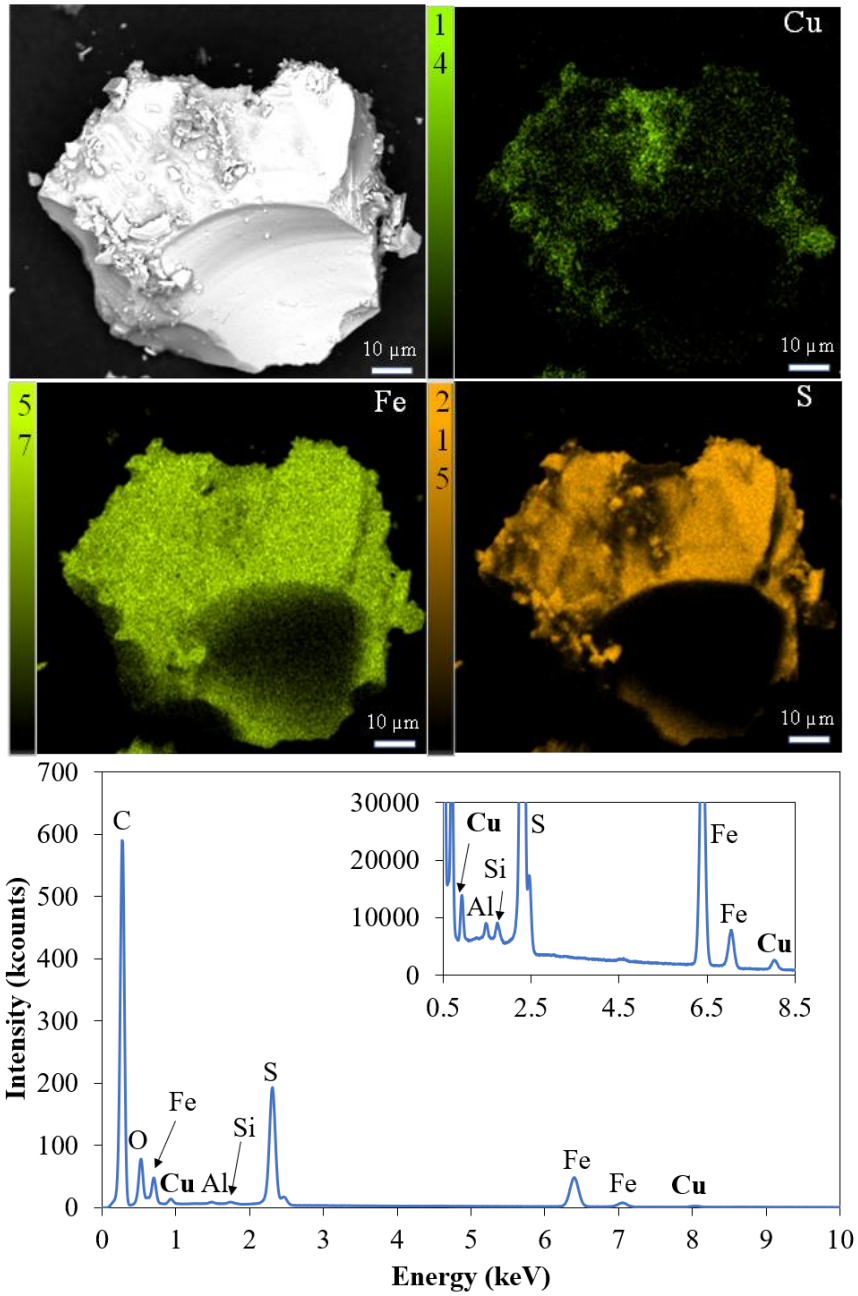


Fig. 4-7. Scanning electron microscopy-energy dispersive X-ray spectroscopy (SEM-EDX) analysis of pyrite treated with $Cu^{2+}$.

To further clarify the change in the pyrite surface after activation, XPS analyses of pyrite treated with $Cu^{2+}$ and untreated pyrite were carried out. Fig. 4-8 shows the Fe 2p, S 2p, Cu 2p, and O 1s XPS spectra of the untreated and treated pyrite samples. As shown in the Fe $2p_{3/2}$ spectrum of untreated pyrite (Fig. 4-8a-(i)), it consists of a strong peak at ~707 eV corresponding to Fe(II)–S in pyrite, along with other peaks representing Fe(III) species such as Fe(III)–S (~ 708.9 eV) and Fe(III)–O (~ 710 eV) (von Oertzen et al., 2006, Li et al., 2021, Park et al., 2020b, Park et al., 2021a, Ejtemaei and Nguyen, 2017, Deng et al., 2021). In the case of treated pyrite (Fig. 4-8a-(ii)), the intensities of the oxidized Fe species were notably increased, indicating that pyrite was oxidized during the activation process.

The S $2p_{3/2}$ spectra of untreated and treated pyrite are shown in Fig. 4-8b. Both spectra contain a dominant peak at approximately 162.4 eV, which corresponds to $S_2^{2-}$ in pyrite (Ejtemaei and Nguyen, 2017, Deng et al., 2021). Meanwhile, another minor peak at around 161.5 eV is observed only in the S $2p_{3/2}$ spectrum of treated pyrite (Fig. 4-8b-(ii)), which is assigned to $S^{2-}$ (Ejtemaei and Nguyen, 2017). This indicates that the activation of pyrite generates new compounds, such as metal sulfides.

The Cu 2p spectrum of untreated pyrite (Fig. 4-8c-(i)) does not show any signals of Cu; however, it is important to note that Cu signals were detected when pyrite was treated with $Cu^{2+}$ (Fig. 4-8c-(ii)). The major peaks of Cu $2p_{1/2}$ (951.5 eV) and Cu $2p_{3/2}$ (932 eV) are coincident with the Cu(I) state of $Cu_2S$ (Zhuge et al., 2009), and the formation of $Cu_2S$ on the surface of treated pyrite is supported by the presence of the $S^{2-}$ peak observed in the S $2p_{3/2}$ spectrum (Fig. 8b-(ii)). There are also two peaks at 953.1 eV and 933.4 eV that are both assigned to Cu(II) species like $CuO/Cu(OH)_2$ (Biesinger et al., 2010). In addition, a shake-up satellite peak is observed at around 942.8 eV, which also indicates that Cu(II) species are present on the surface of treated pyrite (Biesinger et al., 2010, Zhuge et al., 2009).

As shown in Fig. 4-8d, the O 1s spectra of both untreated and treated pyrite samples revealed three types of oxygen species: lattice oxygen ($O^{2-}$) at 530 eV, hydroxyl oxygen ($OH^-$) at 531 eV, and the oxygen of attached water ($\equiv H_2O$) at 533 eV (Deng et al., 2021). It is important to note that the O 1s spectrum of treated pyrite shows a higher intensity of lattice oxygen than that of untreated pyrite, suggesting that the amount of metal oxide(s), such as Fe(III)-oxide and/or Cu(II)-oxide, is increased, as confirmed by Fig. 4-8a-(ii) and Fig. 4-8c-(ii).

SEM-EDX and XPS analyses (Fig. 4-7 and Fig. 4-8) imply that after $Cu^{2+}$ activation, the pyrite surface is covered with Cu-containing compounds (e.g., $Cu_2S$, CuO, and/or $Cu(OH)_2$), and the effects of this on the ability of pyrite as a carrier are discussed in the next section.

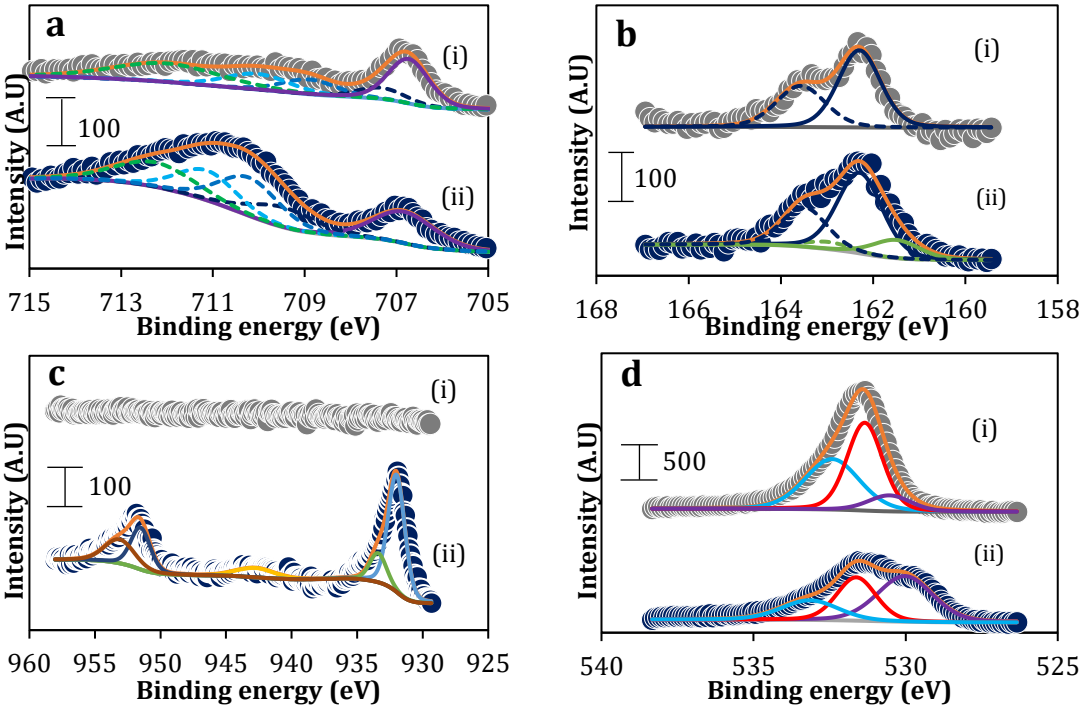


Fig. 4-8. X-ray photoelectron spectroscopy (XPS) spectra of (i) untreated pyrite (ii) pyrite treated with $CuSO_4$ at a pH of 8: (a) Fe 2p, (b) S 2p, (c) Cu 2p, and (d) O 1s. a: This spectrum has three multiplets located at lower and higher binding energies separated by 0.95 eV. b: This spectrum has a doublet located at higher binding energy with 1.18-eV peak separation. The intensity ratio was constrained to one-half with the same Full Width at Half Maximum (FWHM).

#### 4.4.3.2 Particle size distribution analysis

Particle size distribution for the mixture of 20 g of fine chalcopyrite particles and 10 g coarse $Cu^{2+}$-treated pyrite particles suspended in a 400-mL flotation cell after conditioning with KAX were analyzed using Microtrac (Fig. 4-9). The solid black line represents the measured frequency of the mixture, while the dotted line represents the frequency calculated using Eq. (4.2), as described in section 3.1.1. As shown in Fig. 4-9, the comparison of the measured results (solid black lines) with the calculated results (dotted line) shows that the frequency of the fine particles almost disappears while that of the coarse particles increases upon pyrite being treated with $Cu^{2+}$. This suggests that fine chalcopyrite particles were attached to the surface of coarse $Cu^{2+}$-treated pyrite particles before flotation when they were agitated together in the flotation cell after conditioning with KAX.

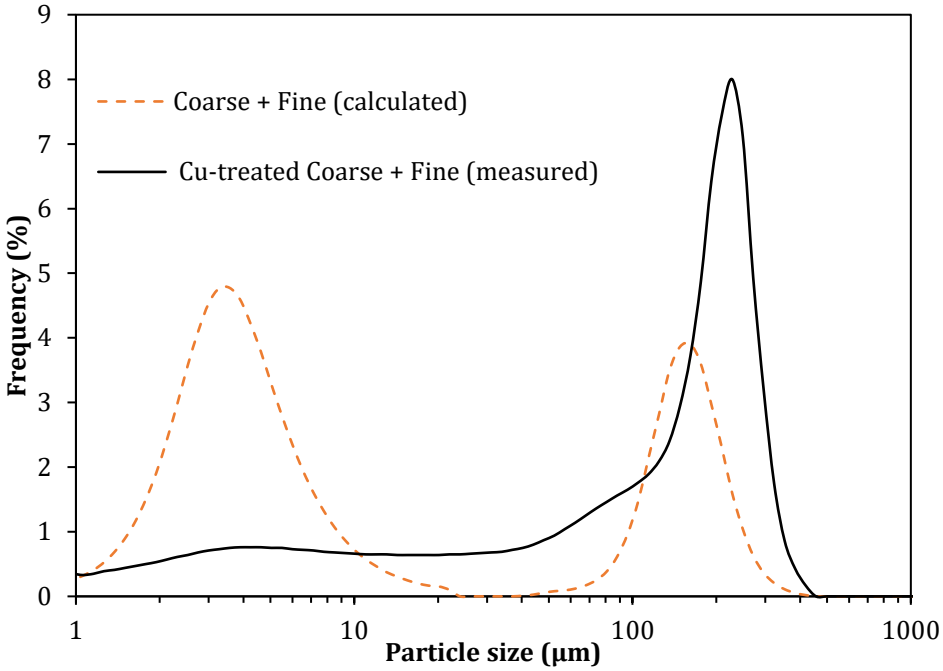


Fig. 4-9. Particle size distribution of the mixture of coarse $Cu^{2+}$-activated pyrite and fine chalcopyrite after conditioning with the collector (measured vs. calculated).

#### 4.4.3.3 Hydrophobic interactions between particles

Based on Eq. (4.3), the hydrophobic interaction energies between coarse $Cu^{2+}$-treated pyrite and fine chalcopyrite particles were calculated and compared to those between coarse untreated pyrite and fine chalcopyrite particles. As shown in Fig. 4-10, the hydrophobic interactions between $Cu^{2+}$-treated pyrite and fine chalcopyrite are much stronger than those between the untreated pyrite and fine chalcopyrite particles, suggesting that the attachment of fine chalcopyrite on the surface of coarse pyrite is enhanced by $Cu^{2+}$ treatment; this is in line with the particle size distribution results shown in Fig. 4-5 and Fig. 4-9.

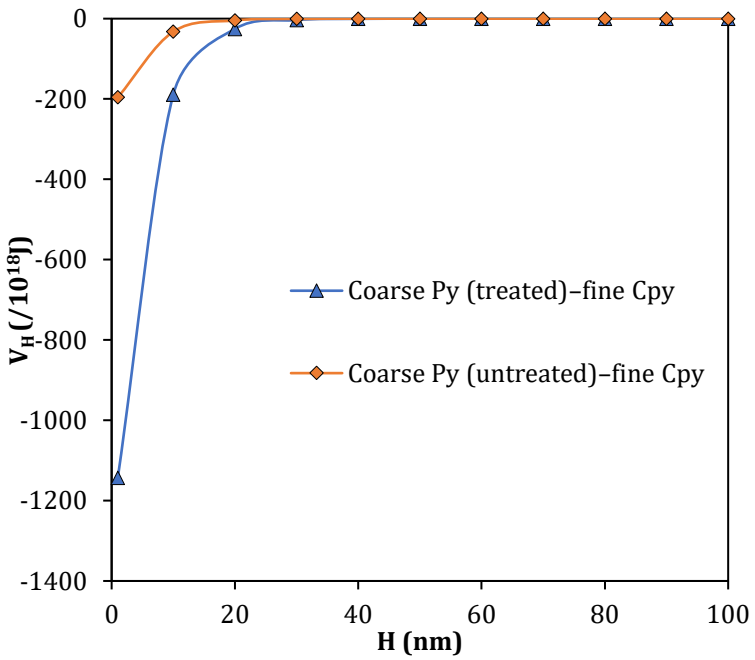


Fig. 4-10. Hydrophobic interactions ($V_H$) between coarse $Cu^{2+}$-treated pyrite and fine chalcopyrite, and those between untreated pyrite and fine chalcopyrite particles.

*4.4.4 Flotation experiments*

To investigate the effects of $Cu^{2+}$-treated coarse pyrite particles as a carrier on the flotation recovery of finely ground chalcopyrite particles, $CuSO_4$ (2,000 g/t) was added to the mixture of fine chalcopyrite and coarse pyrite while maintaining a pH of 8. Fig. 4-11 shows the Cu recovery after 10 min of flotation time, with and without $Cu^{2+}$-treated coarse pyrite particles as a carrier. It can be seen that when coarse $Cu^{2+}$-treated pyrite particles were introduced as a carrier, the recovery of fine chalcopyrite particles improved significantly, from around 70% (with untreated pyrite) to over 90%.

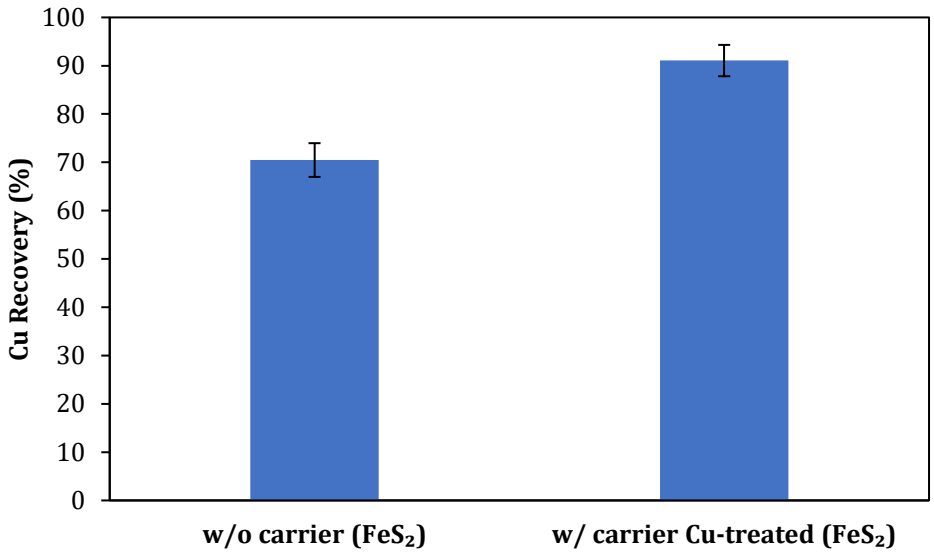


Fig. 4-11. Cu Recovery (%) from fines without (left) and with (right) $Cu^{2+}$-treated pyrite as a carrier: Test conditions: [KAX] = 500 g/t; [MIBC] = 25 µL/L; [$CuSO_4$] = 2,000 g/t; [Carrier size] = –125+106 µm; [Carrier amount] = 10 g.

## 4.5 Conclusions

In this chapter, the effects of two types of coarse pyrite (untreated and $Cu^{2+}$-treated) as a carrier on the flotation behavior of fine chalcopyrite particles ($D_{50}$ ~3 µm) were investigated. When untreated pyrite was used as the carrier, the attachment of fine chalcopyrite to the carrier was limited, and flotation recovery of fine chalcopyrite was not enhanced. When pyrite is treated with $Cu^{2+}$, the pyrite surface is covered with Cu-containing compounds (e.g., $Cu_2S$, CuO, and/or $Cu(OH)_2$), which promotes the adsorption of KAX on the pyrite surface, thereby promoting the attachment of fine chalcopyrite to the surface of $Cu^{2+}$-treated pyrite particles. Therefore, $Cu^{2+}$-treated pyrite can be used as an enhanced carrier to recover fine chalcopyrite particles from tailings.

This chapter was modified from **Bilal, M.;** Ito, M.; Akishino, R.; Bu, X.; Ul Hassan, F.; Park, I.; Jeon, S.; Aikawa, K.; Hiroyoshi, N. Heterogenous carrier flotation technique for recovering finely ground chalcopyrite particles using coarse pyrite particles as a carrier. Miner. Eng. **2022**, 180, 107518.

## References

AIKAWA, K., ITO, M., KUSANO, A., PARK, I., OKI, T., TAKAHASHI, T., FURUYA, H. & HIROYOSHI, N. 2021. Flotation of Seafloor Massive Sulfide Ores: Combination of Surface Cleaning and Deactivation of Lead-Activated Sphalerite to Improve the Separation Efficiency of Chalcopyrite and Sphalerite. *Metals,* 11 DOI: https://doi.org/10.3390/met11020253.

BIESINGER, M. C., LAU, L. W. M., GERSON, A. R. & SMART, R. S. C. 2010. Resolving surface chemical states in XPS analysis of first row transition metals, oxides and

hydroxides: Sc, Ti, V, Cu and Zn. *Applied Surface Science,* 257**,** 887-898 DOI: https://doi.org/10.1016/j.apsusc.2010.07.086.

BOULTON, A., FORNASIERO, D. & RALSTON, J. 2003. Characterisation of sphalerite and pyrite flotation samples by XPS and ToF-SIMS. *International Journal of Mineral Processing,* 70**,** 205-219 DOI: https://doi.org/10.1016/S0301-7516(03)00003-6.

CHENG, W., DENG, Z., TONG, X. & LU, T. 2020. Hydrophobic Agglomeration of Fine Pyrite Particles Induced by Flotation Reagents. *Minerals,* 10 DOI: https://doi.org/10.3390/min10090801.

DENG, Z., CHENG, W., TANG, Y., TONG, X. & LIU, Z. 2021. Adsorption mechanism of copper xanthate on pyrite surfaces. *Physicochemical Problems of Mineral Processing,* 57**,** 46-60 DOI: https://doi.org/10.37190/ppmp/135131.

EJTEMAEI, M. & NGUYEN, A. V. 2017. Characterisation of sphalerite and pyrite surfaces activated by copper sulphate. *Minerals Engineering,* 100**,** 223-232 DOI: https://doi.org/10.1016/j.mineng.2016.11.005.

HU, Y. & DAI, J. 2003. Hydrophobic aggregation of alumina in surfactant solution. *Minerals Engineering,* 16**,** 1167-1172 DOI: https://doi.org/10.1016/j.mineng.2003.07.018.

LI, D., YIN, W., LIU, Q., CAO, S., SUN, Q., ZHAO, C. & YAO, J. 2017. Interactions between fine and coarse hematite particles in aqueous suspension and their implications for flotation. *Minerals Engineering,* 114**,** 74-81 DOI: https://doi.org/10.1016/j.mineng.2017.09.012.

LI, X., PARK, I., TABELIN, C. B., NARUWA, K., GODA, T., HARADA, C., JEON, S., ITO, M. & HIROYOSHI, N. 2021. Enhanced pyrite passivation by carrier-microencapsulation using Fe-catechol and Ti-catechol complexes. *Journal of Hazardous Materials,* 416**,** 126089 DOI: https://doi.org/10.1016/j.jhazmat.2021.126089.

MITCHELL, T. K., NGUYEN, A. V. & EVANS, G. M. 2005. Heterocoagulation of chalcopyrite and pyrite minerals in flotation separation. *Advances in Colloid and Interface Science,* 114-115**,** 227-237 DOI: https://doi.org/10.1016/j.cis.2004.08.009.

NESBITT, H. W. & MUIR, I. J. 1994. X-ray photoelectron spectroscopic study of a pristine pyrite surface reacted with water vapour and air. *Geochimica et Cosmochimica Acta,* 58**,** 4667-4679 DOI: https://doi.org/10.1016/0016-7037(94)90199-6.

PARK, I., HIGUCHI, K., TABELIN, C. B., JEON, S., ITO, M. & HIROYOSHI, N. 2021a. Suppression of arsenopyrite oxidation by microencapsulation using ferric-catecholate complexes and phosphate. *Chemosphere,* 269**,** 129413 DOI: https://doi.org/10.1016/j.chemosphere.2020.129413.

PARK, I., HONG, S., JEON, S., ITO, M. & HIROYOSHI, N. 2020a. Flotation Separation of Chalcopyrite and Molybdenite Assisted by Microencapsulation Using Ferrous and Phosphate Ions: Part I. Selective Coating Formation. *Metals,* 10 DOI: https://doi.org/10.3390/met10121667.

PARK, I., HONG, S., JEON, S., ITO, M. & HIROYOSHI, N. 2021b. Flotation Separation of Chalcopyrite and Molybdenite Assisted by Microencapsulation Using Ferrous and Phosphate Ions: Part II. Flotation. *Metals,* 11 DOI: https://doi.org/10.3390/met11030439.

PARK, I., TABELIN, C. B., SENO, K., JEON, S., INANO, H., ITO, M. & HIROYOSHI, N. 2020b. Carrier-microencapsulation of arsenopyrite using Al-catecholate complex: nature of oxidation products, effects on anodic and cathodic reactions, and coating stability under simulated weathering conditions. *Heliyon,* 6**,** e03189 DOI: https://doi.org/10.1016/j.heliyon.2020.e03189.

SHIRLEY, D. A. 1972. High-Resolution X-Ray Photoemission Spectrum of the Valence Bands of Gold. *Physical Review B,* 5**,** 4709-4714 DOI: https://doi.org/10.1103/PhysRevB.5.4709.

VON OERTZEN, G. U., SKINNER, W. M. & NESBITT, H. W. 2006. Ab initio and XPS studies of pyrite (100) surface states. *Radiation Physics and Chemistry,* 75**,** 1855-1860 DOI: https://doi.org/10.1016/j.radphyschem.2005.07.040.

YANG, B., TONG, X., DENG, Z. & LV, X. 2016. The Adsorption of Cu Species onto Pyrite Surface and Its Effect on Pyrite Flotation. *Journal of Chemistry,* 2016**,** 4627929 DOI: https://doi.org/10.1155/2016/4627929.

YAO, J., YIN, W. & GONG, E. 2016. Depressing effect of fine hydrophilic particles on magnesite reverse flotation. *International Journal of Mineral Processing,* 149**,** 84-93 DOI: https://doi.org/10.1016/j.minpro.2016.02.013.

ZHUGE, F., LI, X., GAO, X., GAN, X. & ZHOU, F. 2009. Synthesis of stable amorphous Cu2S thin film by successive ion layer adsorption and reaction method. *Materials Letters,* 63**,** 652-654 DOI: https://doi.org/10.1016/j.matlet.2008.12.010.

# CHAPTER 5: Detachment of chalcopyrite fines from $Cu^{2+}$-treated pyrite particles

## 5.1 Introduction

In chapter 3, we have investigated the effects of coarse chalcopyrite particles as the carrier. Using coarse chalcopyrite as a carrier, the flotation recovery of finely ground chalcopyrite was improved significantly (Bilal et al., 2021). Moreover, it was revealed that hydrophobic interaction is the key factor in the attachment of fine chalcopyrite pyrite particles to coarse chalcopyrite particles. One of the advantages of autogenous carrier flotation is that it does not require a post-flotation process (Li et al., 2017) and the Cu grade in the final concentrate is maximum.

However, considering tailings as future deposits, this autogenous carrier flotation may have limited applicability because of the non-availability of coarse copper mineral particles at the tailings site. That is why an alternate carrier is required to recover fine copper sulfides from tailings.

Pyrite is a suitable choice as a carrier, because of its abundance at mine sites. In chapter 4, we have investigated the heterogenous carrier flotation technique using coarse $Cu^{2+}$-treated pyrite as a carrier. We demonstrated that by using coarse $Cu^{2+}$-treated pyrite particles as the carrier, flotation recovery of finely ground chalcopyrite particles can be improved significantly. Moreover, it was revealed that hydrophobic interaction is the key factor in the attachment of fine chalcopyrite particles to coarse $Cu^{2+}$-treated pyrite particles (Bilal et al., 2022).

Although effective, heterogeneous carrier flotation using $Cu^{2+}$-treated pyrite as a carrier has a drawback; that is, low Cu grade in the concentrate because a significant amount of coarse pyrite particles is also contained together with fine chalcopyrite particles in the froth. In actual industrial mineral processing operations, a smelter requires a specific grade of copper. Therefore, in the case of heterogeneous carrier flotation using pyrite as a carrier, the development of the post-flotation process to separate attached-fine copper minerals from carrier pyrite is needed to obtain a high-grade Cu concentrate.

In this chapter, two methods (i.e., ultrasonic treatment and acid treatment) were investigated to detach fine chalcopyrite from coarse pyrite (i.e., carrier) by reducing the hydrophobic interaction between them—a major force for these two particles to be attached. Specifically, suitable conditions of these two methods for the detachment were

examined, and the mechanisms of how fine chalcopyrite was detached from coarse pyrite were clarified.

## 5.2 Materials and reagents

### *5.2.1 Materials*

Chalcopyrite and pyrite samples used in these experiments were the same as mentioned in chapter 4.

### *5.2.2 Reagents*

Potassium amyl xanthate (KAX, $C_5H_{11}OCSSK$) (Tokyo Chemical Industry Co., Ltd., Japan) and methyl isobutyl carbinol (MIBC, $C_6H_{14}O$) (Wako Pure Chemical Industries, Ltd., Japan) were used as the collector and frother reagents, respectively. Copper sulfate pentahydrate ($CuSO_45H_2O$) (Wako Pure Chemical Industries, Ltd., Japan) was used as the source of $Cu^{2+}$ for pyrite activation. Diluted HCl (1M) and NaOH (1M) were prepared from concentrated solutions (Wako Pure Chemical Industries, Ltd., Japan) and were used to change the pH of the solution.

## 5.3 Methods

### *5.3.1 Sample preparation*

A jaw crusher (1023-A, Yoshida Manufacturing Co., Ltd, Sapporo, Japan) and disc mill (RS200, Retsch Inc., Haan, Germany) were used to crush and grind the samples, respectively. The particle size distributions of coarse pyrite ($D_{50}$ ~104 μm) and fine chalcopyrite ($D_{50}$ ~3.5 μm) determined by Microtrac (MT3300SX, Nikkiso Co., Ltd., Tokyo, Japan) are shown in Fig. 5-1.

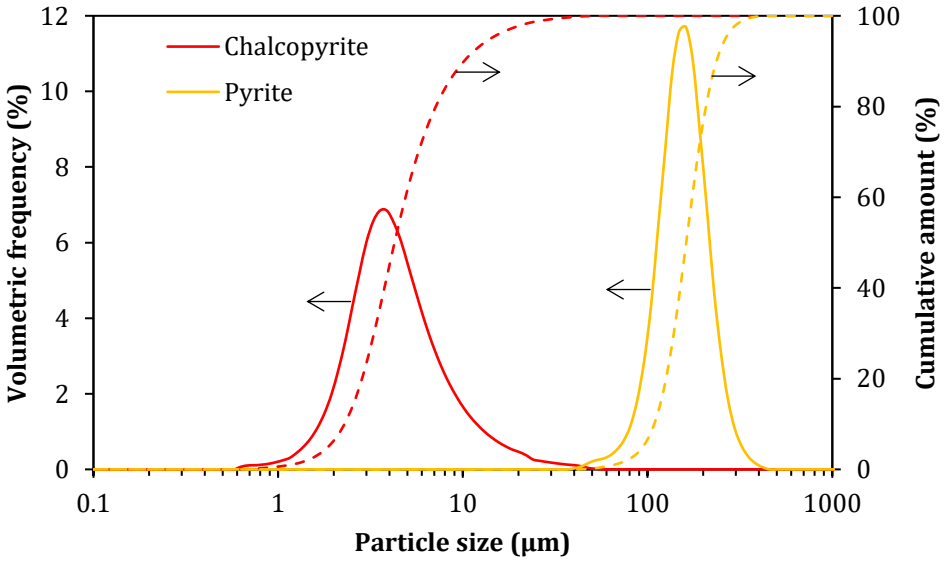


Fig. 5-1. Particle size distributions of the pyrite and chalcopyrite samples.

### *5.3.2 Mixed pyrite–chalcopyrite flotation tests*

Ten grams of coarse pyrite particles and 20 g of fine chalcopyrite particles were conditioned with reagents KAX (500 g/t), MIBC (25 µL/L), and $CuSO_4$ (2000 g/t) for 5, 5, and 3 minutes respectively. The parameters here were the same as already mentioned in section *4.3.4*. The pH of the slurry was 8 and it was kept constant during the conditioning. After the desired conditioning time, air bubbles were introduced into the flotation cell and flotation was carried out for 10 min. The froth product was then analyzed by Microtrac to check the attachment of fines onto the carrier.

### *5.3.3 Detachment of finely ground chalcopyrite from coarse pyrite*

#### 5.3.3.1 Ultrasonic treatment

The froth product obtained after the mixed pyrite-chalcopyrite flotation test was put into a beaker, mixed with 200 mL distilled water, and then treated by an ultrasonicator (W-113, Honda Electronics Co., Ltd., Japan) at 31 Hz for up to 30 min. Afterward, particle size analysis was conducted to check the detachment of finely ground chalcopyrite from coarse pyrite.

#### 5.3.3.2 Acid treatment

Similar to the above subsection, a 200 mL suspension was prepared by mixing the froth product and distilled water. The pH of the suspension was adjusted to 8 using dilute NaOH while stirring at 340 rpm, and a 1mL aliquot was taken and analyzed by a particle size analyzer. Afterward, the pH of the suspension was decreased gradually up to 2 using dilute HCl, and the changes in particle size distributions were measured.

### *5.3.4 XPS analysis*

The surfaces of $Cu^{2+}$-treated pyrite samples treated at different pH were analyzed by X-ray photoelectron spectroscopy (XPS, JPS-9200, JEOL Ltd., Japan) to check whether Cu-compounds formed on the surface of pyrite remained after acid treatment. The XPS analysis was performed using an Al Kα X-ray source (1486.7 eV) operated at 100 W (voltage = 10 kV; current = 10 mA) under ultra-high vacuum conditions (~6.7 × 10−7 Pa). The binding energies of the photoelectrons were calibrated using C 1s (285 eV) as a reference for charge correction. The XPS data were analyzed by Casa XPS, and the spectra were deconvoluted using an 80% Gaussian–20% Lorentzian peak model and a true Shirley background (Nesbitt and Muir, 1994, Shirley, 1972, Park et al., 2020b, Aikawa et al., 2022).

*5.3.5 FTIR measurements*

The $Cu^{2+}$-treated pyrite samples treated at different pH were analyzed by attenuated total reflectance Fourier transform infrared spectroscopy (ATR-FTIR, FT/IR-6200 HFV, and ATR Pro One attachment equipped with a diamond prism, Jasco Analytical Instruments, Japan) to check whether KAX is decomposed or not. $Cu^{2+}$-treated pyrite was conditioned with KAX at different pHs for 20 minutes each in the flotation cell at 1000 rpm. Afterward, the residue was recovered from the suspension by filtration, dried in the vacuum oven at 40 °C for 24 h, and analyzed by ATR-FTIR.

*5.3.6 Dissolution tests of $Cu^{2+}$*

Ten grams of pyrite sample was conditioned with KAX and $CuSO_4$, respectively. Initially, the pH of the sample was adjusted to 8 and conditioned for 13 minutes at 1000 rpm in the flotation cell (same as flotation conditioning time); after this, the leachates were collected by filtration using 0.2 μm syringe-driven membrane filters and immediately analyzed using an inductively coupled plasma atomic emission spectrometer (ICP-AES, ICPE 9820, Shimadzu Corporation, Japan) (margin of error = ±2%) to measure the concentration of $Cu^{2+}$. Similarly, the pH of the suspension was decreased gradually up to 2 using dilute HCl and the samples were taken and analyzed for $Cu^{2+}$ dissolution.

## 5.4 Results and discussion

*5.4.1 Ultrasonic treatment on the detachment of chalcopyrite from $Cu^{2+}$-treated pyrite*

A carrier-flotation experiment for 20 g of fine chalcopyrite was conducted using 10 g of coarse $Cu^{2+}$-treated pyrite particles as carriers with xanthate as the collector. Froth product was suspended in 200 ml of distilled water and agitated, then ultrasonic treatment was applied for 30 min.

Fig. 5-2 shows the particle size distribution of the suspended froth product before ultrasonic treatment. The dotted line is reference data calculated from the amount of chalcopyrite and pyrite in the froth by assuming that there is no attachment of chalcopyrite fines to coarse pyrite particles. In the reference data, there are two peaks corresponding to fine chalcopyrite at around 3.5 μm and coarse pyrite at around 150 μm. In the size distribution curve for the suspended froth product, the peak located at around 3.5 μm was very small, indicating that most of the fine chalcopyrite particles in the froth were attached to coarse $Cu^{2+}$-treated pyrite particles. Moreover, the peak at around 150 μm was shifted to around 250 μm, indicating that fine particles were attached to the surface of coarse pyrite particles as well as the coarse–coarse particles agglomerates were formed.

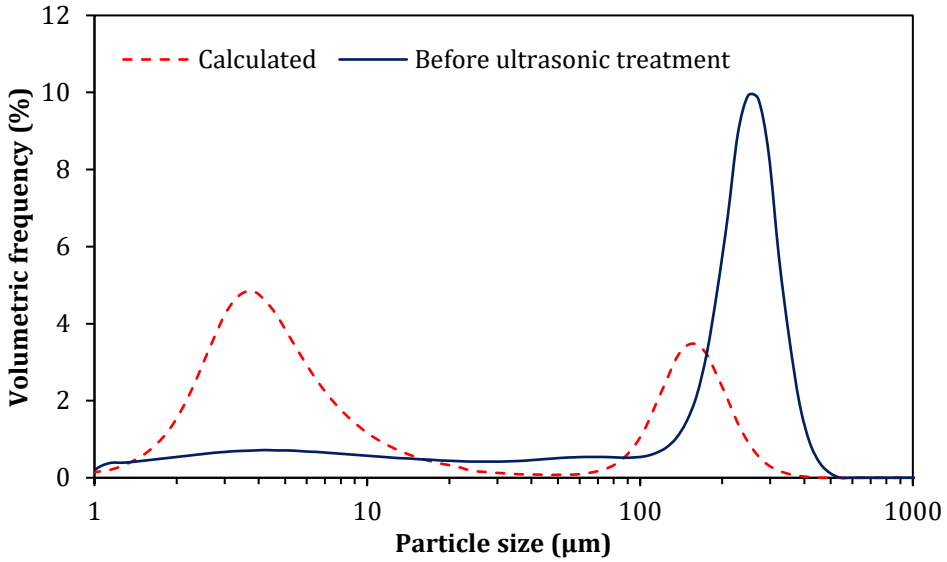


Fig. 5-2. Particle size distribution of the froth product of fine chalcopyrite and coarse pyrite particles before ultrasonic treatment (measured vs. calculated).

Fig. 5-3 shows the effects of the ultra-sonication on the particle size distribution for the suspended froth product. The curve indicated with "0 min (before ultrasonic treatment)" is the same as the solid blue line shown in Fig. 5-2. If fine chalcopyrite particles are detached from coarse pyrite particles, there would be an increase in the peak at 3.5 µm. The observed data, however, showed that there was no significant increase in the peak at 3.5 µm after 30 min of ultrasonic treatment. This suggests that ultrasonic treatment is not effective to detach chalcopyrite fines from $Cu^{2+}$-treated pyrite particles.

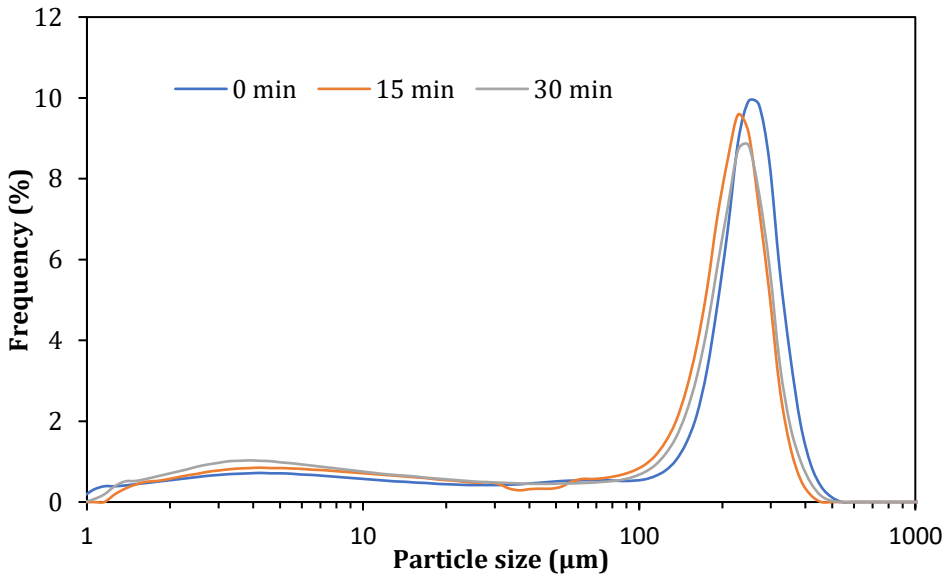


Fig. 5-3. Particle size distribution of the froth product of fine chalcopyrite and coarse pyrite particles at different intervals of ultrasonic treatment time.

In chapter 4, it was found that hydrophobic interaction is the main reason for the attachment of fine chalcopyrite to coarse $Cu^{2+}$-treated pyrite: the potential energy of hydrophobic interaction between fine chalcopyrite and coarse $Cu^{2+}$-treated pyrite was evaluated to be around $-200 \times 10^{18}$ J when the distance between two-particle surfaces is 10 nm (Bilal et al., 2022). As shown in Fig. 5-3, ultrasonic treatment could not detach chalcopyrite fines from $Cu^{2+}$-treated coarse pyrite particles, which indicates two possibilities: (1) the intensity of ultrasonic treatment is not enough to overcome the hydrophobic interaction, and (2) the detachment occurs but the particles get re-attached due to hydrophobic interactions. This suggests that rather than supplying the kinetic energy, a reduction of hydrophobic interaction is needed. In the next section, this approach is discussed.

### *5.4.2 Acid treatment on the detachment of chalcopyrite from $Cu^{2+}$-treated pyrite*

The hydrophobic interaction between chalcopyrite and $Cu^{2+}$-treated pyrite is mainly caused by (1) the CuO/CuS layer formed on the pyrite surface, and (2) collector (KAX) adsorbed on both chalcopyrite and the CuO/CuS layer. It has been reported that at low pH (<4), the collector (KAX) adsorbed onto the surface of the particle could be decomposed (Elizondo-Álvarez et al., 2021). It is also possible that the CuO layer can also be decomposed (or dissolved) in acidic solutions.

Considering the above, acid treatment was applied to reduce the hydrophobic interaction between chalcopyrite and $Cu^{2+}$-treated pyrite. HCl was added to the suspension of the flotation froth product to adjust the pH to ~2. Fig. 5-4 shows the effect of acid treatment on the particle size distribution of the suspended flotation froth product. After 20 min of acid treatment, a significant peak corresponding to fine chalcopyrite (at around 3.5 μm) was observed. The peak at around 250 μm before the treatment was shifted to around 200 μm after acid treatment. This may be due to both the detachment of chalcopyrite from pyrite and the decomposition of pyrite-pyrite agglomerates. This result suggests that acid treatment is effective to reduce the hydrophobic interaction and cause the detachment of fine chalcopyrite from coarse $Cu^{2+}$-treated pyrite.

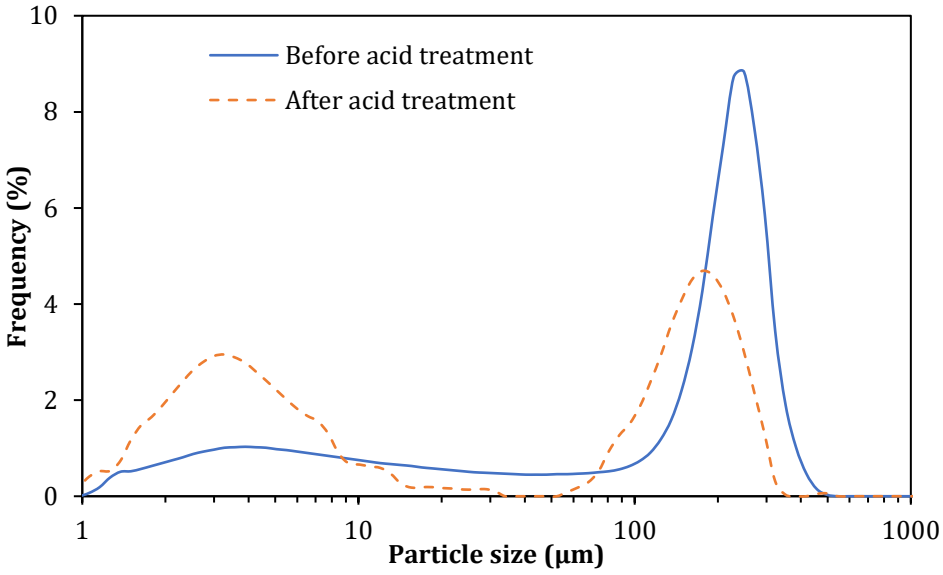


Fig. 5-4. Particle size distribution of the froth product of fine chalcopyrite and coarse pyrite particles before and after acid treatment.

To optimize the pH condition for acid treatment, particle size distributions for the mixture of 20 g of fine chalcopyrite particles and 10 g coarse $Cu^{2+}$-treated pyrite particles suspended in a 400-mL flotation cell after conditioning with KAX at pH 8 and then changing the pH to 5, 4, 3 and 2, were analyzed using Microtrac. For comparison, a calculated size distribution curve for the mixture was obtained, assuming no attachment of chalcopyrite fines to coarse pyrite particles and a comparison has been made with the measured data (Fig. 5-5). From Fig. 5-6, it can be seen that at pH 8, around 38% of fines were attached to coarse $Cu^{2+}$-treated pyrite particles. However, the detachment of fines from coarse $Cu^{2+}$-treated pyrite particles increased with a decrease in pH. The detachment of fines was not significant at pH 4–8 but it was effective at pH <4, i.e., at pH 2, the cumulative frequency of fines was around 97%; suggesting that hydrophobic interactions between coarse and fine particles became weaker. As mentioned earlier, the reduction of hydrophobic interaction has mostly resulted from the dissolution of Cu compounds present on the surface of $Cu^{2+}$-treated pyrite and/or the decomposition of KAX adsorbed on mineral surfaces, which will be clarified in more detail in the following subsections.

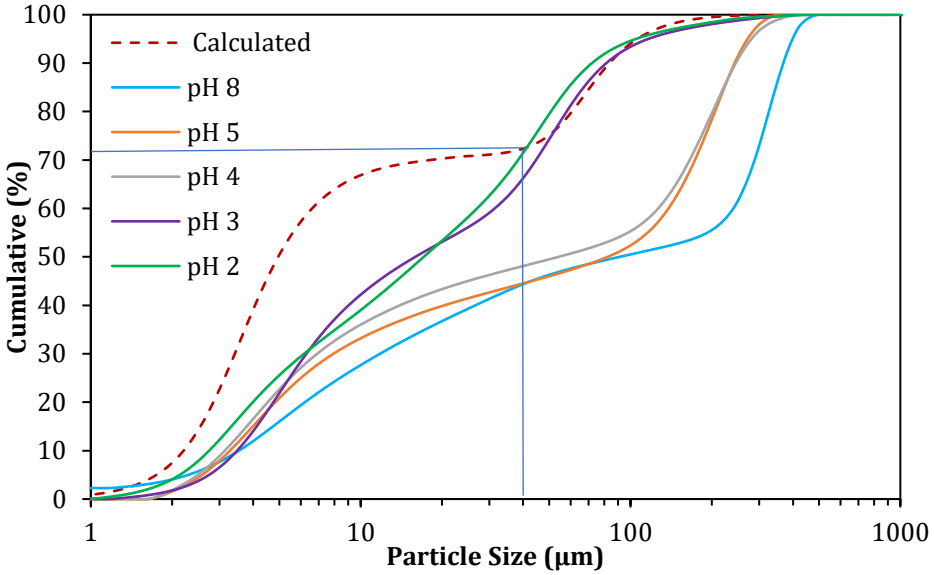


Fig. 5-5. Particle size distribution of the mixture of fine chalcopyrite and coarse $Cu^{2+}$-treated pyrite particles after conditioning (measured vs. calculated).

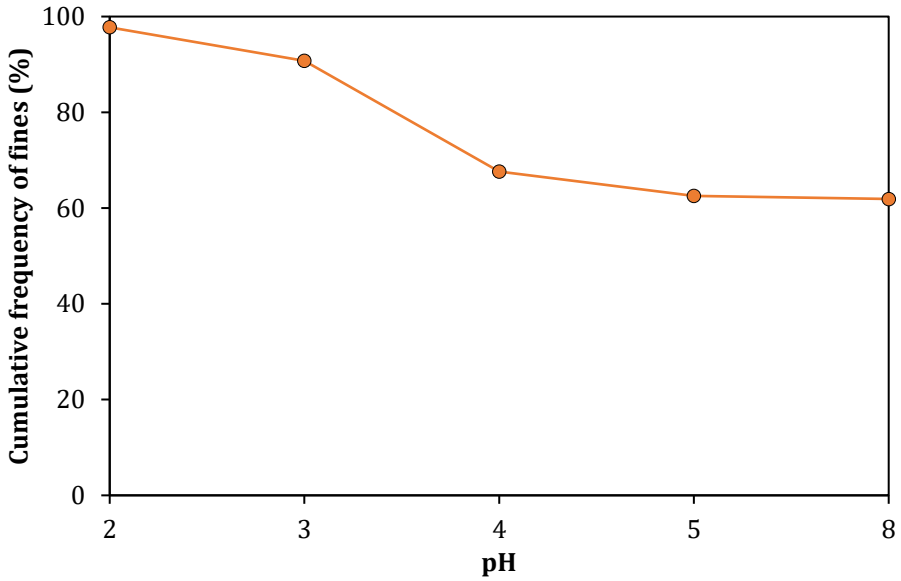


Fig. 5-6. Measured cumulative amount of chalcopyrite fines at different pH.

*5.4.3 Dissolution of Cu compounds formed on the surface of $Cu^{2+}$-treated pyrite at different pH*

Dissolution tests of Cu compounds formed on the surface of $Cu^{2+}$-treated pyrite at different pH were conducted. As shown in Fig. 5-7, almost all of $Cu^{2+}$ was precipitated, when the pH was around 8. However, it can be seen that when pH was decreased, the dissolution of $Cu^{2+}$ increased significantly, i.e., ~ 95% at pH 2.

After dissolution tests, residues were analyzed by XPS to check the changes in the intensities of Cu species present on the surface of pyrite. Fig. 5-8 shows the Cu 2p spectra of $Cu^{2+}$-treated pyrite at different pH. In the Cu $2p_{3/2}$ spectrum of $Cu^{2+}$-treated pyrite at pH

8 (Fig. 5-8 (i)), there is a strong peak at ~ 932 eV corresponding to $Cu_2S$ (Zhuge et al., 2009), as well as minor peaks at around 933.4 eV and 934.9 eV that are both assigned to Cu(II) species like $CuO/Cu(OH)_2$ (Biesinger et al., 2010, Zhuge et al., 2009). However, the intensities of these peaks were reduced when $Cu^{2+}$-activated pyrite was treated at pH 4 (Fig. 5-8 (ii)), and it was further reduced at pH 2 (Fig. 5-8 (iii)), indicating that Cu compounds adsorbed on pyrite surface have been dissolved.

Surface modification is an effective method of controlling mineral hydrophobicity (Aikawa et al., 2021, Park et al., 2020a, Park et al., 2021). The KAX adsorption on pyrite becomes easier when a CuS-like layer or its oxidized products, such as $Cu(OH)_2$, can be formed on the surface of the pyrite (Yang et al., 2016). Pyrite particles would become more hydrophobic, making them better carriers for fine chalcopyrite particles during flotation. Because acid treatment dissolves the CuO layer formed on the pyrite surface (Fig. 5-7 and Fig. 5-8), collector (KAX) adsorbed on the surface of $Cu^{2+}$-treated pyrite could be desorbed, so chalcopyrite fines can be detached from coarse pyrite particles (Fig. *5-5* and Fig. *5-6*). Thus, the dissolution of Cu compounds formed on the surface of pyrite by acid treatment significantly contributes to the detachment of fine chalcopyrite and coarse pyrite.

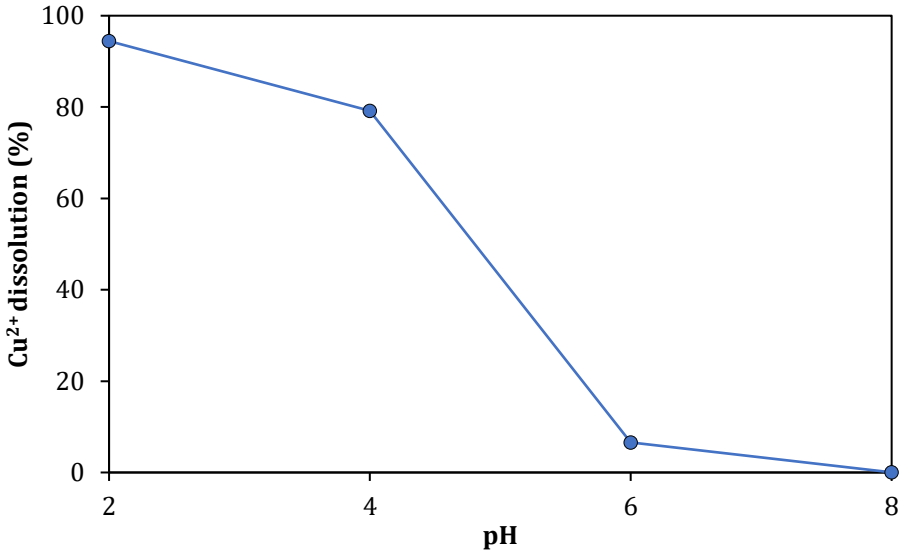

Fig. 5-7. Dissolved Cu concentration after dissolution test.

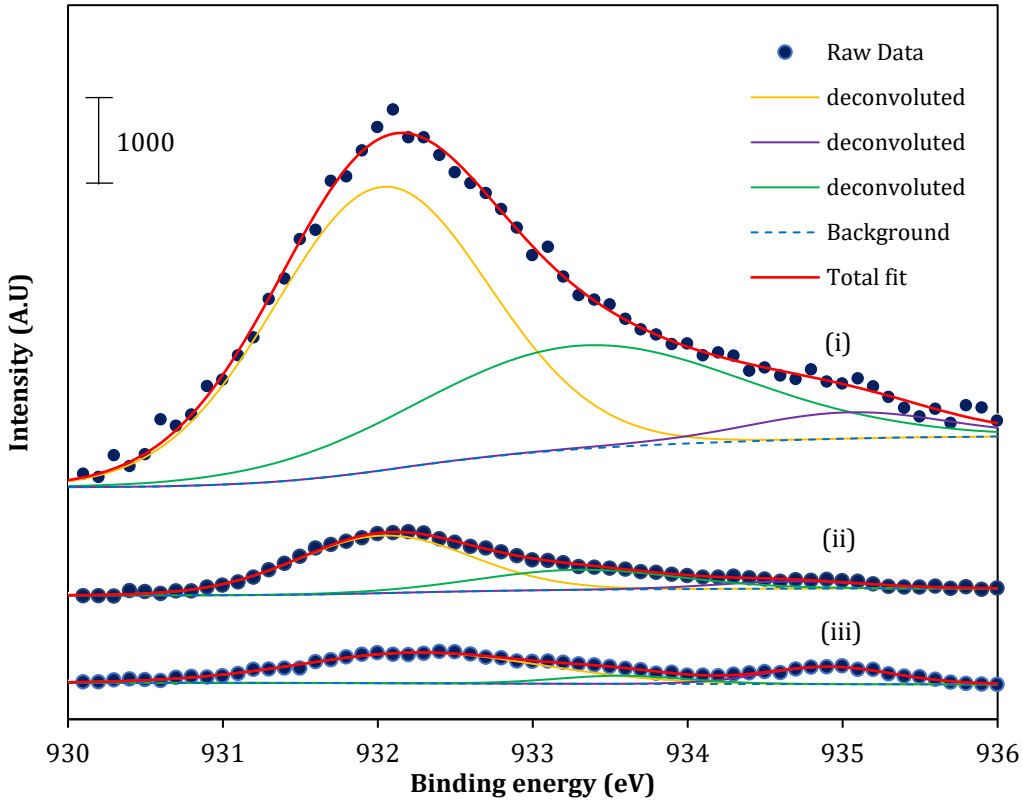

Fig. 5-8. XPS Cu 2p3/2 spectra of $Cu^{2+}$-treated pyrite: (i) pH 8, (ii) pH 4, and (iii) pH 2.

*5.4.4 Decomposition of KAX adsorbed on the surface of pyrite*

Not only the formation of Cu compounds but also the adsorption of KAX plays an important role in improving hydrophobic interaction between fine chalcopyrite and coarse pyrite. Under acidic conditions, it is known that KAX is readily decomposed (Elizondo-Álvarez et al., 2021), so its decomposition was verified by ATR-FTIR analysis of $Cu^{2+}$-activated pyrite treated at various pH (2–8). As shown in Fig. 5-9, the IR spectrum of $Cu^{2+}$-activated pyrite treated with KAX at pH 8 showed the absorption bands of the hydrophobic tail of KAX (e.g., asymmetric, and symmetric stretching bands of $CH_3$–$CH_2$ at 2977, 2927, 2887, and 2830 $cm^{-1}$) (Hornn et al., 2021, Eensalu et al., 2022). Moreover, $Cu^{2+}$-activated pyrite treated with KAX at pH 8 showed only the absorption bands of C–O–C, S–C–S, and C–O–S at 1116 $cm^{-1}$, 1084 $cm^{-1}$and 945 $cm^{-1}$, respectively (Leppinen, 1990, Leppinen et al., 1989). The IR spectrum of $Cu^{2+}$-activated pyrite treated with KAX at pH 4 showed only a weak absorption band of S–C–S detected at 1084 $cm^{-1}$. Meanwhile, IR signatures of KAX were not observed in the spectrum of $Cu^{2+}$-activated pyrite treated with KAX at pH 2, which indicates that KAX started being decomposed at pH 4, and it is completely decomposed at pH 2. This supports our earlier deduction that at low pH (~2),

Cu precipitates could be dissolved and KAX could be decomposed, thereby reducing the hydrophobic attractive force between mineral particles, and promoting detachment.

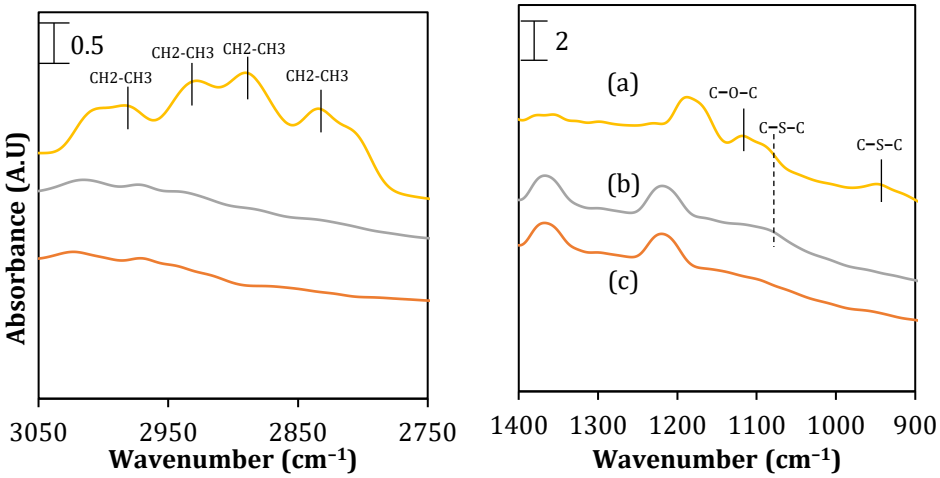


Fig. 5-9. FT-IR spectra of pyrite treated with KAX: (a) pH 8, (b) pH 4, and (c) pH 2.

*5.4.5 Proposed flow sheet for heterogeneous carrier flotation*

To separate fine chalcopyrite particles from $Cu^{2+}$-treated pyrite particles, suspension of the acid-treated froth product was poured on the screen of 75 µm. The results showed that around 90% of Cu in the froth was recovered as a passing product and it was separated from the retained product, which is mainly composed of coarse pyrite. Based on the results a flow sheet was proposed, to integrate the heterogenous carrier flotation into the existing flotation circuits to recover fine copper sulfides from low-grade deposits/tailings and reuse the coarse pyrite as the carrier (Fig. 5-10). Tailings may contain fine pyrite particles and during copper activation, they may attach to coarse pyrite particles. To avoid this, it was proposed that coarse pyrite particles should be pre-treated with $CuSO_4$ separately, this will allow only fine copper sulfides particles to attach with coarse treated pyrite particles and fine pyrite particles will not attach to coarse treated pyrite particles.

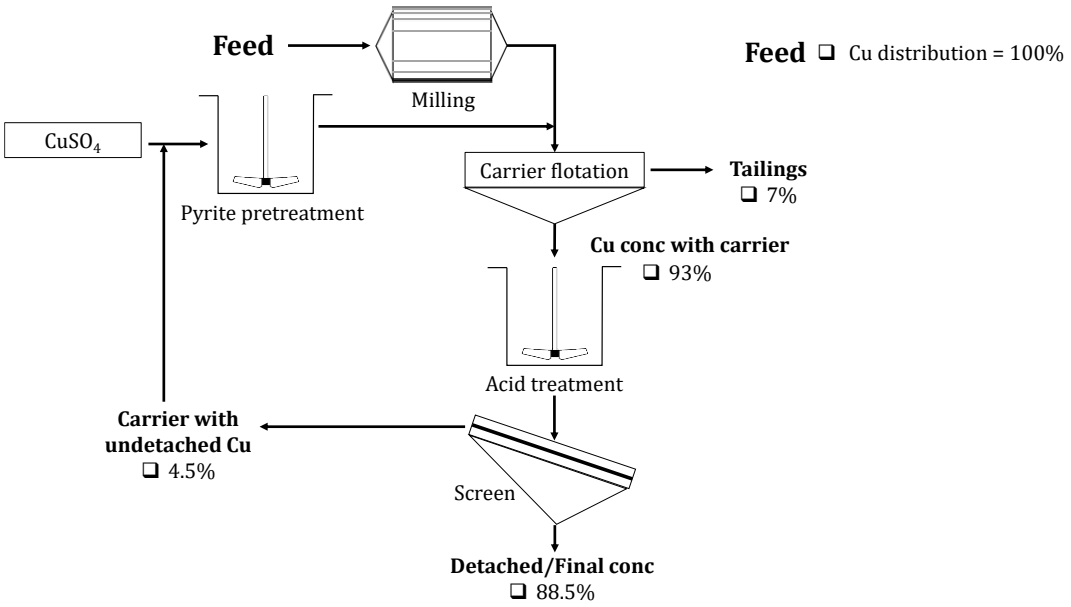


Fig. 5-10. Proposed flow-sheet of heterogeneous carrier flotation for low-grade deposits/tailings.

## 5.5 Conclusion

In this chapter, the effects of ultrasonic treatment and acid treatment were compared for the detachment efficiency of chalcopyrite fines from $Cu^{2+}$-treated coarse pyrite particles. Particle size distribution analysis of the froth product (fine chalcopyrite and $Cu^{2+}$-treated coarse pyrite particles) suspended in water showed that ultrasonic treatment was not effective, while acid treatment was effective to detach fine chalcopyrite from carrier (coarse pyrite). After acid treatment, the overall copper recovery was around 90% (with carrier flotation) compared to that of 70% (without carrier flotation). This suggests that after heterogeneous carrier flotation combined with acid treatment (post flotation), not only coarse pyrite may be reused as a carrier but also the grade of final Cu concentrate could be improved.

This chapter was modified from **Bilal, M.;** Ito, M.; Park, I.; Ul Hassan, F.; Aikawa, K.; Jeon, S.; Hiroyoshi, N. Heterogenous carrier flotation technique for recovering finely ground chalcopyrite particles using coarse pyrite particles as a carrier: Part II. Detachment of finely ground chalcopyrite 3 particles from coarse pyrite particles. Minerals Engineering, MINE-D-22-00996 (Under review).

## References

AIKAWA, K., ITO, M., KUSANO, A., JEON, S., PARK, I. & HIROYOSHI, N. 2022. Development of a Sustainable Process for Complex Sulfide Ores Containing Anglesite: Effect of Anglesite on Sphalerite Floatability, Enhanced Depression of Sphalerite by Extracting Anglesite, and Recovery of Extracted Pb2+ as Zero-Valent Pb by Cementation Using Zero-Valent Fe. *Minerals,* 12 DOI: https://doi.org/10.3390/min12060723.

AIKAWA, K., ITO, M., KUSANO, A., PARK, I., OKI, T., TAKAHASHI, T., FURUYA, H. & HIROYOSHI, N. 2021. Flotation of Seafloor Massive Sulfide Ores: Combination of Surface Cleaning and Deactivation of Lead-Activated Sphalerite to Improve the Separation Efficiency of Chalcopyrite and Sphalerite. *Metals,* 11 DOI: https://doi.org/10.3390/met11020253.

BIESINGER, M. C., LAU, L. W. M., GERSON, A. R. & SMART, R. S. C. 2010. Resolving surface chemical states in XPS analysis of first row transition metals, oxides and hydroxides: Sc, Ti, V, Cu and Zn. *Applied Surface Science,* 257**,** 887-898 DOI: https://doi.org/10.1016/j.apsusc.2010.07.086.

BILAL, M., ITO, M., AKISHINO, R., BU, X., UL HASSAN, F., PARK, I., JEON, S., AIKAWA, K. & HIROYOSHI, N. 2022. Heterogenous carrier flotation technique for recovering finely ground chalcopyrite particles using coarse pyrite particles as a carrier. *Minerals Engineering,* 180**,** 107518 DOI: https://doi.org/10.1016/j.mineng.2022.107518.

BILAL, M., ITO, M., KOIKE, K., HORNN, V., UL HASSAN, F., JEON, S., PARK, I. & HIROYOSHI, N. 2021. Effects of coarse chalcopyrite on flotation behavior of fine chalcopyrite. *Minerals Engineering,* 163**,** 106776 DOI: https://doi.org/10.1016/j.mineng.2021.106776.

EENSALU, J. S., TÕNSUAADU, K., ADAMSON, J., OJA ACIK, I. & KRUNKS, M. 2022. Thermal decomposition of tris(O-ethyldithiocarbonato)-antimony(III)—a single-source precursor for antimony sulfide thin films. *Journal of Thermal Analysis and Calorimetry,* 147**,** 4899-4913 DOI: 10.1007/s10973-021-10885-1.

ELIZONDO-ÁLVAREZ, M. A., URIBE-SALAS, A. & BELLO-TEODORO, S. 2021. Chemical stability of xanthates, dithiophosphinates and hydroxamic acids in aqueous solutions and their environmental implications. *Ecotoxicology and Environmental Safety,* 207**,** 111509 DOI: https://doi.org/10.1016/j.ecoenv.2020.111509.

HORNN, V., PARK, I., ITO, M., SHIMADA, H., SUTO, T., TABELIN, C. B., JEON, S. & HIROYOSHI, N. 2021. Agglomeration-flotation of finely ground chalcopyrite using surfactant-stabilized oil emulsions: Effects of co-existing minerals and ions. *Minerals Engineering,* 171**,** 107076 DOI: https://doi.org/10.1016/j.mineng.2021.107076.

LEPPINEN, J. O. 1990. FTIR and flotation investigation of the adsorption of ethyl xanthate on activated and non-activated sulfide minerals. *International Journal of Mineral Processing,* 30**,** 245-263 DOI: https://doi.org/10.1016/0301-7516(90)90018-T.

LEPPINEN, J. O., BASILIO, C. I. & YOON, R. H. 1989. In-situ FTIR study of ethyl xanthate adsorption on sulfide minerals under conditions of controlled potential. *International Journal of Mineral Processing,* 26**,** 259-274 DOI: https://doi.org/10.1016/0301-7516(89)90032-X.

LI, D., YIN, W., LIU, Q., CAO, S., SUN, Q., ZHAO, C. & YAO, J. 2017. Interactions between fine and coarse hematite particles in aqueous suspension and their implications for flotation. *Minerals Engineering,* 114**,** 74-81 DOI: https://doi.org/10.1016/j.mineng.2017.09.012.

NESBITT, H. W. & MUIR, I. J. 1994. X-ray photoelectron spectroscopic study of a pristine pyrite surface reacted with water vapour and air. *Geochimica et Cosmochimica Acta,* 58**,** 4667-4679 DOI: https://doi.org/10.1016/0016-7037(94)90199-6.

PARK, I., HONG, S., JEON, S., ITO, M. & HIROYOSHI, N. 2020a. Flotation Separation of Chalcopyrite and Molybdenite Assisted by Microencapsulation Using Ferrous and Phosphate Ions: Part I. Selective Coating Formation. *Metals,* 10 DOI: https://doi.org/10.3390/met10121667.

PARK, I., HONG, S., JEON, S., ITO, M. & HIROYOSHI, N. 2021. Flotation Separation of Chalcopyrite and Molybdenite Assisted by Microencapsulation Using Ferrous and Phosphate Ions: Part II. Flotation. *Metals,* 11 DOI: https://doi.org/10.3390/met11030439.

PARK, I., TABELIN, C. B., SENO, K., JEON, S., INANO, H., ITO, M. & HIROYOSHI, N. 2020b. Carrier-microencapsulation of arsenopyrite using Al-catecholate complex: nature of oxidation products, effects on anodic and cathodic reactions, and coating stability under simulated weathering conditions. *Heliyon,* 6**,** e03189 DOI: https://doi.org/10.1016/j.heliyon.2020.e03189.

SHIRLEY, D. A. 1972. High-Resolution X-Ray Photoemission Spectrum of the Valence Bands of Gold. *Physical Review B,* 5**,** 4709-4714 DOI: https://doi.org/10.1103/PhysRevB.5.4709.

YANG, B., TONG, X., DENG, Z. & LV, X. 2016. The Adsorption of Cu Species onto Pyrite Surface and Its Effect on Pyrite Flotation. *Journal of Chemistry,* 2016**,** 4627929 DOI: https://doi.org/10.1155/2016/4627929.

ZHUGE, F., LI, X., GAO, X., GAN, X. & ZHOU, F. 2009. Synthesis of stable amorphous Cu2S thin film by successive ion layer adsorption and reaction method. *Materials Letters,* 63**,** 652-654 DOI: https://doi.org/10.1016/j.matlet.2008.12.010.

# CHAPTER 6: General conclusion and recommendations

## 6.1 Conclusion

A comprehensive review of different flotation techniques to recover fine copper sulfides from tailings was conducted. Based on the review it was suggested that carrier flotation can be more effective to recover fine copper sulfides from tailings.

In this dissertation, innovative methods, the effects of coarse chalcopyrite (autogenous carrier flotation) and $Cu^{2+}$-activated coarse pyrite (heterogenous carrier flotation) particles as carriers to recover finely ground chalcopyrite particles were investigated. It was observed that fine chalcopyrite particles recovery was improved when coarse chalcopyrite and $Cu^{2+}$-activated coarse pyrite particles were used as carriers.

Brief background of mineral processing of copper ore is presented in chapter 1. Moreover, the problems related to fine particles recovery and the objective of this study are also described in chapter 1.

In chapter 2, the challenges, and prospects to recover copper sulfides from tailings are discussed in detail. Ultrafine copper sulfide mineral particles are least likely to collide with air bubbles in the flotation cell, and coarse copper sulfide particles associated with gangue minerals are not attached to air bubbles, causing the tailing loss of these copper sulfides. Hence, regrinding of the coarse unliberated particle will further produce ultrafine particles. Therefore, the development of flotation methods for fine particles is much needed. Flotation methods for fine particles recovery such as microbubble flotation, column flotation, nanobubble flotation, oil agglomeration, shear flocculation, polymer flocculation, and carrier flotation were reviewed; and their applications and limitations were discussed in detail.

In chapter 3, the autogenous carrier flotation technique was used to recover finely ground chalcopyrite particles using coarse chalcopyrite particles as carriers. Using coarse chalcopyrite particles as carriers significantly improved the recovery of finely ground chalcopyrite particles. Moreover, from particle size distribution results and SEM observations, it was confirmed that fine chalcopyrite particles were selectively attached to the surface of coarse chalcopyrite particles. Based on EDLVO calculations, it was revealed that hydrophobic interaction plays an important role in the attachment of chalcopyrite fines to the surface of coarse carrier particles.

The heterogeneous carrier flotation technique using coarse pyrite particles as carriers for finely ground chalcopyrite particles was investigated in chapter 4. It was observed that adding coarse pyrite particles did not act as carriers, however, when pyrite was pre-treated with $CuSO_4$ solution, the hydrophobic interactions between fine chalcopyrite and $Cu^{2+}$-treated pyrite particles became stronger, and the fine chalcopyrite were attached to the surface of $Cu^{2+}$-treated pyrite particles, which improved fine chalcopyrite recovery significantly.

In chapter 5, the post-flotation separation of $Cu^{2+}$-treated pyrite and finely ground chalcopyrite particles was investigated. It was observed that using an ultrasonic treatment for particles suspended in water did not effectively separate the particles. However, with acid treatment, the KAX could be dissolved, and the fine particles attached to coarse $Cu^{2+}$-treated pyrite particles were efficiently detached.

### 6.2 Recommendations for future work

The findings from this research work indicate that using coarse chalcopyrite particles as well as $Cu^{2+}$-treated pyrite particles as carriers improved the finely ground chalcopyrite recovery. However, further studies are needed to investigate the autogenous and heterogenous carrier flotation techniques at pilot and industrial scales using low-grade ores.